The potential of bamboo corals to record environmental conditions in their calcitic skeletons

Dissertation

zur Erlangung des Doktorgrades

Dr. rer. nat.

der Mathematisch-Naturwissenschaftlichen Fakultät

der Christian-Albrechts-Universität zu Kiel

vorgelegt von

Sebastian B. Flöter

Kiel, 2019

Erster Gutachter:	Prof. Anton Eisenhauer
Zweite Gutachterin:	Dr. Claire Rollion-Bard

Eingereicht am:	05. November 2019
Tag der mündlichen Prüfung:	20. Dezember 2019

Eidesstattliche Erklärung

Hiermit versichere ich an Eides statt, dass ich diese Dissertation selbständig und nur mit Hilfe der angegebenen Quellen und Hilfsmittel erstellt habe. Diese Arbeit ist unter Einhaltung der Regeln guter wissenschaftlicher Praxis der Deutschen Forschungsgemeinschaft entstanden und wurde weder ganz, noch in Teilen an anderer Stelle im Rahmen eines Prüfungsverfahrens eingereicht. Teile dieser Arbeit sind bereits veröffentlicht oder in Vorbereitung eingereicht zu werden. Ein akademischer Grad wurde mir nicht entzogen.

Kiel, den 05.11.2019

Sebastian B. Flöter

Contents

"Denn ein Weg zur Wirklichkeit geht über Bilder."

Elias Canetti

Abstract

The ocean's physicochemical variability (e.g. temperature) is not well understood despite its importance for the world's climate because of rare instrumental time series. This issue can be resolved through natural archives that recorded past environmental conditions such as corals. The cosmopolitan calcitic bamboo corals (Isididae) belong to the subclass of Octocorallia and are long-lived, thus offering the potential to record environmental parameters over a wide range of oceanic conditions. This study provides a detailed look into the chemical composition of bamboo coral skeletons to distinguish between environmental and biomineralisation controls over the skeletal composition.

The ability of bamboo corals to record seawater temperature and nutrient conditions was investigated in chapter two this thesis. For this purpose the distribution of Mg and Ba, respectively, in the calcitic internode of an Atlantic specimen from the Blake Plateau off Florida was measured. We observed that the mean Mg/Ca composition of a bamboo coral can be used to reconstruct the ambient seawater temperature while mean Ba/Ca was found to record $[Ba]_{SW}$. Conversely, microscale variations suggest environmental variability which cannot reflect ambient seawater conditions. Instead, the coral physiology has a strong impact on skeletal formation and with that on the micron-scale skeletal Mg and Ba composition. The physiological impact on the skeletal composition is further indicated by chemical patterns formed along regions of nearly simultaneous growth excluding an environmental impact for the origin of these patterns. If ambient seawater conditions exerted the sole control over these elemental ratios, a certain environmental parameter such as temperature should cause the same response everywhere along the region of simultaneous growth. Further, we propose that the observed isolated microscale compositional features are related to tissue attachment. Taken together, these results suggest that bamboo corals can be used as temperature and $[Ba]_{SW}$ recorder when utilising mean skeletal compositions, while variations on the micrometre scale exceed that ambient conditions and are hence controlled by internal physiological processes.

The use of skeletal Na and S contents as environmental proxies in marine calcifiers is debated. Therefore it was evaluated in chapter three whether these potential proxies record ambient seawater conditions in two Atlantic bamboo corals from the Bear Seamount and the Blake Plateau during the time of their growth. The microscale distribution of Na and S can show a concentric structure and zig zag patterns as found for Mg. The comparison of the variability of two Atlantic samples revealed that with increasing variability of salinity, the variations of Na in the sample are higher. Nevertheless, we cannot exclude a coincidence. As seen in chapter two for Mg and Ba, the microscale heterogeneity indicates a main control of the coral physiology over the skeletal composition. We present a calcification model that is capable of explaining the Na and S inverse correlation. This model includes Ca pumping and bicarbonate active transport while assuming conservative behaviour of Na and S in the calcifying fluid. Although the inverse correlation of Na and S can be explained without the involvement of skeletal organic matter, it cannot be excluded as an additional minor influence on the skeletal incorporation of these two elements. The results suggest that the skeletal microscale distribution of both Na and S are mainly influenced by physiological processes rather than ambient environmental conditions.

The B elemental as well as its isotopic composition in calcium carbonates have been used to study the carbonate system, and in particular ambient pH, of the calcifying fluid. Chapter four describes the B/C and B isotopic spatial distribution in an Atlantic (Bear Seamount) and a Pacific (Monterey Canyon) bamboo coral specimen measured in the bulk internode material and the purified calcite fraction. We found a correlation between bulk δ^{11}B values and B/C on the samples employing the laser ablation approach, allowing for a preliminary estimate on potential δ^{11}B variations based on the B distribution in bamboo corals. The range of the δ^{11}B values collected with laser ablation sampling is larger than obtained from the drill sampling. This observation can be explained with averaging significantly larger areas by drill sampling but mainly with the compositional difference of the skeletal phases we

measured. We found that the solution-based measurements indicate a lower pH up-regulation of the calcifying fluid than scleractinian corals which agrees with earlier studies. Nevertheless, our results suggest that the skeletal boron isotopic composition of bamboo corals might besides CF pH be influenced by borate influx to the CF, organic matter induced isotope fractionation or kinetic isotope effects.

Zusammenfassung

Die Variabilität physikalisch-chemischer Eigenschaften der Ozeane ist trotz ihrer Bedeutung für das Weltklima aufgrund der Seltenheit von instrumentellen Zeitreihen nicht sehr gut bekannt. Das Fehlen dieser Zeitreihen könnte durch die Nutzung von natürlichen Umweltarchiven wie Korallen gelöst werden. Bambuskorallen sind langlebige und kosmopolitische kalzitische Oktokorallen und bieten daher das Potenzial, marine Umweltbedingungen über einen weiten räumlichen und zeitlichen Bereich aufzuzeichnen. Diese Dissertation untersucht detailliert die chemische Zusammensetzung von Bambuskorallen mit dem Ziel, zwischen dem Einfluss von Umweltfaktoren und Biomineralisation auf die Skelettzusammensetzung unterscheiden zu können.

Die Fähigkeit von Bambuskorallen, die Temperatur und die Nährstoffbedingungen des Meerwassers zu erfassen, wurde durch die Verteilung von Mg und Ba im kalzitischen Internodium einer atlantischen Probe vom Blake Plateau vor Florida in Kapitel zwei untersucht. Die Resultate zeigen, dass die mittlere Mg/Ca-Zusammensetzung der Probe verwendet werden kann, um die langfristige Umgebungstemperatur des Meerwassers zu rekonstruieren, während das durchschnittliche Ba/Ca Verhältnis über $[Ba]_{SW}$ Auskunft geben kann. Gleichzeitig deuten mikroskalige Variationen auf eine Umgebungsvariabilität hin, die die Umgebungsbedingungen nicht widerspiegeln kann. Deshalb ist es wahrscheinlicher, dass die Korallenphysiologie einen starken Einfluss auf die Skelettbildung und damit auf die kleinräumige Skelettkonzentration von Mg und Ba hat. Die physiologische Wirkung wird außerdem durch feinskalige Muster auf der Probe angedeutet, die sich entlang von Regionen mit nahezu gleichzeitigem Wachstum bildeten. Dadurch liegt die Ursache für den Ursprung dieser Muster höchstwahrscheinlich nicht in Schwankungen der Umgebungswasserparameter. Weiterhin schlagen wir vor, dass beobachtbare isolierte mikroskalige Zusammensetzungsmerkmale mit der Anhaftung des Korallengewebes am Skelett zusammenhängen. Bambuskorallen können demnach als Temperatur- und $[Ba]_{SW}$-Archive verwendet werden, wenn die mittlere Skelettzusammensetzung verwendet wird, wobei die Variation im Bereich

von Mikrometern eindeutig die Schwankungen der Umgebungsbedingungen überschreitet.

Die Verwendung der Na- und S-Konzentrationen als Umweltproxys in marinen Kalzifizierern ist Gegenstand gegenwärtiger Diskussion. In Kapitel drei wurde untersucht, ob diese potentiellen Proxies die Umgebungsbedingungen zweier atlantischer Bambuskorallen zur Zeit ihres Wachstums widergeben können. Die mikroskalige Verteilung von Na/Ca und S/Ca, kann wie bereits bei der Verteilung von Mg/Ca und Ba/Ca zu sehen war, eine konzentrische Struktur und Zickzackmuster aufweisen. Der Vergleich der Variabilität von zwei atlantischen Proben ergab eine höhere Variation von Na/Ca in der Probe mit einer höheren Variabilität des Salzgehalts. Dennoch können wir eine Koinzidenz nicht ausschließen. Weiterhin legt, wie bei Mg, die mikroskalige Heterogenität den Haupteinfluss der Korallenphysiologie auf die Skelettzusammensetzung nahe. Na und S weisen eine inverse Korrelation auf, die durch ein Kalzifikationsmodell erklärt werden kann. Dieses Modell beinhaltet Ca-Pumpen und aktiven Bikarbonattransport unter der Annahme konservativen Verhaltens von Na und S in der Fällungslösung. Obwohl die inverse Korrelation von Na und S ohne Beteiligung skelettgebundener organischer Substanz erklärt werden kann, kann sie als zusätzlicher wenn auch schwacher Einfluss auf den Einbau dieser beiden Elemente in Skelett nicht ausgeschlossen werden. Die Ergebnisse deuten darauf hin, dass die mikroskalige Verteilung von Na und S im Skelett hauptsächlich durch interne physiologische Prozesse und nicht durch äußere Umweltbedingungen bestimmt werden.

Die Zusammensetzung von Kalziumkarbonaten bezüglich ihrer B-Konzentration und -Isotopie wurde verwendet, um einzelne Karbonatparameter und vor allem den pH-Wert der Fällungsflüssigkeit zu ermitteln. Kapitel vier zeigt die Verteilung von B/C und δ^{11}B-Werten im Internodium an je einer atlantischen und pazifischen Bambuskorallenprobe, die an Bulkmaterial sowie am Kalzit bestimmt wurde. Wir fanden eine Korrelation zwischen den Borisotopenverhältnissen, die im Bulkmaterial bestimmt wurde und dem B/C Verhältnis der Proben. Dies erlaubt eine vorläufige Schätzung der möglichen räumlichen δ^{11}B Variation aufgrund der B-Verteilung

in Bambuskorallen. Die Variation von δ^{11}B-Werten der Bulkproben ist größer als jene der lösungsbasiert gemessenen Kalzitproben. Diese Beobachtung lässt sich hauptsächlich durch den Unterschied in der Zusammensetzung des gemessenen Materials erklären, wobei die individuelle Probengröße bei laserablationsbasierten Messungen wesentlich geringer war. Die lösungsbasierten Messungen am kalzitischen Material deuten auf eine weniger starke pH-Wert-Erhöhung der Kalkflüssigkeit hin, als bei skleraktinischen Korallen, was die Ergebnisse früherer Studien bestätigt. Dennoch deuten unsere Ergebnisse darauf hin, dass die isotopenchemische Zusammensetzung des Skeletts, neben dem pH-Wert der Kalzifikationslösung auch durch Borattransport in die Kalzifikationslösung, Isotopenfraktierung durch organisches Material oder kinetische Isotopeneffekte beeinflusst wird.

Contributions to this thesis

Chapter two was already published in *Geochimica et Cosmochimica Acta* authored by Sebastian B. Flöter, Jan Fietzke, Marcus Gutjahr, Jesse Farmer, Bärbel Hönisch, Gernot Nehrke, and Anton Eisenhauer under the title: "The influence of skeletal micro-structures on potential proxy records in a bamboo coral" (DOI: 10.1016/j.gca.2018.12.027). Individual contributions of various authors are as follows: I prepared the sample, measured it with the help of Mario Thöner and Jan Fietzke, analysed the data and wrote the manuscript under the guidance of Marcus Gutjahr and Jan Fietzke. The study was designed by me, Jan Fietzke and Marcus Gutjahr. Bärbel Hönisch and Jesse Farmer provided the sample. Confocal Raman spectroscopy data were provided by Gernot Nehrke. All co-authors contributed to the discussion and improved the text of the manuscript. The manuscript was further improved by the associated editor Thomas Marchitto and three anonymous reviewers.

Chapter three is in preparation for submission to *Chemical Geology* in the following month. Authors will be Sebastian B. Flöter, Jan Fietzke, Marcus Gutjahr, Bärbel Hönisch, Gernot Nehrke and Anton Eisenhauer. Individual contributions of various authors are as follows: I prepared the samples, measured these with the help of Jan Fietzke and Mario Thöner, analysed the data and wrote the manuscript under the guidance of Marcus Gutjahr and Jan Fietzke. The study was designed by me, Jan Fietzke and Marcus Gutjahr. Samples were provided by Bärbel Hönisch and Jesse Farmer. Gernot Nehrke provided the confocal Raman spectroscopy data. Jan Fietzke and Marcus Gutjahr guided the writing process and the finalisation of the discussion.

Chapter four is planned for publication in *Chemical Geology*. I prepared and measured the samples on their solution based boron isotopic composition, analysed the data and wrote the manuscript. I, Marcus Gutjahr and Jan Fietzke designed the study. Laser ablation based data were provided by Jan Fietzke. Bärbel Hönisch and Jesse Farmer provided the samples. Jan Fietzke and Marcus Gutjahr guided the writing process and the finalisation of the discussion.

Acknowledgements

First I would like to thank my supervisor Prof. Anton Eisenhauer for offering the position, for his supervision and the opportunity to realise my own project. I would also like to thank the thesis assessment committee, Prof. Christian Berndt, Toni, Dr. Claire Rollion-Bard, and Prof. Martin Frank, for their time and effort to evaluate my thesis.

I am grateful for all the invaluable advice I got from Dr. Jan Fietzke and Dr. Marcus Gutjahr and the numerous hours they have spent with me to discuss my research. Marcus is especially thanked for teaching me the essential skills for the boron column chemistry and measurement at the Neptune and his detailed feedback during the write-up period of my thesis. I am indebted to Jan for the invaluable insights into statistics, biomineralisation processes and chemical mapping but also on the conversations about philosophy and science in general.

Tyler Goepfert is thanked for always helping with challenges appearing during the Neptune sessions even during weekends and sharing his knowledge on technical details of several instruments.

I would like to thank all my collaborators who have supported me on my way. Prof. Bärbel Hönisch (Lamont Doherty Earth Observatory) and Dr. Jesse Framer (Princeton University) provided the bamboo corals for the project and offered valuable discussion. Dr. Gernot Nehrke from AWI is thanked for offering the opportunity to include confocal Raman spectroscopy into this study.

Mario Thöner greatly advised me with the measurements undertaken at the electron microprobe and Dr. Matthias Frische with help with the laser ablation at the ATTOM.

The time Dr. Phil Alderslade (CSIRO), Dr. Chris Meinen (NOAA) and Rainer Zantopp (GEOMAR) invested in discussions on the growth and the environment of bamboo corals greatly improved my understanding of these topics.

In particular, I would like to mention the support by Prof. Wolf-Christian Dullo who always supported me and made the participation in the R/V Meteor cruise M122 to the cold-water coral seamounts off Angola and Namibia possible.

HOSST is thanked for partially financing my PhD and the opportunity to get to know great people from around the world. The unforgettable summer schools on Cape Verdes and in Halifax widened my horizon in the field of marine science.

Further, I would like to thank Dr. Clara Manno (Britisch Antarctic Survey) for offering the opportunity to participate in the R/V James Clark Ross cruise JR304 off Antarctica.

Finally, I would like to thank my family for always believing in me and their continuous support. Sylvie, I am grateful for all the support, encouragement and patience over the last years. This thesis would not have been possible without you.

1 Introduction

1.1 Objectives and Outline

The ocean as a heat reservoir and CO_2 capacitor has a great impact on Earth's climate system (see e.g. Reid et al., 2009), but is also crucial for the supply of natural resources as for example fish. In a time of rapid anthropogenic climate change, the ability to predict future development is crucial for mediation and adaptation strategies. Biogeochemical and physical processes in the ocean therefore need to be understood to reconstruct past variations and future development. Time series of environmental changes and the analyses of drivers is therefore the key for future predictions. Due to the absence of instrumental time series in vast regions of the ocean, temporal and spatial variations of different parameters have to be reconstructed from natural archives. The tests of foraminifera from sediment cores have been widely used as proxy carriers (Kucera, 2007). Nevertheless their temporal potential to resolve marine processes is limited by sedimentation rate and bioturbation. Long living calcifying organisms are therefore of great advantage. The combination of longevity and in comparison to average sedimentation rates, fast biogenic carbonate growth rates allows a higher temporal resolution compared with sediment cores and reconstruction of processes. Processes such as upwelling events, seasonal current changes or terrestrial erosion peaks can be recorded. For example, corals have been found to represent an archive with continuous sub-annual recording capabilities (Druffel, 1997). However, research has mostly focused on surface dwelling tropical corals for environmental reconstruction. Since the deep ocean contains most of the world's ocean volume and large quantities of dissolved carbon,

deep dwelling cold-water corals are an important archive for palaeoclimatic reconstructions. Several geochemical tools such as the combination of $\delta^{13}C$ and $\delta^{18}O$ values or Mg/Li for temperature studies, or $\delta^{11}B$ values as a pH proxy are promising approaches for environmental reconstruction (Robinson et al., 2014).

This thesis investigates calcitic cold-water corals of the genus Isididae also known as bamboo corals, aiming at a better understanding of their potential to record environmental conditions in their skeleton. Due to their global geographic and depth distribution as well as their longevity, they are promising archives of environmental proxies of growth sites where instrumental records are scarce. In this thesis, high resolution techniques such as laser ablation inductively coupled mass spectrometry, electron microprobe analyses, and confocal Raman spectroscopy has been used to study the intra-skeletal chemical composition. The findings provide new information on the spatial distribution of Ba, Mg, Na, S and $\delta^{11}B$ in bamboo corals on the μm-scale and provide an overview on potential drivers of incorporation and fractionation. Chapter two examines the incorporation of Mg and Ba as proxies of water temperature and $[Ba]_{SW}$ from the Blake Plateau off Florida. The proxy potential of Na and S are assessed in the following chapter on two bamboo coral specimens from the western North Atlantic. Boron isotopes as a potential pH proxy in Isidids in comparison with findings from the other investigated geochemical tools are finally considered in chapter four. Taken together, key findings derived from chapters two to four are brought together in chapter five summarising the findings on the geochemistry and biomineralisation mechanism of bamboo corals.

1.2 Bamboo corals

The corals of the class Anthozoa (phylum Cnidaria) are divided into the subclasses Hexa- and Octocorallia. In the case of octocorals, the number of tentacles of the polyp is fixed to eight, which states the origin of their name. Octocorals are often called soft corals or gorgonians because only some species in this subclass develop a calcareous skeleton. Bamboo corals constitute the family of Isididae which contain the genera of Acanella, Isidella and Keratoisis (Roberts et al., 2009). As common

feature, all these genera have a jointed calcareous skeleton forming from dark proteinaceous nodes that connect high magnesium calcite (HMC) internodes (Noé and Dullo, 2006). These can be branched and form bushes or unbranched whip-like colonies (Bayer and Stefani, 1987). Living tissue covers their skeleton similar to other anthozoans. Most octocorals are colonial, which means that a tissue called coenosarc connects several polyps. The tissue is composed of different layers. The mesoglea separates the outer layer (ectoderm) from the inner layer (endoderm). These layers separate the coelenteron, a space that connects the gastral space of the polyps from seawater. The coelenteron is confined from the skeleton again by an endoderm that is separated by the mesoglea from the calicoblastic layer. The latter tissue layer is involved in the formation of the calcareous coral skeleton. The tissue contains calcitic spicules called sclerites which are an important tool to identify the species (Bayer and Stefani, 1987).

Since gorgonians are suspension feeders, they rely on currents transporting their food to the polyps. The effectivity of capturing food depends on the polyp morphology, food particle size and current velocity as shown on three gorgonian species by Dai and Lin (1993). The pray of polyps that are capable of catching motile food is a mixture of zoo- and phytoplankton as well as particulate organic matter. Further, the proportions of the different food sources are observed to change during the year (e.g. Cocito et al., 2013; Orejas et al., 2003; Picciano and Ferrier-Pages, 2007). Conversely dissolved organic matter does not seem to play an important role for feeding (Coma et al., 1994; Ribes et al., 1999).

Besides currents and food, also the properties of the seafloor are important for settling and growth. Corals in general need hardgrounds to build massive holdfasts to support their skeleton (e.g. Roberts et al., 2009). Nevertheless, some bamboo coral species such as Isidella elongata or Keratoisis sp. can grow on sandy or muddy grounds (e.g. Ingrassia et al., 2019; Mastrototaro et al., 2017; Neves et al., 2014) and are not only endemic to seamounts (Smith et al., 2004). On soft sediments, bamboo corals develop root-like structures to anchor in the ground (Neves et al., 2014).

Bamboo corals are thriving in a wide range of environmental conditions. Thresher

et al. (2016) report bamboo corals to grow in oxygen conditions from 2.1 to 8.0 ml L^{-1} and temperatures from -1.9 to 14.4 °C. Isidids can be found globally from the tropics (e.g. France, 2007) to polar waters (e.g. Thresher et al., 2010) and from surface waters (e.g. Thresher et al., 2016) to about 4000 m depth (e.g. Lapointe and Watling, 2015). Taking into account the high solubility of HMC with a pK^* value of about 5.9 (Woosley et al., 2012) this means that bamboo corals can grow in seawater that is undersaturated relative to HMC.

Another characteristic of Isidids are their slow mean radial growth rates of about 10 to more than 200 µm $year^{-1}$ (e.g. Farmer et al., 2015b; Frenkel et al., 2017; Thresher et al., 2016) and great longevity of over 300 years (Hill et al., 2011.

Bamboo corals are not only of cosmopolitan distribution in the world's ocean, but were also found in various geological periods. The oldest fossil of a bamboo coral was found in deposits from the Late Cretaceous (Helm and Schülke, 2003). Younger fossil specimens from within the Cenozoic era were reported by e.g. Bernecker and Weidlich (2005), Kocurko (1989) or Langer (1989).

1.3 Geochemical tools

1.3.1 Mg/Ca

The Mg/Ca-temperature-proxy is a well investigated and often applied temperature proxy in palaeoceanography (Lea, 2014). It is based on the temperature dependency of the amount of magnesium incorporated into calcite. In inorganic precipitation experiments, temperature shows a large impact on distribution coefficient of Mg in calcite (e.g. Katz, 1973; Mucci, 1987; Oomori et al., 1987). The substitution of Ca with Mg in calcite is an endothermic reaction (Leeuw and Parker, 2000) resulting in a positive Mg/Ca temperature relation, which forms the theoretical basis for the suggested temperature proxy (Rosenthal et al., 1997).

Besides the influence of temperature on the Mg/Ca ratio of calcite non-thermal

influence have been found in abiogenic calcites as well. Several inorganic precipitation experiments have shown that Mg/Ca is invariant over a wide range of precipitation rates (Lopez et al., 2009; Mucci, 1986; Mucci and Morse, 1983). This is in contrast to findings of e.g. Mavromatis et al. (2013) who report an increase of Mg/Ca with precipitation rate and Gabitov et al. (2014a), who observed a decrease.

Experiments by Zhong and Mucci (1989) revealed that rising salinity decreases the incorporation of magnesium into calcite. Also, the absence of sulfate in solution potentially increases the Mg partitioning into calcite (Mucci et al., 1989). Further, dissolved organic matter was found to increase the Mg partitioning coefficient in calcite (Mavromatis et al., 2017; Stephenson et al., 2008). The Mg/Ca ratio of the precipitation solution might raise Mg/Ca calcite with rising Mg/Ca of the solution (e.g. Berner, 1966; Kitano et al., 1979; Mucci and Morse, 1983).

Non-thermal influences of calcites can also change the Mg/Ca ratio in biogenic calcites represented for example by the shell material of foraminifera (e.g. Gray and Evans, 2019). As with other elemental or isotopic proxies, the physiological impact on the Mg partitioning is often summarised by the expression "vital effect" (e.g. Weiner and Dove, 2003) which was coined by Urey et al. (1951). Large species specific and intra shell variabilities were observed for foraminifera (e.g. Branson et al., 2013; Eggins et al., 2003; Kunioka et al., 2006). Reasons for the observed variability can be manifold. These "vital effects" contain for example the precipitation in connection with an organic matrix, the involvement of ACC in calcification and active Mg modulation in the calcifying fluid as reviewed in Bentov and Erez (2006).

In foraminiferal calcite Mg appears like Ca uniformly in octahedral coordination. According to Branson et al. (2013) this shows that Mg is an ideal substitution for Ca in the calcite lattice of foraminifera. Based on the uniform coordination of Mg in the calcite lattice Branson et al. (2013) concluded that Mg in foraminifera is not bound to organic matter.

Besides these vital effects other influences have been found to influence the Mg/Ca ratio of foraminiferal tests. The incorporation of Mg is shown to be higher with increased salinity (e.g. Dissard et al., 2010; Hönisch et al., 2013; Kisakürek et

al., 2008) which is in contrast to inorganic experiments.

Further, ocean carbonate chemistry was found to impact shell Mg/Ca while it decreases with rising pH (e.g. Evans et al., 2016; Lea et al., 1999; Russell et al., 2004). An apparent confirmation was found by high resolution electron microprobe mappings where high Mg/Ca bands in foraminifera were temporarily linked with low external pH (e.g. Fehrenbacher et al., 2017; Sadekov et al., 2005; Spero et al., 2015). Nevertheless, these studies excluded a direct causation but rather suggested a physiological impact like respiration or Mg pumping activity in causing the apparent pH dependency.

Ries (2010) published a review on the influence of secular seawater Mg/Ca variations on the calcification in invertebrates where he reports a decline of skeletal Mg/Ca with reduced seawater Mg/Ca. Seawater Mg/Ca variations can be taken into account by applying a correction term to the temperature reconstruction that links shell Mg/Ca to seawater Mg/Ca with an empirical power function (Evans and Müller, 2012).

Post-depositional dissolution of calcite was found to lower skeletal Mg/Ca in effect lowering reconstructed temperatures (e.g. Brown and Elderfield, 1996; Lohmann, 1995; Regenberg et al., 2014). This can be corrected for by e.g. accounting for core depth, calcite saturation or by applying a species specific size normalised shell weight to the temperature reconstruction (e.g. Dekens et al., 2002; Rosenthal and Lohmann, 2002; Rosenthal et al., 2000).

Numerous studies have successfully calibrated and applied Mg/Ca as a palaeotemperature proxy in several clades of marine calcifiers as for example reviewed by Barker et al. (2005). Mg palaeothermometry was most often applied to planktonic (e.g. Elderfield and Ganssen, 2000; Nürnberg et al., 1996; Rosenthal and Lohmann, 2002) and benthic (e.g. Lear et al., 2000; Roberts et al., 2016a; Rosenthal et al., 1997) foraminifera. Other used species are marine ostracods (e.g. Cronin et al., 2005; De Deckker et al., 1988; Dwyer et al., 1995), bivalves and brachiopods (e.g. Butler et al., 2015; Schöne et al., 2011; Wanamaker Jr et al., 2008). The application of Mg/Ca as a temperature proxy in coccolithophores is challenging due to ineffective removal of

noncarbonate Mg (Stoll et al., 2001). Nevertheless Ra et al. (2010) found a positive correlation with temperature. Coralline algae also have been used to reconstruct water temperature based on the Mg/Ca-temperature proxy (e.g. Halfar et al., 2000; Light et al., 2018; Williams et al., 2018). Calcitic corals have also been studied to reconstruct temperature (e.g. Bond et al., 2005; Mitsuguchi et al., 1996; Thresher et al., 2016).

Temperatures have been reconstructed from Mg/Ca in foraminifera on millennial timescales (e.g. Oppo et al., 2009; Pahnke et al., 2003; Saenger et al., 2011) back to the early Eocene (Lear et al., 2000), during the Palaeocene-Eocene Boundary (Tripati and Elderfield, 2005; Zachos et al., 2003) and even beyond (Bice et al., 2006; Tripati et al., 2003).

The ratio of Mg to Ca in marine biogenic carbonates has been studied extensively to reconstruct water temperature. For palaeoceanographers, Mg/Ca of foraminiferal shells is one of the most useful tools to reconstruct past climate (Lea, 2014). Nevertheless the effect of e.g. salinity, carbonate ion concentration and carbonate dissolution on shell Mg/Ca have to be further investigated to improve the reliability of this proxy.

1.3.2 Ba/Ca

Barium shows a nutrient-like distribution in the water column (e.g. Chan et al., 1977; Jacquet et al., 2004; Monnin et al., 1999) which suggests a relationship to the biological cycle in the ocean (Paytan and Griffith, 2007). Of special importance for this distribution is the formation of barite in close connection with decaying biogenic matter (Bernstein et al., 1998). Fisher et al. (1991) for example reported that Ba is enriched in marine organisms and might represent an important source for abiotic micro-environmental barite precipitation (Paytan and Griffith, 2007). Further Acantharia, a group of radiolaria, contain high concentrations of Ba in their $SrSO_4$ skeletons. After dissolution these can provide Ba and sulfate for barite precipitation in microenvironments (Bernstein and Byrne, 2004). Nevertheless, conservative

mixing of water masses is expected to exert the key control on the dissolved Ba distribution in the ocean (Taylor et al., 2003). Barium concentration in coastal waters is mainly driven by riverine input of suspended material where Ba is adsorbed as surface complexes. During mixing of freshwater with more saline waters, the higher ionic strength of marine water leads to the release of Ba from surface complexes (e.g. Carroll et al., 1993; Hanor and Chan, 1977; Li and Chan, 1979). Further, saltwater intrusion in fresh water aquifers can lead to release of high concentrations of adsorbed Ba and with that contribute to the coastal dissolved Ba (Shaw et al., 1998). Besides this, seasonal runoff changes (Shiller, 1997) and biological activity (Guay and Falkner, 1998; Stecher and Kogut, 1999) might also change the relative importance of Ba sources in coastal environments.

The incorporation of Ba into synthetic and biogenic calcium carbonate has been investigated in several studies. Most inorganic precipitation experiments on calcium carbonate have shown that Ba is depleted in comparison to the solution it precipitated from. This is expressed with the Ba partitioning coefficient D_{Ba} of synthetic aragonite and calcite of < 1. For example, Tesoriero and Pankow (1996) found a D_{Ba} for calcite of 0.012 ± 0.005 and Yoshida et al. (2008) one of 0.016 ± 0.011. Values below unity show that Ba is not readily exchanged with Ca in the carbonate lattice. Possible reasons for this observation are for example the differences in crystal structure, electronegativity, mobility and radius of these two ions (Tesoriero and Pankow, 1996). With 1.43 Å, Ba has for example a greater ionic radius than Ca with 1 Å (Zachara et al., 1991). This led Pingitore (1987) to suggest Ba incorporation by trapping or adsorption. Nevertheless, Lea and Boyle (1989) rejected this proposal and instead suggested lattice incorporation of Ba in foraminiferal calcite. A direct evaluation of the structural state of Ba by X-ray Absorption Near Edge Structure in biogenic aragonite by Finch et al., 2010 was not successful due to the low [Ba].

Numerous studies have applied Ba partitioning in various types of biogenic skeletons to reconstruct environmental conditions. These include e.g. aragonitic (e.g. Anagnostou et al., 2011; Fallon et al., 1999; Quinn and Sampson, 2002) and calcitic corals (e.g. Flöter et al., 2019; LaVigne et al., 2011; Thresher et al., 2016),

planktonic (e.g. Hönisch et al., 2011; Kunioka et al., 2006; Lea and Spero, 1992) and benthic foraminifera (e.g. Hall and Chan, 2004; Lea and Boyle, 1989; Lea, 1993), bivalves (e.g. Gillikin et al., 2006; Schöne et al., 2013; Warter et al., 2018), coralline algae (e.g. Chan et al., 2017; Chan et al., 2011; Hetzinger et al., 2013) or otoliths (e.g. Bath et al., 2000; Dorval et al., 2007; Miller, 2011.

Barium partitioning in synthetic and biogenic calcium carbonate is dependent on various factors resulting in a partitioning range from Ba enrichment to depletion. The D_{Ba} values of synthetic Mg-free calcium carbonate, planktonic foraminiferal carbonates (0.14 – 0.17) (Hönisch et al., 2011; Lea and Spero, 1992) or bivalves (0.07 – 0.1) (Gillikin et al., 2006) are in contrast with that of aragonitic and calcitic coral skeletons. The latter show a D_{Ba} mostly falling between 1 and 2 (e.g. LaVigne et al., 2016; Lea and Boyle, 1989; Spooner et al., 2018) with extremes ranging from 0.5 (Allison et al., 2018) to 3.8 (Pretet et al., 2015). Gabitov et al. (2019) found that the presence of Mg in the carbonate increased the incorporation of Ba into calcite resulting in partitioning coefficients of 0.8 to 1.2. This was explained by the coupled substitution of Ca by the smaller Mg ion together with the larger Ba ion (Mucci and Morse, 1983). Indeed, Dietzel et al. (2004) reported a D_{Ba} value of 1.5 ± 0.1 using Mg containing precipitation solutions. This influence might be an explanation for the difference between synthetic and biogenic partitioning coefficients, where the former are derived from low or Mg-free calcite (Gabitov et al., 2019). Another influence on the Ba partitioning could be the precipitation pathway involving amorphous calcium carbonate (ACC) that would lead to the inclusion of more Ba than classical precipitation pathways (Littlewood et al., 2017). Mavromatis et al. (2018) found a weak positive correlation of D_{Ba} with growth rate for calcite and a stronger one for aragonite. These findings agree with a growth rate dependence of Ba incorporation in calcite as proposed by Tesoriero and Pankow (1996) and Yoshida et al. (2008). Besides growth rate, the influence of organic complex formation on D_{Ba} during precipitation should be considered for the interpretation of skeletal Ba records (Mavromatis et al., 2018).

Barium in biogenic calcium carbonate was used as a proxy for terrigenous sediment flux (e.g. Alibert et al., 2003; McCulloch et al., 2003; Walther et al., 2013), phytoplankton blooms (Stecher et al., 1996), a measure for the Ba concentration of seawater (LaVigne et al., 2016; Lea and Boyle, 1989), spawning patterns and migrations routes of fish (e.g. Bath et al., 2000; Dorval et al., 2007; Thorrold et al., 1997), or upwelling activity (e.g. Lea et al., 1989; Montaggioni et al., 2006; Shen et al., 1992).

Overall barium is a promising and already frequently applied tool to reconstruct environmental conditions. Nevertheless, especially its incorporation mechanism into and host site in calcium carbonate needs more investigation to utilise the full potential of this geochemical tool.

1.3.3 Na/Ca

Besides chloride, sodium is the most abundant dissolved compound in seawater and was suggested for example by Wit et al. (2013) as a palaeosalinity proxy in foraminiferal calcium carbonate. The salinity sensitivity was proposed although Busenberg and Niel Plummer (1985) excluded Na as a salinity proxy based on calcite precipitation experiments and multi species measurements. Due to its long residence time in seawater of about 100 Ma, Hauzer et al. (2018) proposed that Na in biogenic carbonates traced Cenozoic Ca variations in seawater.

Abiotic precipitation experiments found that aragonite accommodates more Na than calcite and that the incorporated Na can reach saturation with [Na] of the precipitation solution approaching the concentration of seawater (Ishikawa and Ichikuni, 1984; Kitano et al., 1975; Okumura and Kitano, 1986). The incorporation of Na into calcium carbonate has been suggested to take place at interstitial sites (Ishikawa and Ichikuni, 1984; Kitano et al., 1975; White, 1977). Incorporation of Na into the calcite lattice by substitution for Ca raises the question of ion charge imbalance. Due to this, studies have for example proposed a compensation by incorporation of trivalent ions with Na (Ragland et al., 1979), replacement of Ca and CO_3^{2-} by monovalent halide anions and Na (Ichikuni, 1979), or lattice defects (White, 1977). Nevertheless, mono- and trivalent ions are not present in sufficient concentrations

in biogenic carbonates to compensate the charge imbalance (e.g. Bastidas and Garcia, 1999; Pingitore Jr et al., 2002). Instead, Yoshimura et al. (2017) and White (1977) suggest an altervalent structural substitution of Ca with two Na by the creation of CO_3^{2-} vacancies for charge compensation. It was proposed that crystal growth rate and Na content are positively correlated (e.g. Busenberg and Niel Plummer, 1985; Evans et al., 2015; Rollion-Bard and Blamart, 2015). This is due to the Na accommodating properties of crystal defects which increase at higher precipitation rates. This was further supported by calcite precipitation experiments with another alkali metal during which Füger et al. (2019) found a positive correlation of Li incorporation with growth rate. These authors also reported an inverse dependence of Li incorporation with pH. A decrease of HCO_3^- with rising pH would lead to a decrease of direct charge compensation of the monovalent Na and therefore reduce incorporation.

Investigations in biogenic calcium carbonates were conducted on foraminifera (e.g. Allen et al., 2016; Delaney et al., 1985; Hauzer et al., 2018), aragonitic corals (e.g.Mitsuguchi et al., 2010; Rollion-Bard and Blamart, 2015; Swart, 1981), otoliths and statoliths (Marohn et al., 2011; Zumholz et al., 2007), echinoderms (Busenberg and Niel Plummer, 1985), barnacles (Gordon et al., 1970), and bivalves (e.g. Ballesta-Artero et al., 2018; Markulin et al., 2019; Zhao et al., 2017). The range of skeletal Na content is between about 103 and 104 ppm as compiled by Yoshimura et al. (2017) and with that lower than its concentration in seawater of about 10'780 ppm at a salinity of 35 (Millero et al., 2008). The partitioning coefficient is therefore often smaller one showing that Na is preferentially excluded from biogenic calcium carbonates.

Studies on Na in downcore records such as by Yoshimura et al. (2017) for foraminifera in a Quaternary record or by Ragland et al. (1979) for molluscs from the late Cretaceous to Holocene have revealed decreasing skeletal [Na] with increasing age. Both studies regard these changes as diagenetic alteration rather than an environmental signal. Further, Rosenthal and Katz (1989) report early diagenetic alteration of skeletal Na in aragonitic freshwater gastropods. Therefore, potential

diagenetic alteration of fossil carbonates taking place even before recrystallisation has to be considered when interpreting downcore records.

1.3.4 S/Ca

The oxyanion sulfate is the most abundant species of sulfur in seawater but the controls over its incorporation to calcite are still rarely investigated. The concentration of sulfate in inorganic calcite was found to be dependent on the sulfur concentration of the precipitation solution (Kitano et al., 1975; Kontrec et al., 2004). Okumura et al., 2018 expanded the range of sulfate concentration in the solution and observed saturation after reaching a sulfate concentration above that in seawater. Busenberg and Niel Plummer (1985) and Wynn et al. (2018) reported that precipitation rate might also be an important driver of sulfate incorporation. Both studies explained their findings with the raising number of crystal defects with rising growth rate. The geochemical parameter S/Ca was recently found to correlate with the carbonate concentration of seawater for foraminifera (Dijk et al., 2017) as suggested by e.g. Yoshimura et al. (2014) or Yoshimura et al. (2013) for bivalves. The correlation might be explained by carbonate substitution in the calcite lattice by sulfate in relation to the carbonate to sulfate ratio in the precipitation solution (Balan et al., 2014). This explanation requires the (apparently valid) assumption that the measured sulfur is solely present as inorganic sulfate. Referring to this suggestion, sulfate in form of carbonate associated sulfate (CAS) was used in several studies to reconstruct the sulfur isotopic composition of seawater (e.g. Burdett et al., 1989; Kampschulte and Strauss, 2004; Strauss, 1999). In contrast, reconstruction of seawater sulfate concentrations by CAS on geological timescales might be complicated due to the changing Ca concentration of seawater (Giri and Swart, 2019). The influence of Ca on the skeletal S composition was observed in culturing experiments with scleractinian corals grown under different Ca concentration scenarios.

The exact incorporation mechanism of sulfate into calcite is not known yet. Staudt et al. (1994) proposed that sulfate might preferentially attach at kink sites of calcite crystals. The incorporation of sulfate is supposed to distort the crystal lattice

of calcite (Kontrec et al., 2004) and is energetically unfavourable (Balan et al., 2014; Fernandez-Diaz et al., 2010). Heberling et al. (2014) calculated that the incorporation of sulfate is highly endothermic and might under standard conditions only be explained by surface entrapment processes. X-ray absorption near edge structure (XANES) studies of hexa- (Farfan et al., 2018; Pingitore et al., 1995) and octocorals (e.g. Nguyen et al., 2014; Perrin et al., 2017; Vielzeuf et al., 2013) state that most sulfur is present as inorganic sulfate while Yoshimura et al. (2013) were not able to distinguish between organic and inorganic sulfate in molluscs. Balan et al. (2017) used the powder infrared spectra of bamboo coral calcite and found that sulfate is dominantly a structural component in the calcite lattice. These authors are emphasising the validity of CAS as a seawater sulfate proxy. For foraminifera Yoshimura et al. (2019) found that sulfate is the dominant sulfur species present in organic and inorganic compounds.

Bound to an organic compound, sulfur can also be incorporated into the skeletons of marine calcifiers as sulfate or in a reduced form. The presence of organic sulfur in calcium carbonate was shown e.g. for corals (e.g. Constantz and Weiner, 1988; Cuif et al., 2003; Nguyen et al., 2014), molluscs (e.g. Dauphin et al., 2003; Fichtner et al., 2018; Yoshimura et al., 2014), brachiopods (Cusack et al., 2008; England et al., 2007), foraminifera (Weiner and Erez, 1984; Yoshimura et al., 2019) and also for synthetic calcite (Chalmin et al., 2013). Therefore, sulfur was suggested as a tracer for organic compounds in biogenic calcium carbonates. Organic matrix molecules were found to influence biomineralisation in a variety of ways. These can result in modification of physical properties, mineral surface stabilisation, formation of microenvironments and mineral nucleation (e.g. Mann, 2001). Of special importance in that context are glycoproteins which are acidic macromolecules covalently linking proteins to polysaccharide side chains. The sidechains often contain sulfate groups like chondroitin sulfate which electrostatically attract Ca and therefore might influence calcification (e.g. Constantz and Weiner, 1988).

Since the exact control mechanism of organic and inorganic sulfur incorporation is not known yet, significant uncertainties in the interpretation of measured sulfur

signals remain. Further, lack of a firm understanding of the sulfur speciation is a major hurdle to better understand the skeletal elemental sulfur signal in connection to environmental parameters.

1.3.5 Boron

Boron is an essential element for terrestrial and marine organisms (e.g. Carrano et al., 2009; Goldbach and Wimmer, 2007; Uluisik et al., 2018). It is transported to the oceans by riverine and groundwater discharge, mud volcanoes and hydrothermal vents, gaseous absorption and aerosol deposition (Park and Schlesinger, 2002). Currently, human activity alters the riverine input drastically. While natural weathering input by rivers is 0.15 Tg B yr^{-1}, the input of B from anthropogenic origin by far exceeds the latter with 0.65 Tg B yr^{-1} (Schlesinger and Vengosh, 2016). Boron is exported from the water column most importantly by sea-salt aerosol emission (1.44 Tg B yr^{-1}) but also by precipitation into calcium carbonate and more importantly by adsorption to terrigenous sediments at a total flux of < 0.3 Tg yr^{-1} (Schlesinger and Vengosh, 2016). The latter process is especially important for the B isotopic composition of seawater. Adsorption on clay (Palmer et al., 1987) and the interaction of B with fresh basalt at ocean ridges (Spivack and Edmond, 1987) were reported as the main drivers of enrichment of heavy B isotopes in seawater. A total amount of 4.3 Tg B is annually cycled in the living biomass of the oceans while $6.2*10^6$ Tg B are dissolved in seawater (Schlesinger and Vengosh, 2016).

The B elemental and its isotopic composition in calcium carbonate have been used as environmental and calcification proxies. The elemental ratio has been shown to record pH in synthetic calcite (He et al., 2013; Sanyal et al., 2000) and in cultured planktonic foraminifera (e.g. Allen and Hönisch, 2012; Henehan et al., 2015; Holland et al., 2017). Nevertheless, Henehan et al. (2015) could not observe a pH dependence of foraminiferal B/Ca in open ocean sediments. Further, this is also in contrast to biogenic aragonite where no pH dependence was found (Allison and Finch, 2010; Sinclair, 2005; Trotter et al., 2011). The B content of calcite was additionally suggested as a carbonate ion proxy (Rae et al., 2011; Yu and Elderfield, 2007; Yu

et al., 2010). Downcore records of foraminiferal B contents were used to study former seawater $[B(OH)_4^-]/[HCO_3^-]$ ratios to reconstruct pCO_2 (e.g. Foster, 2008; Seki et al., 2010; Tripati et al., 2011). Uncertainties arise from secondary factors like seasonal light variability (Babila et al., 2014), growth rate (Quintana Krupinski et al., 2017; Salmon et al., 2016), or seawater phosphate concentrations (Henehan et al., 2015) that may influence the B/Ca proxy.

$$\delta^{11}B = \left(\left(\frac{\left(\frac{^{11}B}{^{10}B}\right)_{sample}}{\left(\frac{^{11}B}{^{10}B}\right)_{NIST951}} \right) - 1 \right) * 1000 \tag{1.1}$$

The B isotopic composition of calcium carbonate is expressed as $\delta^{11}B$. This is the $^{11}B/^{10}B$ ratio in the sample relative to the pure boric acid reference material NIST SRM 951 (Eq. 1.1). $\delta^{11}B$ was shown to record seawater pH as demonstrated by e.g. Hemming and Hanson (1992), Rae et al. (2011) or Vengosh et al. (1991). It was used to reconstruct past seawater pH with planktonic (e.g. Foster, 2008; Palmer et al., 1998; Pearson et al., 2009) and benthic foraminifera (e.g.Hönisch et al., 2008; Raitzsch and Hönisch, 2013; Sanyal et al., 1997) as well as with aragonitic corals (e.g. Douville et al., 2010; Kubota et al., 2014; Pelejero et al., 2005). Seawater pH reconstructions have to take the $\delta^{11}B$ of seawater into account, which is currently 39.61 ‰ (Foster et al., 2010). The $\delta^{11}B$ of seawater changed over geological time scales due to the residence time of B in seawater (14 to 20 Ma) (Lemarchand et al., 2000; Spivack and Edmond, 1987). Reconstructions focusing on the variability with time were conducted by (Greenop et al., 2017; Lemarchand et al., 2002; Raitzsch and Hönisch, 2013) who found an increase of $\delta^{11}B$ values from the early to middle Miocene (about 23 to 15 Ma) of approximately 37.5 ‰ to the recent value. In addition to reconstructions of seawater pH, skeletal $\delta^{11}B$ is used to infer the pH of the calcifying fluid (CF) of corals (e.g. Allison et al., 2014; Krief et al., 2010; McCulloch et al., 2017). This is due to growing evidence that the CF pH might be actively upregulated and does not reflect seawater pH (e.g. Al-Horani et al., 2003; Sevilgen et al., 2019; Venn et al., 2011).

The theoretical base of these applications is rooted in the incorporation of B into

calcium carbonates. Boron exists in seawater in mainly two species: namely boric acid ($B(OH)_3$) and borate ($B(OH)_4^-$). The distribution of the two species is dependent on seawater pH. While at low pH boric acid is the main component, increasing proportions of borate ion are present at elevated pH (Dickson, 1990). In early investigations, borate was found to be the only species incorporated into calcium carbonates (Hemming and Hanson, 1992; Hemming et al., 1995) suggesting an application of B/Ca and $\delta^{11}B$ values as environmental proxies. This initial view on the incorporation mechanism was challenged by more recent investigations. These suggested that B incorporation in calcite might involve not only borate ions and that isotopic fractionation during incorporation takes place (e.g. Holcomb et al., 2016; Mavromatis et al., 2015; Uchikawa et al., 2015).

The equilibrium between two B species of trigonal $B(OH)_3$ and tetragonal $B(OH)_4^-$ is pH dependent with a pK_B of ≈ 8.6 under current surface ocean conditions. The distribution coefficient further depends on the ambient temperature and pressure of the solution (Dickson, 1990; Hain et al., 2015), which becomes important when comparing surface and deep ocean conditions or compositional changes of seawater over geological timescales. Current ocean conditions also imply B concentrations of about 430 μmol kg^{-1} under which other B species such as $B_3O_3(OH)_4^-$ and $B_3O_3(OH)_5^{2-}$ become negligible (Hönisch et al., 2019 and references therein).

Experiments with precipitation of synthetic aragonite and calcite show that B is more easily incorporated into aragonite than into calcite (Hemming et al., 1995; Kitano et al., 1978; Mavromatis et al., 2015). This can be expressed through the partitioning coefficient while multiple definitions complicate the comparability of studies. The various definitions arise from the fact that B does not substitute for the cation Ca, but sits at the anion site in the precipitate. The partitioning coefficient is for example calculated as carbonate [B]/[Ca] in relation to solution $[B(OH)_4^-]/[HCO_3^-]$ (Hemming et al., 1995), [total B]/[DIC] (Uchikawa et al., 2015) or $[B(OH)_4^-]/[CO_3^{2-}]$ (Mavromatis et al., 2015). Through a comparison of different definitions, Uchikawa et al. (2015) found B/Ca systematics in calcite to be best explained in relation with the growth rate and [total B]/[DIC]. Holcomb et al. (2016)

found $[B(OH)_4^-]/[CO_3^{2-}]$ 0.5 to be the best fit for their aragonite precipitation experiments, an expression which Uchikawa et al. (2015) had not considered.

The reason for a preferential incorporation of B into aragonite over calcite is the crystal lattice structure. Hemming and Hanson (1992) proposed that B might be incorporated as HBO_3^{2-} in substitution for CO_3^{2-}. The incorporation of the negatively charged borate ion will preferentially attach to the crystal surface due to an observed positive surface charge as documented for seawater-like conditions by Moulin and Roques (2003) and Wolthers et al. (2008). For aragonite, B is structurally incorporated mainly in tetrahedral coordination (Klochko et al., 2009; Mavromatis et al., 2015; Rollion-Bard et al., 2011). This might be related to the slight asymmetric arrangement of Ca around the anion positions in aragonite. This lattice distortion leads to aragonite showing larger anion sites, which could better fit tetrahedral impurity ions than calcite (Balan et al., 2016). For calcite, several studies have shown that B is hosted in tetrahedral and/or trigonal coordination (e.g. Cusack et al., 2015; Rollion-Bard et al., 2011; Sen et al., 1994). Balan et al. (2016) suggested that tetrahedral B has to be transformed to trigonal B prior to incorporation. Nevertheless the final coordination state provides no information on the incorporation mechanism due to re-coordination during incorporation (Balan et al., 2016; Hemming et al., 1995; Klochko et al., 2009).

The exchange of the two stable isotopes ^{10}B and ^{11}B between $B(OH)_3$ and borate leads to preferential accumulation of ^{11}B in $B(OH)_3$ due to the stronger B-O bond (Hemming and Hanson, 1992). This leads to an equilibrium fractionation between the two boron species of approximately 25 to 27 ‰ in water (Nir et al., 2015) (Fig. 1.1). The most commonly applied value is 27.2 ‰ and was spectrophotometrically determined by Klochko et al. (2006). Other studies determined similar values for example through theoretical calculation (Kakihana, 1977; Rustad et al., 2010; Zeebe, 2005) or experimentally by measuring the isotopic composition of only $B(OH)_3$ gained through reverse osmosis (Nir et al., 2015). Rapid adjustment of the isotope equilibrium, occurring faster than B incorporation during calcification,

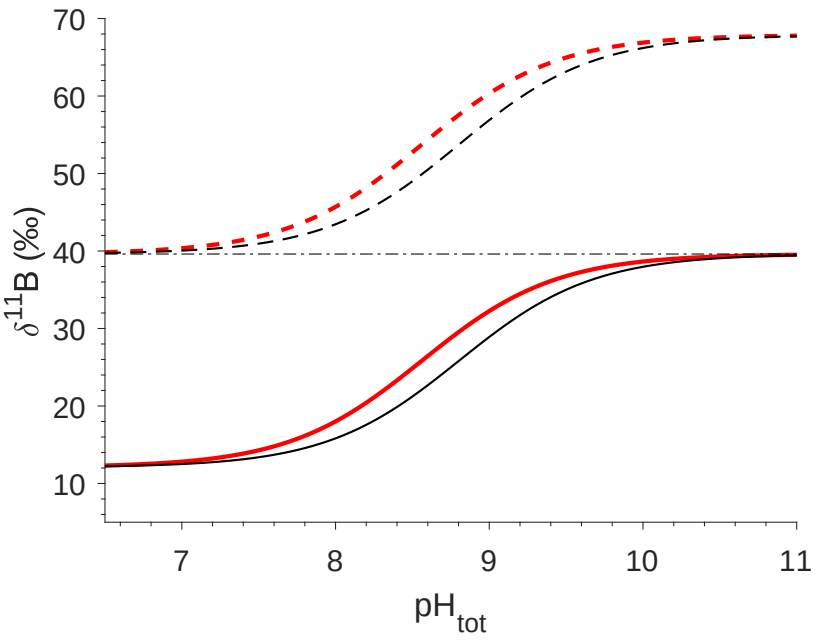

FIGURE 1.1: The isotopic composition of boric acid (dashed) and the borate ion (solid) changes with pH (given here at total scale) and temperatures (red 25°C, black 5 °C) (calculated after Rae (2018)).

should preclude any isotope fractionation (Zeebe and Wolf-Gladrow, 2001). Synthetic aragonite indeed follows this prediction where carbonate δ^{11}B values represent solution δ^{11}B values (Noireaux et al., 2015). Nevertheless, positive offsets from the theoretical borate fractionation curve are observed for example in cultured calcitic foraminifera (e.g. Henehan et al., 2013; Rollion-Bard et al., 2010; Rollion-Bard et al., 2011) but also in synthetic calcite free of potential vital effects (e.g. Farmer et al., 2019; Noireaux et al., 2015; Sanyal et al., 2000). Causes for the deviation from the theoretical borate isotope fractionation curve in synthetic calcite arise from the less favourable incorporation of borate into anion sites in calcite. Consequently the deviations might be explained by incorporation of boric acid (Noireaux et al., 2015; Uchikawa et al., 2015) or isotope fractionation due to kinetic effects during incorporation (e.g. Balan et al., 2018; Pagani et al., 2005; Saldi et al., 2018) but might also come from fluid inclusions or contaminant phases (Branson et al., 2015). In biogenic carbonates, additional physiological processes have to be considered (Hemming and Hanson, 1992; Vengosh et al., 1991). These may include removal of borate

from the CF (Rae et al., 2011) and an increased pH in the diffusive boundary layer of symbiont bearing foraminifera (Rink et al., 1998; Zeebe et al., 1999). Active pH regulation of the CF has to be considered in reconstructions from skeletal δ^{11}B values as already proposed in the pioneering study of Hemming and Hanson (1992). An upregulation of CF pH was observed in aragonitic corals (e.g. Holcomb et al., 2014; McCulloch et al., 2017; Trotter et al., 2011), coccolithophores (Liu et al., 2018), brachiopods (Jurikova et al., 2019), or coralline algae (Cornwall et al., 2017). Farmer et al. (2019) report that the offset from the theoretical borate fractionation curve decreases with pH. This decrease is explained by the latter authors with preferential attachment of isotopically light borate over the heavier boric acid at higher growth rate. The higher growth rate was a result of increased pH during the precipitation experiments. Although open questions on the exact incorporation mechanism of boron into calcium carbonate remain, this will not invalidate the empirical δ^{11}B-pH-proxy.

1.4 Crystal and skeletal growth models

Crystal growth can be divided in classical and non-classical growth as reviewed by De Yoreo et al. (2015). Crystals may form in the classical view after two models. The first model includes nucleation of monomers driven by differences in total Gibbs free energy of the solution to the crystalline phase. Subsequently, monomers or molecules attach according to the terrace ledge kink (TLK) model (Fig. 1.2) which describes preferential attachment at low energy bonding sites of the crystal surface-like kinks and steps (e.g. De Yoreo and Vekilov, 2003). The non-classical growth model describes the formation and the attachment of ACC to the crystal surface. ACC can be formed by aggregation of stable pre-nucleation clusters (Gebauer et al., 2008). At the crystal surface attached ACC can be transformed by dehydration (Ihli et al., 2014) into crystalline calcium carbonate or, in presence of a stabilising additive, kept in a nanogranular structure (Rodriguez-Navarro et al., 2016). An alternative way of crystal growth is oriented attachment of nanocrystals, while the nanocrystals themselves can be formed by classical or non-classical crystal growth

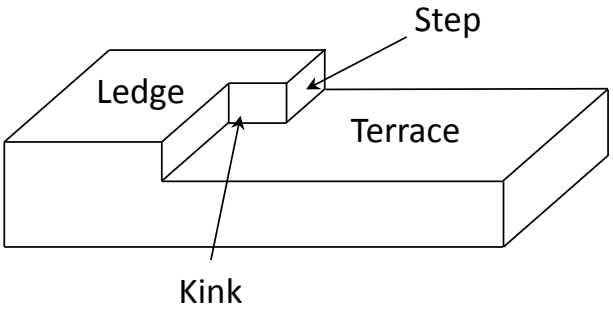

FIGURE 1.2: The TLK growth model describes the growth of crystals by preferential attachment of monomers at low energy kink sites. These sites propagate on the crystal surface with the growth of monomer-thick layers (after Branson (2018)).

(De Yoreo et al., 2015). This growth mechanism is responsible for the formation of mesocrystals which is an abbreviation for "mesoscopically structured crystals" (Song and Colfen, 2010). These mesocrystals might eventually form a single larger crystal by fusion (Rodriguez-Navarro et al., 2016).

Currently, several models exist on skeletal calcium carbonate formation. Lowenstam and Weiner (1989) proposed division into biologically induced and biologically controlled mechanisms. The latter can be subdivided into two groups, namely physico-chemical and organic matrix-controlled models (Cohen and McConnaughey, 2003). While Tambutte et al. (2011) refined it and proposed two physico-chemical and one organic matrix model. The two physico-chemical models are called "bio-inorganic" and "additive mediated" models. The bio-inorganic model describes control mechanisms of the coral to calcify in the CF by changing the saturation state. This can be realised by e.g. removing crystallisation inhibitors, ion pumping, facilitating diffusion or introducing enzymes such as carbonic anhydrase to accelerate chemical reactions (Tambutte et al., 2011). The additive mediated model involves substances interacting directly with the crystal surface and not only a mechanism that varies the saturation state. Those interactions can inhibit growth at certain crystal faces, promote crystal nucleation or generally inhibit calcification (Tambutte et al., 2011). The third model is the organic matrix template model, describing calcification in a three dimensional organic envelope that controls the initiation of crystal growth and morphology (Tambutte et al., 2011).

As shown above, multiple models for skeletal and crystal formation have been proposed. While the non-classical crystal formation mechanisms seems to be the one present under natural conditions, the classical one was found to take place under idealised and simplified laboratory conditions e.g. as reported by Mavromatis et al. (2015) or Uchikawa et al. (2015) (Branson, 2018). Future research needs to identify the ultimate mechanism by which corals form their skeleton whereby idealised and simplified calcification models and experiments might pave the way for a better understanding.

References

Al-Horani, F. A., S. M. Al-Moghrabi, and D. de Beer (2003). "Microsensor study of photosynthesis and calcification in the scleractinian coral, Galaxea fascicularis: active internal carbon cycle". In: *Journal of Experimental Marine Biology and Ecology* 288.1, pp. 1–15.

Alibert, C., L. Kinsley, S. J. Fallon, M. T. McCulloch, R. Berkelmans, and F. McAllister (2003). "Source of trace element variability in Great Barrier Reef corals affected by the Burdekin flood plumes". In: *Geochimica Et Cosmochimica Acta* 67.2, pp. 231–246.

Allen, K. A. and B. Hönisch (2012). "The planktic foraminiferal B/Ca proxy for seawater carbonate chemistry: A critical evaluation". In: *Earth and Planetary Science Letters* 345, pp. 203–211.

Allen, K. A., B. Hönisch, S. M. Eggins, L. L. Haynes, Y. Rosenthal, and J. M. Yu (2016). "Trace element proxies for surface ocean conditions: A synthesis of culture calibrations with planktic foraminifera". In: *Geochimica Et Cosmochimica Acta* 193, pp. 197–221.

Allison, N., I. Cohen, A. A. Finch, J. Erez, A. W. Tudhope, and F. Edinburgh Ion Microprobe (2014). "Corals concentrate dissolved inorganic carbon to facilitate calcification". In: *Nat Commun* 5, p. 5741.

Allison, N., C. Cole, C. Hintz, K. Hintz, and A. A. Finch (2018). "Influences of coral genotype and seawater pCO 2 on skeletal Ba/Ca and Mg/Ca in cultured massive Porites spp. corals". In: *Palaeogeography, Palaeoclimatology, Palaeoecology*.

Allison, N. and A. A. Finch (2010). "δ11B, Sr, Mg and B in a modern Porites coral: the relationship between calcification site pH and skeletal chemistry". In: *Geochimica et Cosmochimica Acta* 74.6, pp. 1790–1800.

Anagnostou, E., R. M. Sherrell, A. Gagnon, M. LaVigne, M. P. Field, and W. F. McDonough (2011). "Seawater nutrient and carbonate ion concentrations recorded as P/Ca, Ba/Ca, and U/Ca in the deep-sea coral Desmophyllum dianthus". In: *Geochimica Et Cosmochimica Acta* 75.9, pp. 2529–2543.

Babila, T. L., Y. Rosenthal, and M. H. Conte (2014). "Evaluation of the biogeochemical controls on B/Ca of Globigerinoides ruber white from the Oceanic Flux Program, Bermuda". In: *Earth and Planetary Science Letters* 404, pp. 67–76.

Balan, E., F. Pietrucci, C. Gervais, M. Blanchard, J. Schott, and J. Gaillardet (2016). "First-principles study of boron speciation in calcite and aragonite". In: *Geochimica et Cosmochimica Acta* 193, pp. 119–131.

Balan, E., J. Aufort, S. Pouillé, M. Dabos, M. Blanchard, M. Lazzeri, C. Rollion-Bard, and D. Blamart (2017). "Infrared spectroscopic study of sulfate-bearing calcite from deep-sea bamboo coral". In: *European Journal of Mineralogy* 29.3, pp. 397–408.

Balan, E., J. Noireaux, V. Mavromatis, G. D. Saldi, V. Montouillout, M. Blanchard, F. Pietrucci, C. Gervais, J. R. Rustad, J. Schott, and J. Gaillardet (2018). "Theoretical isotopic fractionation between structural boron in carbonates and aqueous boric acid and borate ion". In: *Geochimica Et Cosmochimica Acta* 222, pp. 117–129.

Balan, E., M. Blanchard, C. Pinilla, and M. Lazzeri (2014). "First-principles modeling of sulfate incorporation and 34S/32S isotopic fractionation in different calcium carbonates". In: *Chemical Geology* 374-375, pp. 84–91.

Ballesta-Artero, I., L. Zhao, S. Milano, R. Mertz-Kraus, B. R. Schone, J. van der Meer, and R. Witbaard (2018). "Environmental and biological factors influencing trace elemental and microstructural properties of Arctica islandica shells". In: *Sci Total Environ* 645, pp. 913–923.

Barker, S., I. Cacho, H. Benway, and K. Tachikawa (2005). "Planktonic foraminiferal Mg/Ca as a proxy for past oceanic temperatures: a methodological overview and data compilation for the Last Glacial Maximum". In: *Quaternary Science Reviews* 24.7-9, pp. 821–834.

Bastidas, C. and E. Garcia (1999). "Metal content on the reef coral Porites astreoides: an evaluation of river influence and 35 years of chronology". In: *Marine Pollution Bulletin* 38.10, pp. 899–907.

Bath, G. E., S. R. Thorrold, C. M. Jones, S. E. Campana, J. W. McLaren, and J. W. H. Lam (2000). "Strontium and barium uptake in aragonitic otoliths of marine fish". In: *Geochimica Et Cosmochimica Acta* 64.10, pp. 1705–1714.

Bayer, F. M. and J. Stefani (1987). "New and Previously Known Taxa of Isidid Octocorals (Coelenterata, Gorgonacea), Partly from Antarctic Waters". In: *Proceedings of the Biological Society of Washington* 100.4, pp. 937–991.

Bentov, S. and J. Erez (2006). "Impact of biomineralization processes on the Mg content of foraminiferal shells: A biological perspective". In: *Geochemistry Geophysics Geosystems* 7.1.

Bernecker, M. and O. Weidlich (2005). "Azooxanthellate corals in the Late Maastrichtian - Early Paleocene of the Danish basin: bryozoan and coral mounds in a boreal shelf setting". In: *Cold-Water Corals and Ecosystems*. Ed. by A. Freiwald and J. M. Roberts. Erlangen Earth Conference Series. Berlin, Heidelberg: Springer Berlin Heidelberg. Chap. Chapter 1, pp. 3–25.

Berner, R. A. (1966). "Diagenesis of carbonate sediments: interaction of magnesium in sea water with mineral grains". In: *Science* 153.3732, pp. 188–91.

Bernstein, R. E. and R. H. Byrne (2004). "Acantharians and marine barite". In: *Marine Chemistry* 86.1-2, pp. 45–50.

Bernstein, R. E., R. H. Byrne, and J. Schijf (1998). "Acantharians: a missing link in the oceanic biogeochemistry of barium". In: *Deep-Sea Research Part I-Oceanographic Research Papers* 45.2-3, pp. 491–505.

Bice, K. L., D. Birgel, P. A. Meyers, K. A. Dahl, K. U. Hinrichs, and R. D. Norris (2006). "A multiple proxy and model study of Cretaceous upper ocean temperatures and atmospheric CO2 concentrations". In: *Paleoceanography* 21.2.

Bond, Z. A., A. L. Cohen, S. R. Smith, and W. J. Jenkins (2005). "Growth and composition of high-Mg calcite in the skeleton of a Bermudian gorgonian (Plexaurella dichotoma): Potential for paleothermometry". In: *Geochemistry Geophysics Geosystems* 6.8.

Branson, O. (2018). "Boron Incorporation into Marine CaCO3". In: *Boron Isotopes*. Ed. by H. Marschall and G. Foster. Advances in Isotope Geochemistry. Cham: Springer International Publishing. Chap. Chapter 4, pp. 71–105.

Branson, O., S. A. T. Redfern, T. Tyliszczak, A. Sadekov, G. Langer, K. Kimoto, and H. Elderfield (2013). "The coordination of Mg in foraminiferal calcite". In: *Earth and Planetary Science Letters* 383, pp. 134–141.

Branson, O., K. Kaczmarek, S. A. T. Redfern, S. Misra, G. Langer, T. Tyliszczak, J. Bijma, and H. Elderfield (2015). "The coordination and distribution of B in foraminiferal calcite". In: *Earth and Planetary Science Letters* 416, pp. 67–72.

Brown, S. J. and H. Elderfield (1996). "Variations in Mg/Ca and Sr/Ca ratios of planktonic foraminifera caused by postdepositional dissolution: Evidence of shallow Mg-dependent dissolution". In: *Paleoceanography* 11.5, pp. 543–551.

Burdett, J. W., M. A. Arthur, and M. J. Richardson (1989). "A Neogene seawater sulfur isotope age curve from calcareous pelagic microfossils". In: *Earth and Planetary Science Letters* 94.3, pp. 189–198.

Busenberg, E. and L. Niel Plummer (1985). "Kinetic and thermodynamic factors controlling the distribution of SO32- and Na+ in calcites and selected aragonites". In: *Geochimica et Cosmochimica Acta* 49.3, pp. 713–725.

Butler, S., T. R. Bailey, C. H. Lear, G. B. Curry, L. Cherns, and I. McDonald (2015). "The Mg/Ca-temperature relationship in brachiopod shells: Calibrating a potential palaeoseasonality proxy". In: *Chemical Geology* 397, pp. 106–117.

Carrano, C. J., S. Schellenberg, S. A. Amin, D. H. Green, and F. C. Küpper (2009). "Boron and marine life: A new look at an enigmatic bioelement". In: *Marine Biotechnology* 11.4, pp. 431–440.

Carroll, J., k. K. Falkner, E. T. Brown, and W. S. Moore (1993). "The role of the Ganges-Brahmaputra mixing zone in supplying barium and226Ra to the Bay of Bengal". In: *Geochimica et Cosmochimica Acta* 57.13, pp. 2981–2990.

Chalmin, E., Y. Perrette, B. Fanget, and J. Susini (2013). "Investigation of organic matter entrapped in synthetic carbonates–a multimethod approach". In: *Microsc Microanal* 19.1, pp. 132–44.

Chan, L. H., D. Drummond, J. M. Edmond, and B. Grant (1977). "On the barium data from the Atlantic GEOSECS expedition". In: *Deep Sea Research* 24.7, pp. 613–649.

Chan, P., J. Halfar, B. Williams, S. Hetzinger, R. Steneck, T. Zack, and D. E. Jacob (2011). "Freshening of the Alaska Coastal Current recorded by coralline algal Ba/Ca ratios". In: *Journal of Geophysical Research-Biogeosciences* 116.G1, pp. 1–8.

Chan, P., J. Halfar, W. Adey, S. Hetzinger, T. Zack, G. W. K. Moore, U. G. Wortmann, B. Williams, and A. Hou (2017). "Multicentennial record of Labrador Sea primary productivity and sea-ice variability archived in coralline algal barium". In: *Nat Commun* 8, p. 15543.

Cocito, S., C. Ferrier-Pages, R. Cupido, C. Rottier, W. Meier-Augenstein, H. Kemp, S. Reynaud, and A. Peirano (2013). "Nutrient acquisition in four Mediterranean gorgonian species". In: *Marine Ecology Progress Series* 473, pp. 179–188.

Cohen, A. L. and T. A. McConnaughey (2003). "Geochemical perspectives on coral mineralization". In: *Biomineralization* 54.1, pp. 151–187.

Coma, R., J. M. Gili, M. Zabala, and T. Riera (1994). "Feeding and Prey Capture Cycles in the Aposymbiontic Gorgonian Paramuricea-Clavata". In: *Marine Ecology Progress Series* 115.3, pp. 257–270.

Constantz, B. and S. Weiner (1988). "Acidic macromolecules associated with the mineral phase of scleractinian coral skeletons". In: *Journal of Experimental Zoology* 248.3, pp. 253–258.

Cornwall, C. E., S. Comeau, and M. T. McCulloch (2017). "Coralline algae elevate pH at the site of calcification under ocean acidification". In: *Glob Chang Biol* 23.10, pp. 4245–4256.

Cronin, T. M., H. J. Dowsett, G. S. Dwyer, P. A. Baker, and M. A. Chandler (2005). "Mid-pliocene deep-sea bottom-water temperatures based on ostracode Mg/Ca ratios". In: *Marine Micropaleontology* 54.3-4, pp. 249–261.

Cuif, J. P., Y. Dauphin, J. Doucet, M. Salome, and J. Susini (2003). "XANES mapping of organic sulfate in three scleractinian coral skeletons". In: *Geochimica Et Cosmochimica Acta* 67.1, pp. 75–83.

Cusack, M., Y. Dauphin, J. P. Cuif, M. Salome, A. Freer, and H. Yin (2008). "Micro-XANES mapping of sulphur and its association with magnesium and phosphorus in the shell of the brachiopod, Terebratulina retusa". In: *Chemical Geology* 253.3-4, pp. 172–179.

Cusack, M., N. A. Kamenos, C. Rollion-Bard, and G. Tricot (2015). "Red coralline algae assessed as marine pH proxies using 11B MAS NMR". In: *Sci Rep* 5, p. 8175.

Dai, C. and M. Lin (1993). "The effects of flow on feeding of three gorgonians from southern Taiwan". In: *Journal of Experimental Marine Biology and Ecology* 173.1, pp. 57–69.

Dauphin, Y., J. P. Cuif, J. Doucet, M. Salome, J. Susini, and C. T. Willams (2003). "In situ chemical speciation of sulfur in calcitic biominerals and the simple prism concept". In: *J Struct Biol* 142.2, pp. 272–80.

De Deckker, P., A. R. Chivas, J. M. G. Shelley, and T. Torgersen (1988). "Ostracod shell chemistry: A new palaeoenvironmental indicator applied to a regressive/transgressive record from the gulf of Carpentaria, Australia". In: *Palaeogeography, Palaeoclimatology, Palaeoecology* 66.3–4, pp. 231–241.

De Yoreo, J. J. and P. G. Vekilov (2003). "Principles of crystal nucleation and growth". In: *Biomineralization* 54.1, pp. 57–93.

De Yoreo, J. J., P. U. Gilbert, N. A. Sommerdijk, R. L. Penn, S. Whitelam, D. Joester, H. Zhang, J. D. Rimer, A. Navrotsky, J. F. Banfield, A. F. Wallace, F. M. Michel, F. C. Meldrum, H. Colfen, and P. M. Dove (2015). "Crystallization by particle attachment in synthetic, biogenic, and geologic environments". In: *Science* 349.6247, aaa6760.

Dekens, P. S., D. W. Lea, D. K. Pak, and H. J. Spero (2002). "Core top calibration of Mg/Ca in tropical foraminifera: Refining paleotemperature estimation". In: *Geochemistry Geophysics Geosystems* 3.4, pp. 1–29.

Delaney, M. L., A. W. H. Be, and E. A. Boyle (1985). "Li, Sr, Mg, and Na in Foraminiferal Calcite Shells from Laboratory Culture, Sediment Traps, and Sediment Cores". In: *Geochimica Et Cosmochimica Acta* 49.6, pp. 1327–1341.

Dickson, A. G. (1990). "Thermodynamics of the Dissociation of Boric-Acid in Synthetic Seawater from 273.15-K to 318.15-K". In: *Deep-Sea Research Part a-Oceanographic Research Papers* 37.5, pp. 755–766.

Dietzel, M., N. Gussone, and A. Eisenhauer (2004). "Co-precipitation of Sr2+ and Ba2+ with aragonite by membrane diffusion of CO2 between 10 and 50 °C". In: *Chemical Geology* 203.1-2, pp. 139–151.

Dijk, I. van, L. J. de Nooijer, W. Boer, and G. J. Reichart (2017). "Sulfur in foraminiferal calcite as a potential proxy for seawater carbonate ion concentration". In: *Earth and Planetary Science Letters* 470, pp. 64–72.

Dissard, D., G. Nehrke, G. J. Reichart, and J. Bijma (2010). "The impact of salinity on the Mg/Ca and Sr/Ca ratio in the benthic foraminifera Ammonia tepida: Results from culture experiments". In: *Geochimica Et Cosmochimica Acta* 74.3, pp. 928–940.

Dorval, E., C. M. Jones, R. Hannigan, and J. van Montfrans (2007). "Relating otolith chemistry to surface water chemistry in a coastal plain estuary". In: *Canadian Journal of Fisheries and Aquatic Sciences* 64.3, pp. 411–424.

Douville, E., M. Paterne, G. Cabioch, P. Louvat, J. Gaillardet, A. Juillet-Leclerc, and L. Ayliffe (2010). "Abrupt sea surface pH change at the end of the Younger Dryas in the central sub-equatorial Pacific inferred from boron isotope abundance in corals (Porites)". In: *Biogeosciences* 7.8, pp. 2445–2459.

Druffel, E. R. (1997). "Geochemistry of corals: proxies of past ocean chemistry, ocean circulation, and climate". In: *Proc Natl Acad Sci U S A* 94.16, pp. 8354–61.

Dwyer, G. S., T. M. Cronin, P. A. Baker, M. E. Raymo, J. S. Buzas, and T. Corr ge (1995). "North Atlantic Deepwater Temperature Change During Late Pliocene and Late Quaternary Climatic Cycles". In: *Science* 270.5240, pp. 1347–1351.

Eggins, S., P. De Deckker, and J. Marshall (2003). "Mg/Ca variation in planktonic foraminifera tests: implications for reconstructing palaeo-seawater temperature and habitat migration". In: *Earth and Planetary Science Letters* 212.3, pp. 291–306.

Elderfield, H. and G. Ganssen (2000). "Past temperature and [delta]18O of surface ocean waters inferred from foraminiferal Mg/Ca ratios". In: *Nature* 405.6785, pp. 442–445.

England, J., M. Cusack, and M. R. Lee (2007). "Magnesium and sulphur in the calcite shells of two brachiopods, Terebratulina retusa and Novocrania anomala". In: *Lethaia* 40.1, pp. 2–10.

Evans, D. and W. Müller (2012). "Deep time foraminifera Mg/Ca paleothermometry: Nonlinear correction for secular change in seawater Mg/Ca". In: *Paleoceanography* 27.4, n/a–n/a.

Evans, D., J. Erez, S. Oron, and W. Muller (2015). "Mg/Ca-temperature and seawater-test chemistry relationships in the shallow-dwelling large benthic foraminifera Operculina ammonoides". In: *Geochimica Et Cosmochimica Acta* 148, pp. 325–342.

Evans, D., B. S. Wade, M. Henehan, J. Erez, and W. Müller (2016). "Revisiting carbonate chemistry controls on planktic foraminifera Mg / Ca: Implications for sea surface temperature and hydrology shifts over the Paleocene-Eocene Thermal Maximum and Eocene-Oligocene transition". In: *Climate of the Past* 12.4, pp. 819–835.

Fallon, S. J., M. T. McCulloch, R. Van Woesik, and D. J. Sinclair (1999). "Corals at their latitudinal limits: Laser ablation trace element systematics in Porites from Shirigai Bay, Japan". In: *Earth and Planetary Science Letters* 172.3-4, pp. 221–238.

Farfan, G. A., A. Apprill, S. M. Webb, and C. M. Hansel (2018). "Coupled X-ray Fluorescence and X-ray Absorption Spectroscopy for Microscale Imaging and Identification of Sulfur Species within Tissues and Skeletons of Scleractinian Corals". In: *Anal Chem* 90.21, pp. 12559–12566.

Farmer, J. R., L. F. Robinson, and B. Hönisch (2015b). "Growth rate determinations from radiocarbon in bamboo corals (genus Keratoisis)". In: *Deep-Sea Research Part I-Oceanographic Research Papers* 105, pp. 26–40.

Farmer, J. R., O. Branson, J. Uchikawa, D. E. Penman, B. Honisch, and R. E. Zeebe (2019). "Boric acid and borate incorporation in inorganic calcite inferred from B/Ca, boron isotopes and surface kinetic modeling". In: *Geochimica Et Cosmochimica Acta* 244, pp. 229–247.

Fehrenbacher, J. S., A. D. Russell, C. V. Davis, A. C. Gagnon, H. J. Spero, J. B. Cliff, Z. Zhu, and P. Martin (2017). "Link between light-triggered Mg-banding and chamber formation in the planktic foraminifera Neogloboquadrina dutertrei". In: *Nat Commun* 8, p. 15441.

Fernandez-Diaz, L., A. Fernandez-Gonzalez, and M. Prieto (2010). "The role of sulfate groups in controlling CaCO3 polymorphism". In: *Geochimica Et Cosmochimica Acta* 74.21, pp. 6064–6076.

Füger, A., F. Konrad, A. Leis, M. Dietzel, and V. Mavromatis (2019). "Effect of growth rate and pH on lithium incorporation in calcite". In: *Geochimica Et Cosmochimica Acta* 248, pp. 14–24.

Fichtner, V., H. Strauss, V. Mavromatis, M. Dietzel, T. Huthwelker, C. N. Borca, P. Guagliardo, M. R. Kilburn, J. Gottlicher, C. L. Pederson, E. Griesshaber, W. W. Schmahl, and A. Immenhauser (2018). "Incorporation and subsequent diagenetic alteration of sulfur in Arctica islandica". In: *Chemical Geology* 482, pp. 72–90.

Finch, A. A., N. Allison, H. Steaggles, C. V. Wood, and J. F. W. Mosselmans (2010). "Ba XAFS in Ba-rich standard minerals and the potential for determining Ba structural state in calcium carbonate". In: *Chemical Geology* 270.1-4, pp. 179–185.

Fisher, N. S., R. R. L. Guillard, and D. C. Bankston (1991). "The Accumulation of Barium by Marine-Phytoplankton Grown in Culture". In: *Journal of Marine Research* 49.2, pp. 339–354.

Flöter, S., J. Fietzke, M. Gutjahr, J. Farmer, B. Hönisch, G. Nehrke, and A. Eisenhauer (2019). "The influence of skeletal micro-structures on potential proxy records in a bamboo coral". In: *Geochimica Et Cosmochimica Acta* 248, pp. 43–60.

Foster, G. L. (2008). "Seawater pH, pCO_2 and [CO_3^{2-}] variations in the Caribbean Sea over the last 130 kyr: A boron isotope and B/Ca study of planktic forminifera". In: *Earth and Planetary Science Letters* 271.1-4, pp. 254–266.

Foster, G. L., P. A. E. Pogge von Strandmann, and J. W. B. Rae (2010). "Boron and magnesium isotopic composition of seawater". In: *Geochemistry Geophysics Geosystems* 11.

France, S. C. (2007). "Genetic analysis of bamboo corals (Cnidaria: Octocorallia: Isididae): Does lack of colony branching distinguish Lepidisis from Keratoisis?" In: *Bulletin of Marine Science* 81.3, pp. 323–333.

Frenkel, M. M., M. LaVigne, H. R. Miller, T. M. Hill, A. McNichol, and M. L. Gaylord (2017). "Quantifying bamboo coral growth rate nonlinearity with the radiocarbon bomb spike: A new model for paleoceanographic chronology development". In: *Deep-Sea Research Part I-Oceanographic Research Papers* 125, pp. 26–39.

Gabitov, R. I., A. Sadekov, and A. Leinweber (2014a). "Crystal growth rate effect on Mg/Ca and Sr/Ca partitioning between calcite and fluid: An in situ approach". In: *Chemical Geology* 367, pp. 70–82.

Gabitov, R., A. Sadekov, V. Yapaskurt, C. Borrelli, A. Bychkov, K. Sabourin, and A. Perez-Huerta (2019). "Elemental Uptake by Calcite Slowly Grown From Seawater Solution: An in-situ Study via Depth Profiling". In: *Frontiers in Earth Science* 7.51.

Gebauer, D., A. Volkel, and H. Colfen (2008). "Stable prenucleation calcium carbonate clusters". In: *Science* 322.5909, pp. 1819–22.

Gillikin, D. P., F. Dehairs, A. Lorrain, D. Steenmans, W. Baeyens, and L. André (2006). "Barium uptake into the shells of the common mussel (Mytilus edulis) and the potential for estuarine paleo-chemistry reconstruction". In: *Geochimica et Cosmochimica Acta* 70.2, pp. 395–407.

Giri, S. J. and P. K. Swart (2019). "The influence of seawater chemistry on carbonate-associated sulfate derived from coral skeletons". In: *Palaeogeography Palaeoclimatology Palaeoecology* 521, pp. 72–81.

Goldbach, H. E. and M. A. Wimmer (2007). "Boron in plants and animals: Is there a role beyond cell-wall structure?" In: *Journal of Plant Nutrition and Soil Science* 170.1, pp. 39–48.

Gordon, C. M., R. A. Carr, and R. E. Larson (1970). "The Influence of Environmental Factors on the Sodium and Manganese Content of Barnacle Shells". In: *Limnology and Oceanography* 15.3, pp. 461–466.

Gray, W. R. and D. Evans (2019). "Nonthermal Influences on Mg/Ca in Planktonic Foraminifera: A Review of Culture Studies and Application to the Last Glacial Maximum". In: *Paleoceanography and Paleoclimatology* 34.3, pp. 306–315.

Greenop, R., M. P. Hain, S. M. Sosdian, K. I. C. Oliver, P. Goodwin, T. B. Chalk, C. H. Lear, P. A. Wilson, and G. L. Foster (2017). "A record of Neogene seawater δ11B reconstructed from paired δ11B analyses on benthic and planktic foraminifera". In: *Climate of the Past* 13.2, pp. 149–170.

Guay, C. K. and K. K. Falkner (1998). "A survey of dissolved barium in the estuaries of major Arctic rivers and adjacent seas". In: *Continental Shelf Research* 18.8, pp. 859–882.

Hain, M. P., D. M. Sigman, J. A. Higgins, and G. H. Haug (2015). "The effects of secular calcium and magnesium concentration changes on the thermodynamics of seawater acid/base chemistry: Implications for Eocene and Cretaceous ocean carbon chemistry and buffering". In: *Global Biogeochemical Cycles* 29.5, pp. 517–533.

Halfar, J., T. Zack, A. Kronz, and J. C. Zachos (2000). "Growth and high-resolution paleoenvironmental signals of rhodoliths (coralline red algae): A new biogenic archive". In: *Journal of Geophysical Research-Oceans* 105.C9, pp. 22107–22116.

Hall, J. M. and L. H. Chan (2004). "Ba/Ca in benthic foraminifera: Thermocline and middepth circulation in the North Atlantic during the last glaciation". In: *Paleoceanography* 19.4, pp. 1–13.

Hanor, J. S. and L. H. Chan (1977). "Non-Conservative Behavior of Barium during Mixing of Mississippi River and Gulf of Mexico Waters". In: *Earth and Planetary Science Letters* 37.2, pp. 242–250.

Hauzer, H., D. Evans, W. Muller, Y. Rosenthal, and J. Erez (2018). "Calibration of Na partitioning in the calcitic foraminifer Operculina ammonoides under variable Ca concentration: Toward reconstructing past seawater composition". In: *Earth and Planetary Science Letters* 497, pp. 80–91.

He, M. Y., Y. K. Xiao, Z. D. Jin, W. G. Liu, Y. Q. Ma, Y. L. Zhang, and C. G. Luo (2013). "Quantification of boron incorporation into synthetic calcite under controlled

pH and temperature conditions using a differential solubility technique". In: *Chemical Geology* 337, pp. 67–74.

Heberling, F., D. Bosbach, J.-D. Eckhardt, U. Fischer, J. Glowacky, M. Haist, U. Kramar, S. Loos, H. S. Müller, T. Neumann, C. Pust, T. Schäfer, J. Stelling, M. Ukrainczyk, V. Vinograd, M. Vučak, and B. Winkler (2014). "Reactivity of the calcite–water-interface, from molecular scale processes to geochemical engineering". In: *Applied Geochemistry* 45, pp. 158–190.

Helm, C. and I. Schülke (2003). "An almost complete specimen of the Late Cretaceous (Campanian) octocoral 'Isis' ramosa Voigt (Gorgonacea) from the Lower Saxony Basin, northwest Germany". In: *Cretaceous Research* 24.1, pp. 35–40.

Hemming, N. G. and G. N. Hanson (1992). "Boron Isotopic Composition and Concentration in Modern Marine Carbonates". In: *Geochimica Et Cosmochimica Acta* 56.1, pp. 537–543.

Hemming, N. G., R. J. Reeder, and G. N. Hanson (1995). "Mineral-fluid partitioning and isotopic fractionation of boron in synthetic calcium carbonate". In: *Geochimica et Cosmochimica Acta* 59.2, pp. 371–379.

Henehan, M. J., J. W. B. Rae, G. L. Foster, J. Erez, K. C. Prentice, M. Kucera, H. C. Bostock, M. A. Martinez-Boti, J. A. Milton, P. A. Wilson, B. J. Marshall, and T. Elliott (2013). "Calibration of the boron isotope proxy in the planktonic foraminifera Globigerinoides ruber for use in palaeo-CO2 reconstruction". In: *Earth and Planetary Science Letters* 364, pp. 111–122.

Henehan, M. J., G. L. Foster, J. W. B. Rae, K. C. Prentice, J. Erez, H. C. Bostock, B. J. Marshall, and P. A. Wilson (2015). "Evaluating the utility of B/Ca ratios in planktic foraminifera as a proxy for the carbonate system: A case study ofGlobigerinoides ruber". In: *Geochemistry, Geophysics, Geosystems* 16.4, pp. 1052–1069.

Hetzinger, S., J. Halfar, T. Zack, J. V. Mecking, B. E. Kunz, D. E. Jacob, and W. H. Adey (2013). "Coralline algal Barium as indicator for 20th century northwestern North Atlantic surface ocean freshwater variability". In: *Scientific Reports* 3, p. 1761.

Hill, T. M., H. J. Spero, T. Guilderson, M. LaVigne, D. Clague, S. Macalello, and N. Jang (2011). "Temperature and vital effect controls on bamboo coral (Isididae) isotope geochemistry: A test of the "lines method"". In: *Geochemistry Geophysics Geosystems* 12.4.

Hönisch, B., T. Bickert, and N. G. Hemming (2008). "Modern and Pleistocene boron isotope composition of the benthic foraminifer Cibicidoides wuellerstorfi". In: *Earth and Planetary Science Letters* 272.1-2, pp. 309–318.

Hönisch, B., K. A. Allen, A. D. Russell, S. M. Eggins, J. Bijma, H. J. Spero, D. W. Lea, and J. M. Yu (2011). "Planktic foraminifers as recorders of seawater Ba/Ca". In: *Marine Micropaleontology* 79.1-2, pp. 52–57.

Hönisch, B., K. A. Allen, D. W. Lea, H. J. Spero, S. M. Eggins, J. Arbuszewski, P. deMenocal, Y. Rosenthal, A. D. Russell, and H. Elderfield (2013). "The influence of salinity on Mg/Ca in planktic foraminifers – Evidence from cultures, core-top sediments and complementary δ18O". In: *Geochimica et Cosmochimica Acta* 121, pp. 196–213.

Hönisch, B., S. M. Eggins, L. L. Haynes, K. A. Allen, K. D. Holland, and K. Lorbacher (2019). *Boron Proxies in Paleoceanography and Paleoclimatology*.

Holcomb, M., A. A. Venn, E. Tambutte, S. Tambutte, D. Allemand, J. Trotter, and M. McCulloch (2014). "Coral calcifying fluid pH dictates response to ocean acidification". In: *Sci Rep* 4, p. 5207.

Holcomb, M., T. M. DeCarlo, G. A. Gaetani, and M. McCulloch (2016). "Factors affecting B/Ca ratios in synthetic aragonite". In: *Chemical Geology* 437, pp. 67–76.

Holland, K., S. M. Eggins, B. Honisch, L. L. Haynes, and O. Branson (2017). "Calcification rate and shell chemistry response of the planktic foraminifer Orbulina universa to changes in microenvironment seawater carbonate chemistry". In: *Earth and Planetary Science Letters* 464, pp. 124–134.

Ichikuni, M. (1979). "Uptake of Fluoride by Aragonite". In: *Chemical Geology* 27.3, pp. 207–214.

Ihli, J., W. C. Wong, E. H. Noel, Y. Y. Kim, A. N. Kulak, H. K. Christenson, M. J. Duer, and F. C. Meldrum (2014). "Dehydration and crystallization of amorphous calcium carbonate in solution and in air". In: *Nat Commun* 5, p. 3169.

Ingrassia, M., E. Martorelli, A. Bosman, and F. L. Chiocci (2019). "Isidella elongata (Cnidaria: Alcyonacea): First report in the Ventotene Basin (Pontine Islands, western Mediterranean Sea)". In: *Regional Studies in Marine Science* 25.

Ishikawa, M. and M. Ichikuni (1984). "Uptake of Sodium and Potassium by Calcite". In: *Chemical Geology* 42.1-4, pp. 137–146.

Jacquet, S. H. M., F. Dehairs, and S. Rintoul (2004). "A high resolution transect of dissolved barium in the Southern Ocean". In: *Geophysical Research Letters* 31.14.

Jurikova, H., V. Liebetrau, M. Gutjahr, C. Rollion-Bard, M. Y. Hu, S. Krause, D. Henkel, C. Hiebenthal, M. Schmidt, J. Laudien, and A. Eisenhauer (2019). "Boron isotope systematics of cultured brachiopods: Response to acidification, vital effects and implications for palaeo-pH reconstruction". In: *Geochimica et Cosmochimica Acta* 248, pp. 370–386.

Kakihana, H (1977). "Fundamental Stidies on the Ion-Exchange Separation of Boron Isotopes". In: *Bulletin of the chemical society of Japan* 50.1, pp. 158 –163.

Kampschulte, A. and H. Strauss (2004). "The sulfur isotopic evolution of Phanerozoic seawater based on the analysis of structurally substituted sulfate in carbonates". In: *Chemical Geology* 204.3-4, pp. 255–286.

Katz, A. (1973). "The interaction of magnesium with calcite during crystal growth at 25–90°C and one atmosphere". In: *Geochimica et Cosmochimica Acta* 37.6, pp. 1563–1586.

Kisakürek, B., A. Eisenhauer, F. Böhm, D. Garbe-Schönberg, and J. Erez (2008). "Controls on shell Mg/Ca and Sr/Ca in cultured planktonic foraminiferan, Globigerinoides ruber (white)". In: *Earth and Planetary Science Letters* 273.3-4, pp. 260–269.

Kitano, Y., M. Okumura, and M. Idogaki (1975). "Incorporation of sodium, chloride and sulfate with calcium carbonate". In: *Geochemical Journal* 9.2, pp. 75 –84.

Kitano, Y., M. Okumura, and M. Idogaki (1978). "Coprecipitation of Borate-Boron with Calcium-Carbonate". In: *Geochemical Journal* 12.3, pp. 183–189.

Kitano, Y., A. Tokuyama, and T. Arakaki (1979). "Magnesian Calcite Synthesis from Calcium Bicarbonate Solution Containing Magnesium and Barium Ions". In: *Geochemical Journal* 13.4, pp. 181–185.

Klochko, K., A. J. Kaufman, W. S. Yao, R. H. Byrne, and J. A. Tossell (2006). "Experimental measurement of boron isotope fractionation in seawater". In: *Earth and Planetary Science Letters* 248.1-2, pp. 276–285.

Klochko, K., G. D. Cody, J. A. Tossell, P. Dera, and A. J. Kaufman (2009). "Re-evaluating boron speciation in biogenic calcite and aragonite using B-11 MAS NMR". In: *Geochimica Et Cosmochimica Acta* 73.7, pp. 1890–1900.

Kocurko, M. J. (1989). "Notes on the fossil octocorals and comparisons of some modern and ancient octocorals remains". In: *Tulane Studies on Geology and Paleontology* 21, pp. 105–115.

Kontrec, J., D. Kralj, L. Brecevic, G. Falini, S. Fermani, V. Noethig-Laslo, and K. Mirosavljevic (2004). "Incorporation of inorganic anions in calcite". In: *European Journal of Inorganic Chemistry* 2004.23, pp. 4579–4585.

Krief, S., E. J. Hendy, M. Fine, R. Yam, A. Meibom, G. L. Foster, and A. Shemesh (2010). "Physiological and isotopic responses of scleractinian corals to ocean acidification". In: *Geochimica Et Cosmochimica Acta* 74.17, pp. 4988–5001.

Kubota, K., Y. Yokoyama, T. Ishikawa, S. Obrochta, and A. Suzuki (2014). "Larger CO2 source at the equatorial Pacific during the last deglaciation". In: *Scientific Reports* 4, p. 5261.

Kucera, M. (2007). "Chapter Six Planktonic Foraminifera as Tracers of Past Oceanic Environments". In: *Proxies in Late Cenozoic Paleoceanography*. Ed. by C. Hillaire–Marcel and A. De Vernal. Vol. 1. Developments in Marine Geology. Elsevier, pp. 213–262.

Kunioka, D., K. Shirai, N. Takahata, Y. Sano, T. Toyofuku, and Y. Ujiie (2006). "Microdistribution of Mg/Ca, Sr/Ca, and Ba/Ca ratios in Pulleniatina obliquiloculata test by using a NanoSIMS: Implication for the vital effect mechanism". In: *Geochemistry Geophysics Geosystems* 7.12, pp. 1–11.

Langer, M. (1989). "Haftorgan, Internodien und Sklerite von Keratoisis melitensis (GOLDFUSS, 1826) (Octocorallia) in den pliozänen Foraminiferenmergeln ("Trubi") von Milazzo (Sizilien)". In: *Paläontologische Zeitschrift*.

Lapointe, A. and L. Watling (2015). "Bamboo corals from the abyssal Pacific: Bathygorgia". In: *Proceedings of the Biological Society of Washington* 128.2, pp. 125–136.

LaVigne, M., T. M. Hill, H. J. Spero, and T. P. Guilderson (2011). "Bamboo coral Ba/Ca: Calibration of a new deep ocean refractory nutrient proxy". In: *Earth and Planetary Science Letters* 312.3-4, pp. 506–515.

LaVigne, M., A. G. Grottoli, J. E. Palardy, and R. M. Sherrell (2016). "Multi-colony calibrations of coral Ba/Ca with a contemporaneous in situ seawater barium record". In: *Geochimica et Cosmochimica Acta* 179, pp. 203–216.

Lea, D. and E. Boyle (1989). "Barium content of benthic foraminifera controlled by bottom-water composition". In: *Nature* 338, p. 751.

Lea, D. W. (2014). "8.14 - Elemental and Isotopic Proxies of Past Ocean Temperatures". In: *Treatise on Geochemistry (Second Edition)*. Ed. by H. D.H. K. Turekian. Oxford: Elsevier, pp. 373–397.

Lea, D. W., G. T. Shen, and E. A. Boyle (1989). "Coralline barium records temporal variability in equatorial Pacific upwelling". In: *Nature* 340.6232, pp. 373–376.

Lea, D. W., T. A. Mashiotta, and H. J. Spero (1999). "Controls on magnesium and strontium uptake in planktonic foraminifera determined by live culturing". In: *Geochimica Et Cosmochimica Acta* 63.16, pp. 2369–2379.

Lea, D. W. (1993). "Constraints on the alkalinity and circulation of glacial circumpolar deep water from benthic foraminiferal barium". In: *Global Biogeochemical Cycles* 7.3, pp. 695–710.

Lea, D. W. and H. J. Spero (1992). "Experimental determination of barium uptake in shells of the planktonic foraminifera Orbulina universa at 22°C". In: *Geochimica et Cosmochimica Acta* 56.7, pp. 2673–2680.

Lear, C. H., H. Elderfield, and P. A. Wilson (2000). "Cenozoic deep-Sea temperatures and global ice volumes from Mg/Ca in benthic foraminiferal calcite". In: *Science* 287.5451, pp. 269–72.

Leeuw, N. H. de and S. C. Parker (2000). "Modeling absorption and segregation of magnesium and cadmium ions to calcite surfaces: Introducing MgCO3 and CdCO3 potential models". In: *The Journal of Chemical Physics* 112.9, pp. 4326–4333.

Lemarchand, D., J. Gaillardet, E. Lewin, and C. J. Allegre (2000). "The influence of rivers on marine boron isotopes and implications for reconstructing past ocean pH". In: *Nature* 408.6815, pp. 951–954.

— (2002). "Boron isotope systematics in large rivers: implications for the marine boron budget and paleo-pH reconstruction over the Cenozoic". In: *Chemical Geology* 190.1-4, pp. 123–140.

Li, Y.-H. and L.-H. Chan (1979). "Desorption of Ba and226Ra from river-borne sediments in the Hudson estuary". In: *Earth and Planetary Science Letters* 43.3, pp. 343–350.

Light, T., B. Williams, J. Halfar, A. Hou, Z. Zajacz, A. Tsay, and W. Adey (2018). "Advancing Mg/Ca Analysis of Coralline Algae as a Climate Proxy by Assessing LA-ICP-OES Sampling and Coupled Mg/Ca-δ18O Analysis". In: *Geochemistry, Geophysics, Geosystems* 19.9, pp. 2876–2894.

Littlewood, J. L., S. Shaw, C. L. Peacock, P. Bots, D. Trivedi, and I. T. Burke (2017). "Mechanism of Enhanced Strontium Uptake into Calcite via an Amorphous Calcium Carbonate Crystallization Pathway". In: *Crystal Growth & Design* 17.3, pp. 1214–1223.

Liu, Y. W., R. A. Eagle, S. M. Aciego, R. E. Gilmore, and J. B. Ries (2018). "A coastal coccolithophore maintains pH homeostasis and switches carbon sources in response to ocean acidification". In: *Nat Commun* 9.1, p. 2857.

Lohmann, G. P. (1995). "A model for variation in the chemistry of planktonic foraminifera due to secondary calcification and selective dissolution". In: *Paleoceanography* 10.3, pp. 445–457.

Lopez, O., P. Zuddas, and D. Faivre (2009). "The influence of temperature and seawater composition on calcite crystal growth mechanisms and kinetics: Implications for Mg incorporation in calcite lattice". In: *Geochimica Et Cosmochimica Acta* 73.2, pp. 337–347.

Lowenstam, H. A. and S. Weiner (1989). *On Biomineralization*. Oxford University Press.

Mann, S. (2001). *Biomineralization: Principles and Concepts in Bioinorganic Materials Chemistry*. Oxford University Press, p. 198.

Markulin, K., M. Peharda, R. Mertz-Kraus, B. R. Schone, H. Uvanovic, Z. Kovac, and I. Janekovic (2019). "Trace and minor element records in aragonitic bivalve shells as environmental proxies". In: *Chemical Geology* 507, pp. 120–133.

Marohn, L., V. Hilge, K. Zumholz, A. Klugel, H. Anders, and R. Hanel (2011). "Temperature dependency of element incorporation into European eel (Anguilla anguilla) otoliths". In: *Anal Bioanal Chem* 399.6, pp. 2175–84.

Mastrototaro, F., G. Chimienti, J. Acosta, J. Blanco, S. Garcia, J. Rivera, and R. Aguilar (2017). "Isidella elongata (Cnidaria: Alcyonacea) facies in the western Mediterranean Sea: visual surveys and descriptions of its ecological role". In: *European Zoological Journal* 84.1, pp. 209–225.

Mavromatis, V., Q. Gautier, O. Bosc, and J. Schott (2013). "Kinetics of Mg partition and Mg stable isotope fractionation during its incorporation in calcite". In: *Geochimica Et Cosmochimica Acta* 114, pp. 188–203.

Mavromatis, V., V. Montouillout, J. Noireaux, J. Gaillardet, and J. Schott (2015). "Characterization of boron incorporation and speciation in calcite and aragonite from co-precipitation experiments under controlled pH, temperature and precipitation rate". In: *Geochimica Et Cosmochimica Acta* 150, pp. 299–313.

Mavromatis, V., A. Immenhauser, D. Buhl, B. Purgstaller, A. Baldermann, and M. Dietzel (2017). "Effect of organic ligands on Mg partitioning and Mg isotope

fractionation during low-temperature precipitation of calcite in the absence of growth rate effects". In: *Geochimica Et Cosmochimica Acta* 207, pp. 139–153.

Mavromatis, V., K. E. Goetschl, C. Grengg, F. Konrad, B. Purgstaller, and M. Dietzel (2018). "Barium partitioning in calcite and aragonite as a function of growth rate". In: *Geochimica Et Cosmochimica Acta* 237, pp. 65–78.

McCulloch, M., S. Fallon, T. Wyndham, E. Hendy, J. Lough, and D. Barnes (2003). "Coral record of increased sediment flux to the inner Great Barrier Reef since European settlement". In: *Nature* 421.6924, pp. 727–730.

McCulloch, M. T., J. P. D'Olivo, J. Falter, M. Holcomb, and J. A. Trotter (2017). "Coral calcification in a changing World and the interactive dynamics of pH and DIC upregulation". In: *Nat Commun* 8, p. 15686.

Miller, J. A. (2011). "Effects of water temperature and barium concentration on otolith composition along a salinity gradient: Implications for migratory reconstructions". In: *Journal of Experimental Marine Biology and Ecology* 405.1-2, pp. 42–52.

Millero, F. J., R. Feistel, D. G. Wright, and T. J. McDougall (2008). "The composition of Standard Seawater and the definition of the Reference-Composition Salinity Scale". In: *Deep-Sea Research Part I-Oceanographic Research Papers* 55.1, pp. 50–72.

Mitsuguchi, T., E. Matsumoto, O. Abe, T. Uchida, and P. J. Isdale (1996). "Mg/Ca Thermometry in Coral Skeletons". In: *Science* 274.5289, pp. 961–963.

Mitsuguchi, T., T. Uchida, and E. Matsumoto (2010). "Na/Ca variability in coral skeletons". In: *Geochemical Journal* 44.4, pp. 261–273.

Monnin, C., C. Jeandel, T. Cattaldo, and F. Dehairs (1999). "The marine barite saturation state of the world's oceans". In: *Marine Chemistry* 65.3-4, pp. 253–261.

Montaggioni, L. F., F. Le Cornec, T. Correge, and G. Cabioch (2006). "Coral barium/calcium record of mid-Holocene upwelling activity in New Caledonia, South-West Pacific". In: *Palaeogeography Palaeoclimatology Palaeoecology* 237.2-4, pp. 436–455.

Moulin, P. and H. Roques (2003). "Zeta potential measurement of calcium carbonate". In: *Journal of Colloid and Interface Science* 261.1, pp. 115–126.

Mucci, A. (1987). "Influence of Temperature on the Composition of Magnesian Calcite Overgrowths Precipitated from Seawater". In: *Geochimica Et Cosmochimica Acta* 51.7, pp. 1977–1984.

Mucci, A. (1986). "Growth kinetics and composition of magnesian calcite overgrowths precipitated from seawater: Quantitative influence of orthophosphate ions". In: *Geochimica et Cosmochimica Acta* 50.10, pp. 2255–2265.

Mucci, A. and J. W. Morse (1983). "The incorporation of Mg2+ and Sr2+ into calcite overgrowths: influences of growth rate and solution composition". In: *Geochimica et Cosmochimica Acta* 47.2, pp. 217–233.

Mucci, A., R. Canuel, and S. Zhong (1989). "The solubility of calcite and aragonite in sulfate-free seawater and the seeded growth kinetics and composition of the precipitates at 25°C". In: *Chemical Geology* 74.3-4, pp. 309–320.

Neves, B. d. M., E. Edinger, C. Hillaire-Marcel, E. H. Saucier, S. C. France, M. A. Treble, and V. E. Wareham (2014). "Deep-water bamboo coral forests in a muddy Arctic environment". In: *Marine Biodiversity* 45.4, pp. 867–871.

Nguyen, L. T., M. A. Rahman, T. Maki, Y. Tamenori, T. Yoshimura, A. Suzuki, N. Iwasaki, and H. Hasegawa (2014). "Distribution of trace element in Japanese red coral Paracorallium japonicum by mu-XRF and sulfur speciation by XANES: Linkage between trace element distribution and growth ring formation". In: *Geochimica Et Cosmochimica Acta* 127, pp. 1–9.

Nir, O., A. Vengosh, J. S. Harkness, G. S. Dwyer, and O. Lahav (2015). "Direct measurement of the boron isotope fractionation factor: Reducing the uncertainty in reconstructing ocean paleo-pH". In: *Earth and Planetary Science Letters* 414, pp. 1–5.

Noé, S. U. and W. C. Dullo (2006). "Skeletal morphogenesis and growth mode of modern and fossil deep-water isidid gorgonians (Octocorallia) in the West Pacific (New Zealand and Sea of Okhotsk)". In: *Coral Reefs* 25.3, pp. 303–320.

Noireaux, J., V. Mavromatis, J. Gaillardet, J. Schott, V. Montouillout, P. Louvat, C. Rollion-Bard, and D. R. Neuville (2015). "Crystallographic control on the boron isotope paleo-pH proxy". In: *Earth and Planetary Science Letters* 430, pp. 398–407.

Nürnberg, D., J. Bijma, and C. Hemleben (1996). "Assessing the reliability of magnesium in foraminiferal calcite as a proxy for water mass temperatures". In: *Geochimica et Cosmochimica Acta* 60.5, pp. 803–814.

Okumura, M. and Y. Kitano (1986). "Coprecipitation of Alkali-Metal Ions with Calcium-Carbonate". In: *Geochimica Et Cosmochimica Acta* 50.1, pp. 49–58.

Okumura, T., H. J. Kim, J. W. Kim, and T. Kogure (2018). "Sulfate-containing calcite: crystallographic characterization of natural and synthetic materials". In: *European Journal of Mineralogy* 30.5, pp. 929–937.

Oomori, T., H. Kaneshima, Y. Maezato, and Y. Kitano (1987). "Distribution coefficient of Mg2+ ions between calcite and solution at 10–50°C". In: *Marine Chemistry* 20.4, pp. 327–336.

Oppo, D. W., Y. Rosenthal, and B. K. Linsley (2009). "2,000-year-long temperature and hydrology reconstructions from the Indo-Pacific warm pool". In: *Nature* 460.7259, pp. 1113–6.

Orejas, C., J. M. Gili, and W. Arntz (2003). "Role of small-plankton communities in the diet of two antarctic octocorals (Primnoisis antarctica and Primnoella sp.)" In: *Marine Ecology Progress Series* 250, pp. 105–116.

Pagani, M., D. Lemarchand, A. Spivack, and J. Gaillardet (2005). "A critical evaluation of the boron isotope-pH proxy: The accuracy of ancient ocean pH estimates". In: *Geochimica Et Cosmochimica Acta* 69.4, pp. 953–961.

Pahnke, K., R. Zahn, H. Elderfield, and M. Schulz (2003). "340,000-year centennial-scale marine record of Southern Hemisphere climatic oscillation". In: *Science* 301.5635, pp. 948–52.

Palmer, M. R., A. J. Spivack, and J. M. Edmond (1987). "Temperature and pH controls over isotopic fractionation during adsorption of boron on marine clay". In: *Geochimica et Cosmochimica Acta* 51.9, pp. 2319–2323.

Palmer, M. R., P. N. Pearson, and S. J. Cobb (1998). "Reconstructing past ocean pH-depth profiles". In: *Science* 282.5393, pp. 1468–71.

Park, H. and W. H. Schlesinger (2002). "Global biogeochemical cycle of boron". In: *Global Biogeochemical Cycles* 16.4.

Paytan, A. and E. M. Griffith (2007). "Marine barite: Recorder of variations in ocean export productivity". In: *Deep-Sea Research Part Ii-Topical Studies in Oceanography* 54.5-7, pp. 687–705.

Pearson, P. N., G. L. Foster, and B. S. Wade (2009). "Atmospheric carbon dioxide through the Eocene-Oligocene climate transition". In: *Nature* 461.7267, pp. 1110–1114.

Pelejero, C., E. Calvo, M. T. McCulloch, J. F. Marshall, M. K. Gagan, J. M. Lough, and B. N. Opdyke (2005). "Preindustrial to modern interdecadal variability in coral reef pH". In: *Science* 309.5744, pp. 2204–2207.

Perrin, J., C. Rivard, D. Vielzeuf, D. Laporte, C. Fonquernie, A. Ricolleau, M. Cotte, and N. Floquet (2017). "The coordination of sulfur in synthetic and biogenic Mg calcites: The red coral case". In: *Geochimica Et Cosmochimica Acta* 197, pp. 226–244.

Picciano, M. and C. Ferrier-Pages (2007). "Ingestion of pico- and nanoplankton by the Mediterranean red coral Corallium rubrum". In: *Marine Biology* 150.5, pp. 773–782.

Pingitore, N. E. (1987). "Modes of Coprecipitation of Ba2+ and Sr2+ with Calcite". In: *Geochemical Processes at Mineral Surfaces*. Vol. 323. ACS Symposium Series. American Chemical Society. Chap. 27, pp. 574–586.

Pingitore, N. E., G. Meitzner, and K. M. Love (1995). "Identification of Sulfate in Natural Carbonates by X-Ray-Absorption Spectroscopy". In: *Geochimica Et Cosmochimica Acta* 59.12, pp. 2477–2483.

Pingitore Jr, N. E., A. Iglesias, A. Bruce, F. Lytle, and G. M. Wellington (2002). "Valences of iron and copper in coral skeleton: X-ray absorption spectroscopy analysis". In: *Microchemical Journal* 71.2-3, pp. 205–210.

Pretet, C., K. van Zuilen, T. F. Nägler, S. Reynaud, M. E. Böttcher, and E. Samankassou (2015). "Constraints on barium isotope fractionation during aragonite precipitation by corals". In: *The Depositional Record* 1.2, pp. 118–129.

Quinn, T. M. and D. E. Sampson (2002). "A multiproxy approach to reconstructing sea surface conditions using coral skeleton geochemistry". In: *Paleoceanography* 17.4, pp. 14–1–14–11.

Quintana Krupinski, N. B., A. D. Russell, D. K. Pak, and A. Paytan (2017). "Core-top calibration of B/Ca in Pacific Ocean Neogloboquadrina incompta and Globigerina bulloides as a surface water carbonate system proxy". In: *Earth and Planetary Science Letters* 466, pp. 139–151.

Ra, K., H. Kitagawa, and Y. Shiraiwa (2010). "Mg isotopes and Mg/Ca values of coccoliths from cultured specimens of the species Emiliania huxleyi and Gephyrocapsa oceanica". In: *Marine Micropaleontology* 77.3-4, pp. 119–124.

Rae, J. W. B. (2018). "Boron Isotopes in Foraminifera: Systematics, Biomineralisation, and CO2 Reconstruction". In: *Boron Isotopes*. Ed. by H. Marschall and G. Foster. Advances in Isotope Geochemistry. Cham: Springer International Publishing. Chap. Chapter 5, pp. 107–143.

Rae, J. W. B., G. L. Foster, D. N. Schmidt, and T. Elliott (2011). "Boron isotopes and B/Ca in benthic foraminifera: Proxies for the deep ocean carbonate system". In: *Earth and Planetary Science Letters* 302.3-4, pp. 403–413.

Ragland, P. C., O. H. Pilkey, and B. W. Blackwelder (1979). "Diagenetic Changes in the Elemental Composition of Unrecrystallized Mollusk Shells". In: *Chemical Geology* 25.1-2, pp. 123–134.

Raitzsch, M. and B. Hönisch (2013). "Cenozoic boron isotope variations in benthic foraminifers". In: *Geology* 41.5, pp. 591–594.

Regenberg, M., A. Regenberg, D. Garbe-Schonberg, and D. W. Lea (2014). "Global dissolution effects on planktonic foraminiferal Mg/Ca ratios controlled by the calcite-saturation state of bottom waters". In: *Paleoceanography* 29.3, pp. 127–142.

Reid, P. C. et al. (2009). "Chapter 1 Impacts of the Oceans on Climate Change". In: *Advances in Marine Biology*. Vol. 56. Academic Press, pp. 1–150.

Ribes, M., R. Coma, and J. M. Gili (1999). "Heterogeneous feeding in benthic suspension feeders: the natural diet and grazing rate of the temperate gorgonian

Paramuricea clavata (Cnidaria: Octocorallia) over a year cycle". In: *Marine Ecology Progress Series* 183, pp. 125–137.

Ries, J. B. (2010). "Review: Geological and experimental evidence for secular variation in seawater Mg/Ca (calcite-aragonite seas) and its effects on marine biological calcification". In: *Biogeosciences* 7.9, pp. 2795–2849.

Rink, S., M. Kühl, J. Bijma, and H. J. Spero (1998). "Microsensor studies of photosynthesis and respiration in the symbiotic foraminifer Orbulina universa". In: *Marine Biology* 131.4, pp. 583–595.

Roberts, J., J. Gottschalk, L. C. Skinner, V. L. Peck, S. Kender, H. Elderfield, C. Waelbroeck, N. Vazquez Riveiros, and D. A. Hodell (2016a). "Evolution of South Atlantic density and chemical stratification across the last deglaciation". In: *Proc Natl Acad Sci U S A* 113.3, pp. 514–9.

Roberts, J. M., A. Wheeler, A. Freiwald, and S. Cairns (2009). *Cold-Water Corals - The Biology and Geology of Deep-Sea Coral Habitats*.

Robinson, L. F., J. F. Adkins, N. Frank, A. C. Gagnon, N. G. Prouty, E. B. Roark, and T. van de Flierdt (2014). "The geochemistry of deep-sea coral skeletons: A review of vital effects and applications for palaeoceanography". In: *Deep-Sea Research Part Ii-Topical Studies in Oceanography* 99, pp. 184–198.

Rodriguez-Navarro, C., E. Ruiz-Agudo, J. Harris, and S. E. Wolf (2016). "Nonclassical crystallization in vivo et in vitro (II): Nanogranular features in biomimetic minerals disclose a general colloid-mediated crystal growth mechanism". In: *J Struct Biol* 196.2, pp. 260–287.

Rollion-Bard, C. and D. Blamart (2015). "Possible controls on Li, Na, and Mg incorporation into aragonite coral skeletons". In: *Chemical Geology* 396, pp. 98–111.

Rollion-Bard, C., D. Blamart, J. P. Cuif, and Y. Dauphin (2010). "In situ measurements of oxygen isotopic composition in deep-sea coral, Lophelia pertusa: Re-examination of the current geochemical models of biomineralization". In: *Geochimica Et Cosmochimica Acta* 74.4, pp. 1338–1349.

Rollion-Bard, C., D. Blamart, J. Trebosc, G. Tricot, A. Mussi, and J.-P. Cuif (2011). "Boron isotopes as pH proxy: A new look at boron speciation in deep-sea corals

using 11B MAS NMR and EELS". In: *Geochimica et Cosmochimica Acta* 75.4, pp. 1003–1012.

Rosenthal, Y. and G. P. Lohmann (2002). "Accurate estimation of sea surface temperatures using dissolution-corrected calibrations for Mg/Ca paleothermometry". In: *Paleoceanography* 17.3, pp. 16–1–16–6.

Rosenthal, Y., E. A. Boyle, and N. Slowey (1997). "Temperature control on the incorporation of magnesium, strontium, fluorine, and cadmium into benthic foraminiferal shells from Little Bahama Bank: Prospects for thermocline paleoceanography". In: *Geochimica Et Cosmochimica Acta* 61.17, pp. 3633–3643.

Rosenthal, Y., G. P. Lohmann, K. C. Lohmann, and R. M. Sherrell (2000). "Incorporation and preservation of Mg in Globigerinoides sacculifer: implications for reconstructing the temperature and 18O/16O of seawater". In: *Paleoceanography* 15.1, pp. 135–145.

Rosenthal, Y. and A. Katz (1989). "The applicability of trace elements in freshwater shells for paleogeochemical studies". In: *Chemical Geology* 78.1, pp. 65–76.

Russell, A. D., B. Hönisch, H. J. Spero, and D. W. Lea (2004). "Effects of seawater carbonate ion concentration and temperature on shell U, Mg, and Sr in cultured planktonic foraminifera". In: *Geochimica Et Cosmochimica Acta* 68.21, pp. 4347–4361.

Rustad, J. R., E. J. Bylaska, V. E. Jackson, and D. A. Dixon (2010). "Calculation of boron-isotope fractionation between B(OH)(3)(aq) and B(OH)(4)(-)(aq)". In: *Geochimica Et Cosmochimica Acta* 74.10, pp. 2843–2850.

Sadekov, A. Y., S. M. Eggins, and P. De Deckker (2005). "Characterization of Mg/Ca distributions in planktonic foraminifera species by electron microprobe mapping". In: *Geochemistry Geophysics Geosystems* 6.

Saenger, C., R. E. Came, D. W. Oppo, L. D. Keigwin, and A. L. Cohen (2011). "Regional climate variability in the western subtropical North Atlantic during the past two millennia". In: *Paleoceanography* 26.2.

Saldi, G. D., J. Noireaux, P. Louvat, L. Faure, E. Balan, J. Schott, and J. Gaillardet (2018). "Boron isotopic fractionation during adsorption by calcite – Implication for the seawater pH proxy". In: *Geochimica et Cosmochimica Acta* 240, pp. 255–273.

Salmon, K. H., P. Anand, P. F. Sexton, and M. Conte (2016). "Calcification and growth processes in planktonic foraminifera complicate the use of B/Ca and U/Ca as carbonate chemistry proxies". In: *Earth and Planetary Science Letters* 449, pp. 372–381.

Sanyal, A., N. G. Hemming, W. S. Broecker, and G. N. Hanson (1997). "Changes in pH in the eastern equatorial Pacific across stage 5-6 boundary based on boron isotopes in foraminifera". In: *Global Biogeochemical Cycles* 11.1, pp. 125–133.

Sanyal, A., M. Nugent, R. J. Reeder, and J. Bijma (2000). "Seawater pH control on the boron isotopic composition of calcite: evidence from inorganic calcite precipitation experiments". In: *Geochimica et Cosmochimica Acta* 64.9, pp. 1551–1555.

Schlesinger, W. H. and A. Vengosh (2016). "Global boron cycle in the Anthropocene". In: *Global Biogeochemical Cycles* 30.2, pp. 219–230.

Schöne, B. R., Z. J. Zhang, P. Radermacher, J. Thebault, D. E. Jacob, E. V. Nunn, and A. F. Maurer (2011). "Sr/Ca and Mg/Ca ratios of ontogenetically old, long-lived bivalve shells (Arctica islandica) and their function as paleotemperature proxies". In: *Palaeogeography Palaeoclimatology Palaeoecology* 302.1-2, pp. 52–64.

Schöne, B. R., P. Radermacher, Z. J. Zhang, and D. E. Jacob (2013). "Crystal fabrics and element impurities (Sr/Ca, Mg/Ca, and Ba/Ca) in shells of Arctica islandica-Implications for paleoclimate reconstructions". In: *Palaeogeography Palaeoclimatology Palaeoecology* 373, pp. 50–59.

Seki, O., G. L. Foster, D. N. Schmidt, A. Mackensen, K. Kawamura, and R. D. Pancost (2010). "Alkenone and boron-based Pliocene pCO(2) records". In: *Earth and Planetary Science Letters* 292.1-2, pp. 201–211.

Sen, S., J. F. Stebbins, N. G. Hemming, and B. Ghosh (1994). "Coordination Environments of B-Impurities in Calcite and Aragonite Polymorphs - a B-11 Mas Nmr-Study". In: *American Mineralogist* 79.9-10, pp. 819–825.

Sevilgen, D. S., A. A. Venn, M. Y. Hu, E. Tambutte, D. de Beer, V. Planas-Bielsa, and S. Tambutte (2019). "Full in vivo characterization of carbonate chemistry at the site of calcification in corals". In: *Sci Adv* 5.1, eaau7447.

Shaw, T. J., W. S. Moore, J. Kloepfer, and M. A. Sochaski (1998). "The flux of barium to the coastal waters of the southeastern USA: The importance of submarine groundwater discharge". In: *Geochimica et Cosmochimica Acta* 62.18, pp. 3047–3054.

Shen, G. T., J. E. Cole, D. W. Lea, L. J. Linn, T. A. McConnaughey, and R. G. Fairbanks (1992). "Surface ocean variability at Galapagos from 1936-1982: Calibration of geochemical tracers in corals". In: *Paleoceanography* 7.5, pp. 563–588.

Shiller, A. M. (1997). "Dissolved trace elements in the Mississippi river: Seasonal, interannual, and decadal variability". In: *Geochimica Et Cosmochimica Acta* 61.20, pp. 4321–4330.

Sinclair, D. J. (2005). "Correlated trace element "vital effects" in tropical corals: A new geochemical tool for probing biomineralization". In: *Geochimica et Cosmochimica Acta* 69.13, pp. 3265–3284.

Smith, P. J., S. M. McVeagh, J. T. Mingoia, and S. C. France (2004). "Mitochondrial DNA sequence variation in deep-sea bamboo coral (Keratoisidinae) species in the southwest and northwest Pacific Ocean". In: *Marine Biology* 144.2, pp. 253–261.

Song, R. Q. and H. Colfen (2010). "Mesocrystals–ordered nanoparticle superstructures". In: *Adv Mater* 22.12, pp. 1301–30.

Spero, H. J., S. M. Eggins, A. D. Russell, L. Vetter, M. R. Kilburn, and B. Honisch (2015). "Timing and mechanism for intratest Mg/Ca variability in a living planktic foraminifer". In: *Earth and Planetary Science Letters* 409, pp. 32–42.

Spivack, A. J. and J. M. Edmond (1987). "Boron isotope exchange between seawater and the oceanic crust". In: *Geochimica et Cosmochimica Acta* 51.5, pp. 1033–1043.

Spooner, P. T., L. F. Robinson, F. Hemsing, P. Morris, and J. A. Stewart (2018). "Extended calibration of cold-water coral Ba/Ca using multiple genera and co-located measurements of dissolved barium concentration". In: *Chemical Geology* 499, pp. 100–110.

Staudt, W. J., R. J. Reeder, and M. A. A. Schoonen (1994). "Surface structural controls on compositional zoning of SO2-4 and SeO2-4 in synthetic calcite single crystals". In: *Geochimica et Cosmochimica Acta* 58.9, pp. 2087–2098.

Stecher, H. A. and M. B. Kogut (1999). "Rapid barium removal in the Delaware estuary". In: *Geochimica Et Cosmochimica Acta* 63.7-8, pp. 1003–1012.

Stecher, H. A., D. E. Krantz, C. J. Lord, G. W. Luther, and K. W. Bock (1996). "Profiles of strontium and barium in Mercenaria mercenaria and Spisula solidissima shells". In: *Geochimica Et Cosmochimica Acta* 60.18, pp. 3445–3456.

Stephenson, A. E., J. J. DeYoreo, L. Wu, K. J. Wu, J. Hoyer, and P. M. Dove (2008). "Peptides enhance magnesium signature in calcite: insights into origins of vital effects". In: *Science* 322.5902, pp. 724–727.

Stoll, H. M., J. R. Encinar, J. I. G. Alonso, Y. Rosenthal, I. Probert, and C. Klaas (2001). "A first look at paleotemperature prospects from Mg in coccolith carbonate: Cleaning techniques and culture measurements". In: *Geochemistry Geophysics Geosystems* 2.

Strauss, H. (1999). "Geological evolution from isotope proxy signals — sulfur". In: *Chemical Geology* 161.1-3, pp. 89–101.

Swart, P. K. (1981). "The strontium, magnesium and sodium composition of recent scleractinian coral skeletons as standards for palaeoenvironmental analysis". In: *Palaeogeography, Palaeoclimatology, Palaeoecology* 34, pp. 115–136.

Tambutte, S., M. Holcomb, C. Ferrier-Pages, S. Reynaud, E. Tambutte, D. Zoccola, and D. Allemand (2011). "Coral biomineralization: From the gene to the environment". In: *Journal of Experimental Marine Biology and Ecology* 408.1-2, pp. 58–78.

Taylor, J. R., K. K. Falkner, U. Schauer, and M. Meredith (2003). "Quantitative considerations of dissolved barium as a tracer in the Arctic Ocean". In: *Journal of Geophysical Research-Oceans* 108.C12, pp. 4–1 –4–13.

Tesoriero, A. J. and J. F. Pankow (1996). "Solid solution partitioning of Sr2+, Ba2+, and Cd2+ to calcite". In: *Geochimica Et Cosmochimica Acta* 60.6, pp. 1053–1063.

Thorrold, S. R., C. M. Jones, and S. E. Campana (1997). "Response of otolith microchemistry to environmental variations experienced by larval and juvenile Atlantic croaker (Micropogonias undulatus)". In: *Limnology and Oceanography* 42.1, pp. 102–111.

Thresher, R. E., N. C. Wilson, C. M. MacRae, and H. Neil (2010). "Temperature effects on the calcite skeletal composition of deep-water gorgonians (Isididae)". In: *Geochimica Et Cosmochimica Acta* 74.16, pp. 4655–4670.

Thresher, R. E., S. J. Fallon, and A. T. Townsend (2016). "A "core-top" screen for trace element proxies of environmental conditions and growth rates in the calcite skeletons of bamboo corals (Isididae)". In: *Geochimica Et Cosmochimica Acta* 193, pp. 75–99.

Tripati, A. and H. Elderfield (2005). "Deep-sea temperature and circulation changes at the Paleocene-Eocene Thermal Maximum". In: *Science* 308.5730, pp. 1894–1898.

Tripati, A. K., M. L. Delaney, J. C. Zachos, L. D. Anderson, D. C. Kelly, and H. Elderfield (2003). "Tropical sea-surface temperature reconstruction for the early Paleogene using Mg/Ca ratios of planktonic foraminifera". In: *Paleoceanography* 18.4.

Tripati, A. K., C. D. Roberts, R. A. Eagle, and G. Li (2011). "A 20 million year record of planktic foraminiferal B/Ca ratios: Systematics and uncertainties in pCO2 reconstructions". In: *Geochimica et Cosmochimica Acta* 75.10, pp. 2582–2610.

Trotter, J., P. Montagna, M. McCulloch, S. Silenzi, S. Reynaud, G. Mortimer, S. Martin, C. Ferrier-Pagès, J. P. Gattuso, and R. Rodolfo-Metalpa (2011). "Quantifying the pH 'vital effect' in the temperate zooxanthellate coral Cladocora caespitosa:

Validation of the boron seawater pH proxy". In: *Earth and Planetary Science Letters* 303.3-4, pp. 163–173.

Uchikawa, J., D. E. Penman, J. C. Zachos, and R. E. Zeebe (2015). "Experimental evidence for kinetic effects on B/Ca in synthetic calcite: Implications for potential B(OH)4- and B(OH)3 incorporation". In: *Geochimica et Cosmochimica Acta* 150, pp. 171–191.

Uluisik, I., H. C. Karakaya, and A. Koc (2018). "The importance of boron in biological systems". In: *J Trace Elem Med Biol* 45, pp. 156–162.

Urey, H. C., H. A. Lowenstam, S. Epstein, and C. R. Mckinney (1951). "Measurement of Paleotemperatures and Temperatures of the Upper Cretaceous of England, Denmark, and the Southeastern United-States". In: *Geological Society of America Bulletin* 62.4, pp. 399–416.

Vengosh, A., Y. Kolodny, A. Starinsky, A. R. Chivas, and M. T. Mcculloch (1991). "Coprecipitation and Isotopic Fractionation of Boron in Modern Biogenic Carbonates". In: *Geochimica Et Cosmochimica Acta* 55.10, pp. 2901–2910.

Venn, A., E. Tambutte, M. Holcomb, D. Allemand, and S. Tambutte (2011). "Live tissue imaging shows reef corals elevate pH under their calcifying tissue relative to seawater". In: *PLoS One* 6.5, e20013.

Vielzeuf, D., J. Garrabou, A. Gagnon, A. Ricolleau, J. Adkins, D. Gunther, K. Hametner, J. L. Devidal, E. Reusser, J. Perrin, and N. Floquet (2013). "Distribution of sulphur and magnesium in the red coral". In: *Chemical Geology* 355, pp. 13–27.

Walther, B. D., M. J. Kingsford, and M. T. McCulloch (2013). "Environmental Records from Great Barrier Reef Corals: Inshore versus Offshore Drivers". In: *PLoS ONE* 8.10.

Wanamaker Jr, A. D., K. J. Kreutz, T. Wilson, H. W. Borns Jr, D. S. Introne, and S. Feindel (2008). "Experimentally determined Mg/Ca and Sr/Ca ratios in juvenile bivalve calcite for Mytilus edulis: Implications for paleotemperature reconstructions". In: *Geo-Marine Letters* 28.5-6, pp. 359–368.

Warter, V., J. Erez, and W. Müller (2018). "Environmental and physiological controls on daily trace element incorporation in Tridacna crocea from combined laboratory culturing and ultra-high resolution LA-ICP-MS analysis". In: *Palaeogeography, Palaeoclimatology, Palaeoecology* 496, pp. 32–47.

Weiner, S. and P. M. Dove (2003). "An overview of biomineralization processes and the problem of the vital effect". In: *Biomineralization* 54, pp. 1–29.

Weiner, S. and J. Erez (1984). "Organic matrix of the shell of the foraminifer, Heterostegina depressa". In: *Journal of Foraminiferal Research* 14.3, pp. 206–212.

White, A. F. (1977). "Sodium and Potassium Coprecipitation in Aragonite". In: *Geochimica Et Cosmochimica Acta* 41.5, pp. 613–625.

Williams, S., J. Halfar, T. Zack, S. Hetzinger, M. Blicher, T. Juul-Pedersen, A. Kronz, B. Noël, M. van den Broeke, and W. J. van de Berg (2018). "Coralline Algae Archive Fjord Surface Water Temperatures in Southwest Greenland". In: *Journal of Geophysical Research: Biogeosciences* 123.8, pp. 2617–2626.

Wit, J. C., L. J. de Nooijer, M. Wolthers, and G. J. Reichart (2013). "A novel salinity proxy based on Na incorporation into foraminiferal calcite". In: *Biogeosciences* 10.10, pp. 6375–6387.

Wolthers, M., L. Charlet, and P. Van Cappellen (2008). "The surface chemistry of divalent metal carbonate minerals; a critical assessment of surface charge and potential data using the charge distribution multi-site ion complexation model". In: *American Journal of Science* 308.8, pp. 905–941.

Woosley, R. J., F. J. Millero, and M. Grosell (2012). "The solubility of fish-produced high magnesium calcite in seawater". In: *Journal of Geophysical Research* 117.C4.

Wynn, P. M., I. J. Fairchild, A. Borsato, C. Spotl, A. Hartland, A. Baker, S. Frisia, and J. U. L. Baldini (2018). "Sulphate partitioning into calcite: Experimental verification of pH control and application to seasonality in speleothems". In: *Geochimica Et Cosmochimica Acta* 226, pp. 69–83.

Yoshida, Y., H. Yoshikawa, and T. Nakanishi (2008). "Partition coefficients of Ra and Ba in calcite". In: *Geochemical Journal* 42.3, pp. 295–304.

Yoshimura, T., Y. Tamenori, H. Kawahata, and A. Suzuki (2014). "Fluctuations of sulfate, S-bearing amino acids and magnesium in a giant clam shell". In: *Biogeosciences* 11.14, pp. 3881–3886.

Yoshimura, T., Y. Tamenori, A. Suzuki, H. Kawahata, N. Iwasaki, H. Hasegawa, L. T. Nguyen, A. Kuroyanagi, T. Yamazaki, J. Kuroda, and N. Ohkouchi (2017). "Altervalent substitution of sodium for calcium in biogenic calcite and aragonite". In: *Geochimica Et Cosmochimica Acta* 202, pp. 21–38.

Yoshimura, T., A. Maeda, Y. Tamenori, A. Suzuki, K. Fujita, and H. Kawahata (2019). "Partitioning and Chemical Environments of Minor Elements in Individual Large Benthic Foraminifera Cultured in Temperature-Controlled Tanks". In: *Frontiers in Earth Science* 7.

Yoshimura, T., Y. Tamenori, A. Suzuki, R. Nakashima, N. Iwasaki, H. Hasegawa, and H. Kawahata (2013). "Element profile and chemical environment of sulfur in a giant clam shell: Insights from μ-XRF and X-ray absorption near-edge structure". In: *Chemical Geology* 352, pp. 170–175.

Yu, J. M. and H. Elderfield (2007). "Benthic foraminiferal B/Ca ratios reflect deep water carbonate saturation state". In: *Earth and Planetary Science Letters* 258.1-2, pp. 73–86.

Yu, J. M., G. L. Foster, H. Elderfield, W. S. Broecker, and E. Clark (2010). "An evaluation of benthic foraminiferal B/Ca and delta B-11 for deep ocean carbonate ion and pH reconstructions". In: *Earth and Planetary Science Letters* 293.1-2, pp. 114–120.

Zachara, J. M., C. E. Cowan, and C. T. Resch (1991). "Sorption of Divalent Metals on Calcite". In: *Geochimica Et Cosmochimica Acta* 55.6, pp. 1549–1562.

Zachos, J. C., M. W. Wara, S. Bohaty, M. L. Delaney, M. R. Petrizzo, A. Brill, T. J. Bralower, and I. Premoli-Silva (2003). "A transient rise in tropical sea surface temperature during the Paleocene-Eocene thermal maximum". In: *Science* 302.5650, pp. 1551–4.

Zeebe, R. E. and D. Wolf-Gladrow (2001). "Chapter 3 Stable isotope fractionation". In: *Elsevier Oceanography Series*. Ed. by R. E. Zeebe and D. Wolf-Gladrow. Vol. Volume 65. Elsevier, pp. 141–250.

Zeebe, R. E., J. Bijma, and D. A. Wolf-Gladrow (1999). "A diffusion-reaction model of carbon isotope fractionation in foraminifera". In: *Marine Chemistry* 64.3, pp. 199–227.

Zeebe, R. E. (2005). "Stable boron isotope fractionation between dissolved B(OH)3 and B(OH)4-". In: *Geochimica et Cosmochimica Acta* 69.11, pp. 2753–2766.

Zhao, L., B. R. Schöne, R. Mertz-Kraus, and F. Yang (2017). "Insights from sodium into the impacts of elevated p CO 2 and temperature on bivalve shell formation". In: *Journal of Experimental Marine Biology and Ecology* 486, pp. 148–154.

Zhong, S. and A. Mucci (1989). "Calcite and aragonite precipitation from seawater solutions of various salinities: Precipitation rates and overgrowth compositions". In: *Chemical Geology* 78.3-4, pp. 283–299.

Zumholz, K., T. Hansteen, F. Hillion, F. Horreard, and U. Piatkowski (2007). "Elemental distribution in cephalopod statoliths: NanoSIMS provides new insights into nano-scale structure". In: *Reviews in Fish Biology and Fisheries* 17.2-3, pp. 487–491.

2 The influence of skeletal micro-structures on potential proxy records in a bamboo coral

2.1 Abstract

Assessing the physicochemical variability of the deeper ocean is currently hampered by limited instrumental time series and proxy records. Bamboo corals (Isididae) form a cosmopolitan family of calcitic deep sea corals that could fill this information gap via geochemical information recorded in their skeletons. Here we evaluate the suitability of high-resolution chemical imaging of bamboo coral skeletons for temperature and nutrient reconstruction. The applied elemental mapping techniques allow to verify the suitability of the chosen transect on the sample section for paleo-reconstructions and enhance the statistical precision of the reconstruction. We measured Mg/Ca via electron microprobe at 1 μm resolution and Ba/Ca via laser ablation ICP-MS at 35 μm resolution in a historic specimen of *Keratoisis grayi* from the Blake Plateau off Eastern Florida. Long-term growth temperatures of 7.1 ± 3.4 °C (2SD) that are in agreement with recent ambient temperature range can be reconstructed from Mg/Ca ratios provided that anomalously Mg-enriched structural features around the central axis and isolated features related to tissue attachment are avoided for reconstruction. Skeletal Ba/Ca measurements reflect mean seawater barium $[Ba]_{SW}$ concentrations ($[Ba]_{SW}$ = 51 ± 24 nmol kg^{-1} (2SD)), in agreement with instrumental data (47 nmol kg^{-1}). We show for the first time that Ba/Ca forms concentric structures in a bamboo coral skeleton section. Our investigations

suggest that, while bamboo coral skeletons do record environmental parameters in their mean chemical composition, the magnitude of environmental variability reconstructed from high-resolution chemical maps exceeds that expected from instrumental time series. This necessitates additional investigation of the factors driving bamboo coral skeletal composition.

2.2 Introduction

Cold-water corals (CWCs) are receiving rising scientific interest as potential proxy recorders of a rarely observed environment. These animals can thrive in the deep sea – a habitat comprising the largest carbon reservoir in the ocean. Importantly, CWCs often inhabit hard substrates in environments where low sedimentation rates otherwise limit or even prohibit reconstructions from the sedimentary archive. Both global trends (such as changes in temperature or pH) and variable local oceanographic conditions (such as organic matter supply or shifting ocean currents) impact life in deep ocean ecosystems (Ruhl and Smith, 2004;Levin and Le Bris, 2015), but the spatial and temporal deficiency of instrumental records is a major hurdle to our understanding of longer term environmental conditions and oceanographic variability in the deep sea. The lack of deep ocean instrumental data may be mitigated using detailed geochemical information from calcifying CWCs (e.g. Robinson et al., 2014). CWCs are surfaceto deep-sea dwellers and have the potential to record environmental signals in their calcareous skeleton at up to subannual resolution (Sherwood and Risk, 2007). The highmagnesium calcite (HMC)-precipitating octocoral family Isididae – also called bamboo corals – lives in a depth range of less than 10 to more than 2000 m (Bostock et al., 2015;Thresher et al., 2016). They can therefore occur in waters well below the aragonite saturation horizon (Guinotte et al., 2006) where only a small fraction of aragonitic CWCs can survive (Cairns, 2007). Reconstructed bamboo coral radial growth rates range from 12–180 $\mu m\ yr^{-1}$ (Farmer et al., 2015b and references therein). Their calcitic ontogeny is sometimes characterised by growth rings (Noé and Dullo, 2006), and "spirallike" structures (Thresher and Neil, 2016), both of which can be observed by the naked eye. Geochemical analyses

of these calcitic structures may therefore offer high-resolution environmental reconstructions, provided that ontogenetic effects on geochemistry can be understood. Because bamboo corals have long lifespans, sometimes in excess of 300 years (Andrews et al., 2009; Hill et al., 2011), splicing geochemical records of temporally overlapping specimens (Prouty et al., 2011) might allow reconstruction of (sub-)annual growth conditions over several hundreds of years.

Various elemental and isotope ratios have been analysed in both the organic nodes and calcareous internodes of bamboo corals (Robinson et al., 2014). For example, previous studies link internodal Mg/Ca to ambient water temperature (Thresher et al., 2004; Thresher et al., 2010; Thresher et al., 2016), $\delta^{11}B$ to ocean pH (Farmer et al., 2015a), and $\delta^{13}C$ and $\delta^{18}O$ to temperature (Hill et al., 2011; Kimball et al., 2014; Saenger et al., 2017). Additionally, bamboo coral Ba/Ca has been proposed as a nutrient proxy, with Ba/Ca indicating $[Ba]_{SW}$ (LaVigne et al., 2011; Thresher et al., 2016; Serrato Marks et al., 2017) and/or $[Si]_{SW}$ (Thresher et al., 2016). In the organic nodes, bulk $\delta^{15}N$ was found to serve as an indicator of food source and ecosystem trophic dynamics (Sherwood et al., 2009; Hill et al., 2014). Furthermore, $\delta^{13}C$ analyses on nodal organic material have been applied to reconstruct the $\delta^{13}C$ of the exported surface ocean primary production (Schiff et al., 2014).

Although previous studies have generally demonstrated the potential of bamboo corals to record environmental conditions, calibrations established with bulk measurements may hamper fine-scale reconstructions of past environmental conditions (e.g. Aranha et al., 2014). In order to assess whether fine-scale environmental information can be extracted from single specimens, skeletal microstructures and their influence on the proxy record need to be investigated. In this study we quantify the spatial and microstructural chemical composition of bamboo corals using element mapping approaches via laser ablation ICPMS, electron microprobe analysis, and confocal Raman microscopy. These techniques allow us to gain detailed information at high spatial resolution regarding elemental composition of bamboo coral internodes, growth structures and mineralogy. Specifically, we assess the ability of bamboo coral Mg/Ca and Ba/Ca to work as high-resolution temperature and

nutrient proxies, respectively. To investigate the distribution of organic material, we mapped fluorescence and sulfur content via confocal Raman microscopy and electron microprobe, respectively. The employed techniques complement one another and shed light on how bamboo corals build their skeleton. Although LA-ICP-MS mapping has been applied as a promising new tool in paleoclimatic (Fietzke et al., 2015) and biomineralisation studies (Evans and Müller, 2013; Oppelt et al., 2017), fine-scale mapping and subsequent reconstruction of environmental parameters presented here are, to the best of our knowledge, the first application to octocorals.

2.3 Oceanographic setting, material and methods

2.3.1 Specimen and sample

We selected *Keratoisis grayi* (Octocorallia, Isididae) specimen number USNM 10496 of the Smithsonian National Museum of Natural History because it grew in the western Atlantic on the Blake Plateau, where the Gulf Stream is formed. Scientific interest for this site is given by the observation that the Gulf Stream waters exert a major influence on the climatic conditions of Europe (Palter, 2015). Sample growth rate was previously constrained using radiocarbon (^{14}C) (Farmer et al., 2015b), and the internodal sample section shows a pronounced visible ring structure that may be associated with compositional variability. The coral was collected alive in 1885 from 805 m water depth at 30.733° N and 79.433° W off East Florida (Fig. 2.1) by the United States Fish Commission. No signs of bioerosion or diagenetic alteration are apparent, suggesting the coral was alive at the time of collection.

2.3.2 Oceanographic setting

Surface ocean circulation over the Blake Plateau is dominated by the Gulf Stream (Fig. 2.1a). This boundary current is formed by the Florida Current (FC), which travels from the Gulf of Mexico through the Florida Strait, and the Antilles Current, which passes along the east coast of the Bahamas (Jahnke and Blanton, 2010).

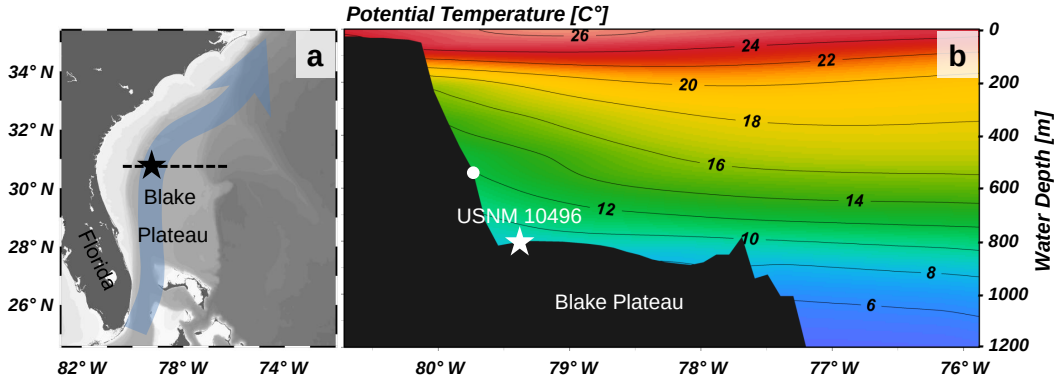

FIGURE 2.1: Bamboo coral USNM 10496 was collected some 150 km of the east coast of Florida on the Blake Plateau (black star (a)), within the flow path of the Florida Current (blue arrow in (a)). (b) displays the vertical temperature distribution along the length of the black dashed line in (a), with oblique isotherms off the outer shelf caused by the geostrophic flow. The white star in (b) marks the sampling site of USNM 10496 while the white dot shows where the sample from Sinclair et al. (2011) was collected. The map and transect were created using Ocean Data View (Schlitzer, 2018) and modified manually. (For interpretation of the references to colour in this figure legend, the reader is referred to the web version of this article.)

Ocean bottom water at the sampling site consists of modified Antarctic Intermediate Water, which is colder and less saline than the overlying water mass (Atkinson, 1983; Kashgarian and Tanaka, 1991). Mean bottom water temperatures measured at mooring stations 80 km away from the sampling site (30.0° N and 79.4° W at 794 m depth) were 7.6 ± 1.2 °C (2SD) for March to September 1981 and 8.1 ± 1.2 °C (2SD) for September 1981 to March 1982 (Lee and Waddell, 1983). Gridded potential temperatures according to the nearest 0.25°×0.25° World Ocean Atlas 2013 (WOA) grid point at 30.625° N and 79.375° W at 800 m depth were 9 °C (Locarnini et al., 2013) (Fig. 2.1b). While the seasonal temperature variation at the exact sampling location is unknown, available hydrographic data suggest the coral was likely bathed in highly variable ocean bottom temperatures. For example, Lee and Waddell (1983) found a total annual thermal variation of 3.9 °C above seafloor at the mooring closest to our sampling site. Seventeen years of CTD casts east of Abaco Island (Bahamas) show a longterm temperature variation of 6.0 °C around a mean of 10.3 ± 2.6 °C (2SD) at 800 m depth (data were collected as part of NOAA's Deep Western Boundary Current Time Series (DWBC) and are available at `www.aoml.noaa.gov/phod/wbts/`. The FC

exhibits a strong seasonal cycle with maximum current strength during summer in addition to inter-annual variability in water transport (Baringer and Larsen, 2001). Strong ocean bottom currents on the Blake Plateau (flow $\approx$ 5 to > 40 cm s^{-1}, Pratt (1963)) limit deposition of sinking particles and expose hard phosphorite grounds (Filippelli, 2011) and manganese pavements (Pratt and McFarlin, 1966) in otherwise calcareous sand (Milliman et al., 1972). The hard substrate and high currents on the Blake Plateau provide suitable habitats for deep-sea coral growth (Reed et al., 2006; Edinger et al., 2011).

2.3.3 Confocal Raman microscopy

To prepare USNM 10496 for analysis, we embedded a slice of the basal internode in Araldite resin under vacuum, dried it overnight at 50 °C in an oven and polished it in a graded series with Struers Dia Pro water based diamond emulsion of 9 μm, 3 μm, and 1 μm grain size with a Struers TegraPol polishing machine. The sample was rinsed with demineralised water after each polishing step.

The polished sample section was used to determine the mineralogical composition and distribution of organic components within the sample by means of confocal Raman microscopy (CRM). CRM measurements were performed using a WITec alpha 300 R instrument and a diode laser having an excitation wavelength of 488 nm at the Alfred Wegener Institute, Helmholtz Centre for Polar and Marine Research in Bremerhaven, Germany. A Zeiss 20 Epiplan lens (NA 0.4) was used for scanning larger areas of the sample. Dedicated areas within these larger areas were subsequently scanned with a higher spatial resolution using a Nikon 100 lens (NA 0.9). High spectral resolution of the Raman spectrum was obtained by using a UHTS300 ultra high throughput spectrometer (WITec GmbH, Ulm, Germany) equipped with 1800 mm^{-1} grating blazed at 500 nm. Data were measured and analysed using WITec ProjectFOUR software. An optical clear calcite single crystal (Iceland-spar from Mexico) was used as an in-house standard to obtain a calcite Raman spectrum under sample measurement conditions. Wall and Nehrke (2012) demonstrated that

enhanced fluorescence in the Raman spectrum of corals correlates well with the distribution of organic compounds within the skeleton. We used this method to create Raman maps showing the distribution of enhanced fluorescence (using the spectral range from 2000–2400 cm^{-1}), i.e. the distribution of organic components within the skeleton.

2.3.4 Electron microprobe analyses

Calcium, magnesium and sulfur concentrations in the sample were determined by electron microprobe (EMPA) using a JEOL JXA 8200 at GEOMAR Helmholtz Centre for Ocean Research Kiel. Prior to analysis, the sample section was sputtered with carbon to avoid sample charging. Element distributions were simultaneously measured by wavelength-dispersive spectrometers. Ca was measured by using PET (pentaerythritol), Mg using TAPH (thallium acid phthalate, high intensity) and S using PETH (pentaerythritol, high intensity) as diffraction crystals, respectively. An overview map of the whole sample was established with a 15 µm electron beam size, a dwell time of 25 ms $pixel^{-1}$ and a current of 100 nA. A high resolution transect across the radius with a width of 300 µm was performed with a 1 µm beam, a dwell time of 45 ms $pixel^{-1}$, and a current of 100 nA. The dwell time and current were chosen to assure high signal intensity while preventing the carbon coating from being removed by the electron beam. We can exclude sample damage via comparison of the actual Ca counts in a calcite standard with their theoretical counts based on the determined calibration factors from non-carbonate standards (see Appendix Fig. 2.10). All maps were created integrating once on a single spot. Depending on the necessities of further comparison the element concentrations are given as absolute concentration in wt% based on the concentration calibration for one element or the relative concentration in mol mol^{-1} based on the concentration calibration for two elements. The latter is calculated under the assumption that the sample material is only composed of calcium carbonate. Detection limits for 1 µm resolution were calculated as three times the standard deviation (SD) of the background signal for Ca, Mg and S for a single pixel analysis, and were 2.33, 0.46 and 0.01 wt%, respectively.

The two-sided 2r relative variation of a single pixel's Mg/Ca ratio was based on counting statistics and is about ±15 %. These are the upper limits, which improved threefold upon averaging nine (three times three) neighbouring pixels for smoothing the Mg/Ca maps compared to a single pixel. About the same improvement was achieved by averaging 10 parallel Mg/Ca lines used for temperature reconstruction. S content was initially mapped as a potential indicator of organic matter distribution as proposed for scleractinians (Cuif et al., 2003). Electron backscatter images indicating the mean atomic number of the sample volume were taken after elemental maps were recorded.

2.3.5 Laser ablation inductively coupled plasma mass spectrometry

The fine-scale abundance of Ba and Ca was mapped by laser ablation inductively coupled plasma mass spectrometry (LA-ICP-MS) with a Nu AttoM sector field ICP-MS coupled to an Electro Scientific Industries NWR 193 nm excimer laser at GEOMAR Helmholtz Centre for Ocean Research Kiel. The sample was investigated with CRM and EMPA prior to LA-ICP-MS to avoid multiple polishing steps, since laser ablation roughens the sample surface. The same section previously analysed with high resolution EMPA was chosen for comparability. Instrumental settings were tuned for hot plasma conditions according to Fietzke and Frische (2016). Any potential surface contamination and the carbon coating from EMPA measurements was removed by a previous measurement at the same site. The laser beam for data acquisition moved with 25 μm s^{-1} over the sample, had a diameter of 35 μm, a pulse rate of 25 Hz and a fluence of 2.5 J cm^{-2}. The map was created by four runs of 20 parallel line scans with 10 μm overlap each. Upon completion of each of these four runs, a gas blank and a NIST SRM 610 glass standard were measured under the same ablation conditions. Data acquisition was performed during two sessions.

As the data reduction applied here is not a standard procedure, it is described in detail below. Data reduction was carried out offline, using ^{44}Ca as an internal standard and NIST SRM 610 for external calibration. Individual lines were aligned based on the ^{44}Ca intensity, separating the ablation from the background signal. By

averaging 2 ×3 data points, a smoothed map of background subtracted values was created and statistical noise was lowered. The detection limits for a single pixel were 20 ppm for Ba and 250 ppm for Ca after smoothing. The $^{138}Ba/^{44}Ca$ ratios were then calculated after the smoothing procedure was applied to the raw counts per second of Ba and Ca. The offset between the four single maps was removed by averaging representative regions on all maps and subsequent application of a factor (0.94–1.07) to match the mean concentration ofall selected regions. The resulting map of every ratio is 1.8 ×4.6 mm in size and contains 20,500 pixels. For $[Ba]_{SW}$ reconstruction the mean of 20 parallel lines was used which resulted in a 2σ relative variation of Ba/Ca lower than ±0.1 % based on counting statistics. This was done in addition to the initial smoothing applied to the raw counts of the Ba and Ca maps.

2.3.6 Etching and secondary electron imaging

After completing its chemical characterisation via CRM, EMPA and LA-ICP-MS, the sample was polished again using a 1 μm polishing emulsion, then etched for 5 minutes in 0.1 M HCl and rinsed with deionised water to visualise growth structures and crystals. The sample was then coated again with carbon and secondary electron images were produced with a JEOL JXA 8200 microprobe. Etching of the sample was carried out after chemical mapping to avoid potential partial leaching of the investigated elements and compounds.

2.3.7 Age model

For temporal analysis of our geochemical mapping data, we used the linear ^{14}C age model of Farmer et al. (2015b), which is based on three radiocarbon dates and yields a mean growth rate of 29 ± 10 $\mu m\ yr^{-1}$. A fourth innermost value was excluded due to potential infilling. While more complex nonlinear growth modes have been postulated for bamboo corals (e.g., Frenkel et al. (2017)), we prefer the simple linear model for this sample, given the limited available chronological data and relative calendar age imprecision of the pre-bomb ^{14}C dates. An absolute (calendar) age

model was established for this specimen using the collection date (1886) and estimated mean growth rate (29 ± 10 μm yr^{-1}). To estimate the relative dating precision for a given sampling point, we started with the sampling date (1886) and integrated the growth rate uncertainty published by Farmer et al. (2015b). This leads to an increase from no uncertainty in 1886 when the sample was collected alive, to +40 and -80 years at about 1740, when the coral is supposed to have started growing. The one-sided dating uncertainty Δ_t in years was calculated as follows:

$$\Delta t_{+;-} = \left| \left(\frac{d}{GR_m} + A_{abs} \right) - \left(\frac{d}{GR_{+;-}} + A_{abs} \right) \right| \tag{2.1}$$

where d is the distance from the outer rim in lm, GR_m is the mean growth rate in μm yr^{-1}, $GR_{+;-}$; are the respective upper and lower growth rate estimates in μm yr^{-1}, and A_{abs} is the year of sampling.

2.4 Results

2.4.1 Visual sample description

Micrograph optical properties

The internodal cross section of bamboo coral specimen USNM 10496 shows concentric visible rings and patterns of elongated opaque structures that are tilted with respect to the radial growth direction and more transparent areas between them (Fig. 2.2). Three drill holes from preceding growth rate investigations (Farmer et al., 2015b) are clearly visible, while drilling the innermost sample filled the otherwise hollow central axis with drilling dust. One concentric crack can be observed about 0.8 mm away from and parallel to the rim of the internode. Along this interruption two sites display a bump in the otherwise concentric visible growth rings. The sample exhibits two major bright ring features. More general features are the multiple alternating opaque-translucent inclined patterns embedded between two growth rings and will be referred to as inter-ring structures below. These patterns

change orientation in one band from clockwise to counter clockwise with an apparently wavelike structure. The inter-ring structure is hardly visible within the 1.6 mm radius of the central axis. This inner increment is more uniformly opaque than the outer increment, where pronounced darker and brighter rings can be seen.

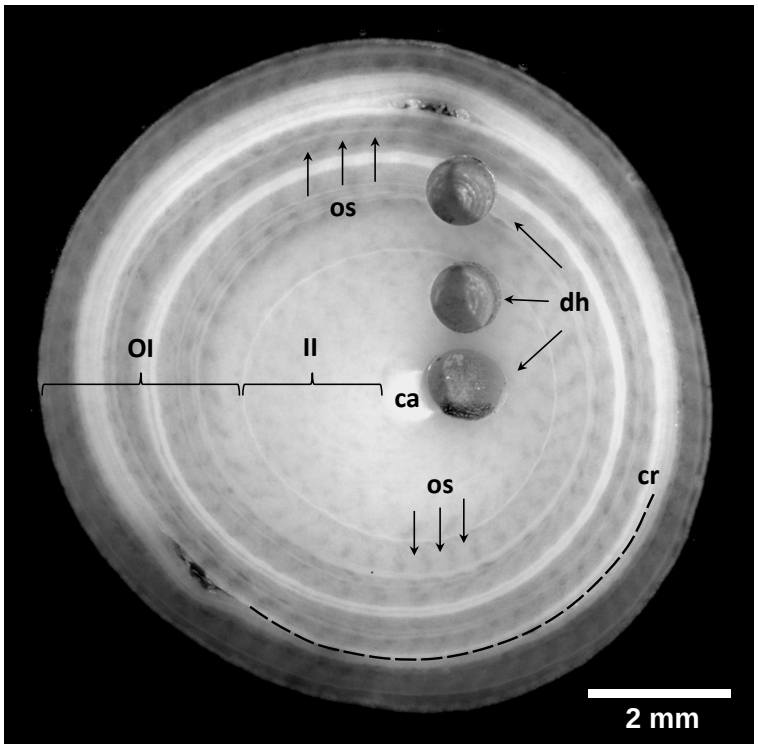

FIGURE 2.2: Micrograph of a section from bamboo coral USNM 10496 from the Blake Plateau. Three drill holes (dh), the drilling dust filled central axis (ca), concentric growth rings and inclined alternating opaque structures (os) are visible. Additionally, a crack (cr) marked by the dashed black line can be seen. The inner (II) and an outer increment (OI) are microstructurally and geochemically distinct (see text for details). Note that the inner increment does not include the central cavity.

Etched surface structure

The etched sample surface shows concentric macroscopic bands, crystallite fascicles and microscopic mineralisation features of which the outer boundary forms a fan- or rivetlike shape (Fig. 2.3). The younger outer increment shows irregular banding while no growth banding is visible in the older inner increment. Etched bands resemble the optical properties of the unetched sample surface (Fig. 2.2). The centre and outermost layer contain smaller crystals than the remaining parts.

Crystallites are generally flat in shape. The orientation of crystallite bundles is generally perpendicular to the growth direction but crosses it in various directions with a wavy microstructure (Fig. 2.3d). Microscale fan-shaped structures always widen in growth direction while the narrow part of the fan is located after a dark band on the secondary electron images. The arrangement of these fans (Fig. 2.4a) mirrors patches of optical opacity (Fig. 2.2) that occur between growth rings. The sizes of the fans are about 20 µm wide at their base 20–30 µm long. None of these fans can be observed in proximity to the dark bands in the 270 µm radius around the central axis in which also a finer less structured surface exists (Fig. 2.3b). In contrast, the remaining outer part of the inner increment does show fans.

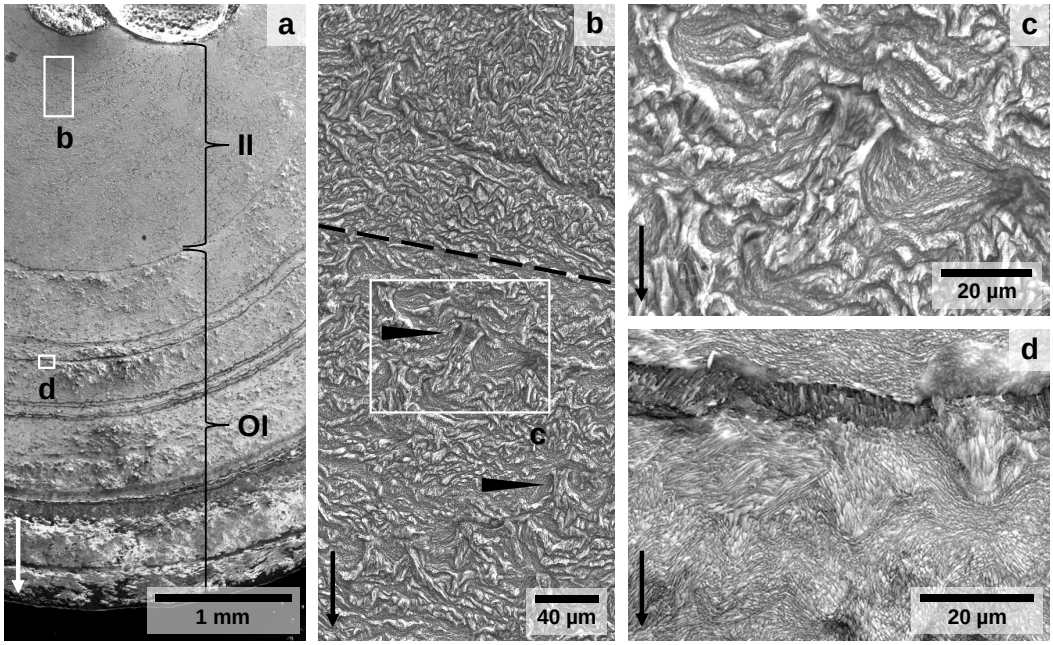

FIGURE 2.3: The transect of the etched surface of a sample section of bamboo coral USNM 10496 from the Blake Plateau shows dark growth rings in the outer increment (OI) and a finer structure in the inner increment (II) (a). (b) depicts a detail of II (a), which is characterised by a finer but still crystalline structure in the upper part above the dashed line, and fanlike structures (arrows) in the lower portion of the image (below the dashed line). (c) shows the fanlike structures marked in (b) presumably formed through desmocyte attachment. Note the blurred base of the fanlike structure which might show the cup-shaped basal lamina overlapping the crystallites. A wavelike pattern is formed by the several crystallite bundles surrounding a here darker growth ring of crystallites shown in figure (d). The arrows in the lower left in each figure display the direction towards the outer rim.

2.4.2 Sample geochemistry

Mineralogy and organic matter distribution

CRM measurements identify calcite as the only mineral phase present within the sample. The distribution of organic components (based on the fluorescence intensity images) can be seen from Fig. 2.4. The presence and absence of short organic bands in fluorescence resemble the pattern of inter-ring structures observed in visual opacity. The observed fluorescent bands are 20–80 μm in length and 1–2 μm in width and form steplike single or multiple row patterns (Fig. 2.4). The shape of these bands forms a wide U with the open part generally facing toward the growth direction.

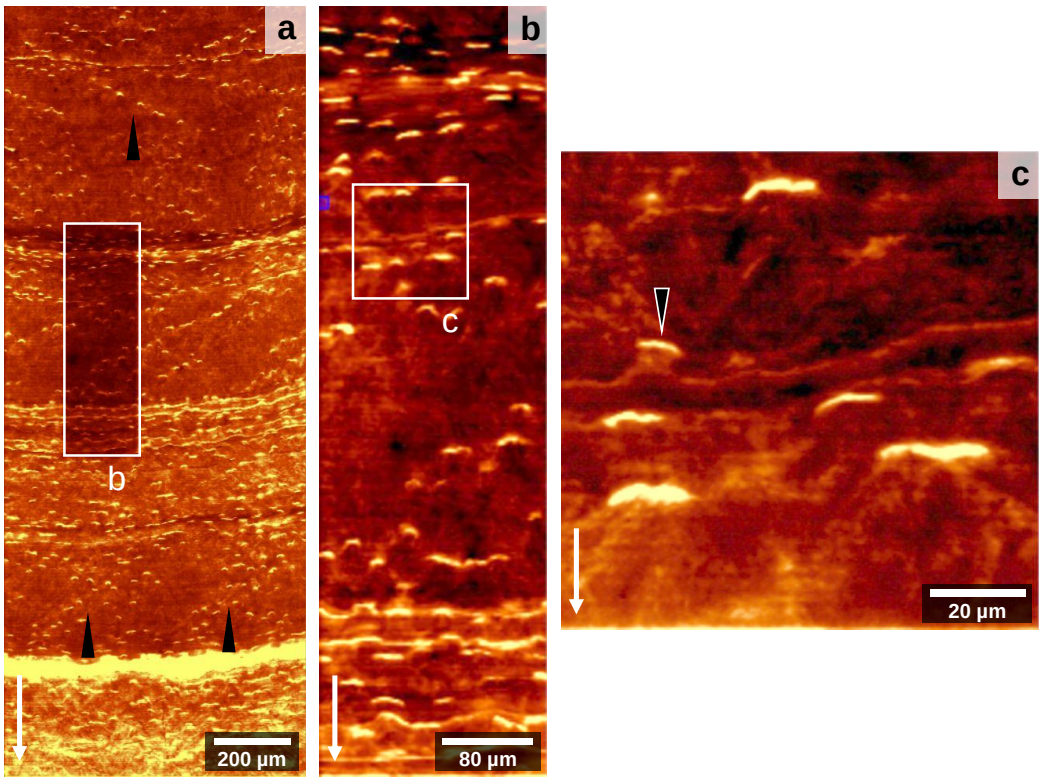

FIGURE 2.4: (a) Fluorescence mapping of a section of bamboo coral USNM 10496 from the Blake Plateau shows high fluorescent (brighter colours) short organic bands which form concave thicker concentric bands and steplike patterns (arrowheads). (b) and (c) The strongly fluorescing short bands have a length of 10–20 μm and are convex in shape relative to the growth direction. Sample growth direction of each figure is indicated by the arrows in the lower left.

Mg and S distribution

The EMPA scans resolve regular, non-stochastic growth patterns for Mg and S. The concentric banding (Fig. 2.5a and b) as well as the amount of data per analysed growth interval shown in Fig. 2.5c demonstrates that the observed Mg/Ca peaks are not random enrichments caused by measurement uncertainty. The counting statistics limit the precision of individual Mg and Ca data to about ±7 % and ±2 % (1SD) respectively at 1 μm resolution. Concentric Mg/Ca rings as well as granular Mg/Ca increases are visible (Fig. 2.5b). The Mg/Ca rings are clearly distinguished in the outer 2.6 mm of the section, but are not as clearly developed in the inner increment of the internode. No continuous rings in the range of tens of μm (the expected annual growth rate) could be identified. In general, Mg/Ca decreases from the central axis to the outside of the internode. The greatest Mg/Ca decrease is observed in an about 0.4 mm wide band surrounding the central axis. Mg/Ca is roughly constant between 0.4 mm and 1.8 mm distance from the central axis, followed by a sharp decrease to another generally constant level. The location of this steplike change in Mg/Ca corresponds to the alteration in etched surface structure between what we define as the inner and outer increments (Figs. 2.2 and 2.3), with Mg/Ca ring patterns restricted to the outer increment. While Mg/Ca decreases from 130 to about 93 mmol mol^{-1} in the inner increment, Mg/Ca is near constant at about 89 mmol mol^{-1} in the outer increment. The total Mg/Ca range, excluding the innermost high Mg/Ca ring, is slightly less pronounced in the inner increment (26.8 mmol mol^{-1}) of the skeleton than in the outer increment (32.3 mmol mol^{-1}). Also, the Mg/Ca variability (2SD) of the detrended increments is lower in the inner increment (7.7 mmol mol^{-1}) than in the outer increment (9.1 mmol mol^{-1}). The area of elevated Mg/Ca around the central axis coincides with the absence of fanlike structures observed by secondary electron imaging of the etched surface (Fig. 2.3b).

The high-resolution EMPA scan (1 μm spot size) of the outermost 1 mm of coral calcite shows well defined Mg/Ca growth rings that are sometimes disturbed by elongated features of high Mg/Ca ratios (Figs. 2.5b and 2.6a). These features always start at bands with low Ca content and low density shown in the electron

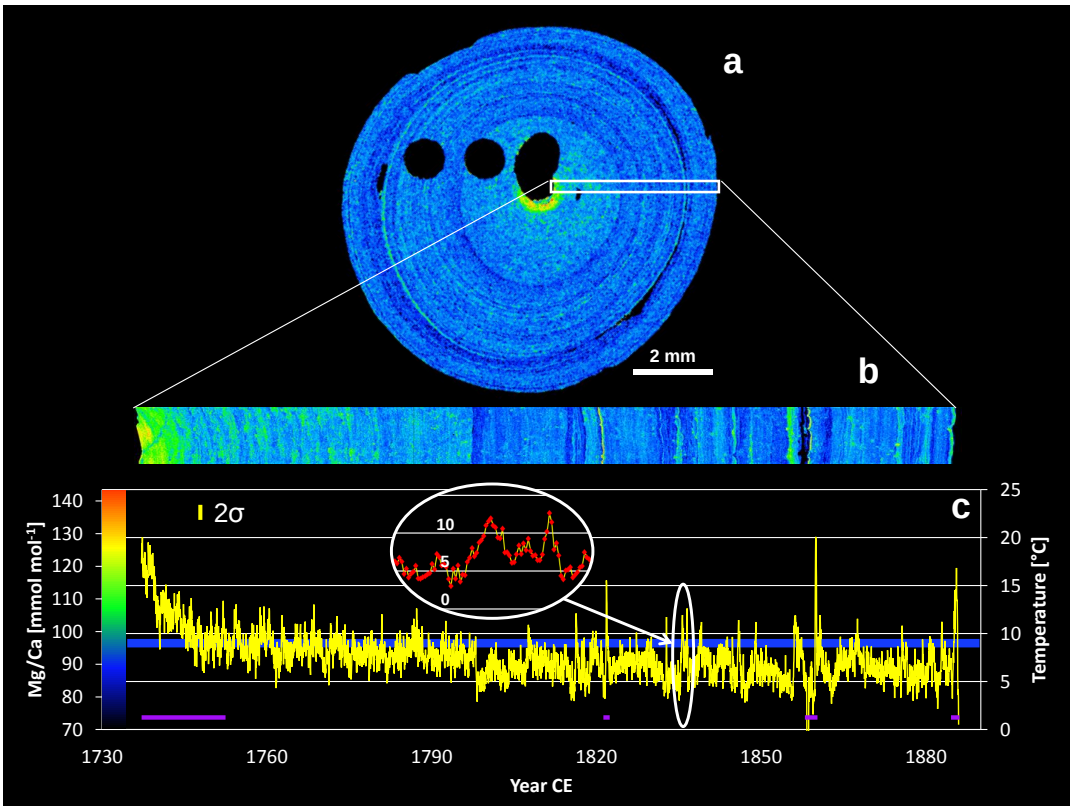

FIGURE 2.5: EMPA scan of a section of bamboo coral USNM 10496 from the Blake Plateau. (a) Mg/Ca overview scan with 15 lm spot size shows ring structures and high Mg/Ca ratios around the central channel. (b) The high-resolution scan (1 μm spot size) resolves concentric growth rings and spots of elevated Mg/Ca. (c) Mg/Ca variation along (b) is the average of 10 parallel lines after elimination of local enrichments. Growth temperatures are estimated using the calibration of Thresher et al., 2016; the scale is shown on the right. The inset in (c) gives a detailed view of the data density (30 data points per reconstructed year). The 2 σerror bar shows the calculated 5 % measurement error based on the mean count statistics for Mg/Ca. The horizontal blue line shows recent mean water temperature in the sampling region while the data excluded from statistical considerations are marked in purple at the bottom. (For interpretation of the references to colour in this figure legend, the reader is referred to the web version of this article.)

backscatter (EBS) images (Fig. 2.6b and c). The low-Ca bands observed here have the same size and shape as the ones imaged by Raman-spectroscopy (Fig. 2.4c). The detailed EBS scan shows that these short bands are the beginning of fans that widen always in growth direction. We also find fan-shaped cavities where the bands are located close to the concentric crack in the sample (Figs. 2.2 and 2.6d).

Mg and S show broadly opposite concentration distributions (Fig. 2.7). In particular, S/Ca is lower in the ring structures (<10 mmol mol^{-1}) and the innermost part around the central axis (<9 mmol mol^{-1}) of the coral section where Mg/Ca is higher (Fig. 2.5a). The inner increment shows a mean S/Ca value of 9.5 ± 1.7 mmol mol^{-1} (2SD) while the outer increment yields S/Ca = 10.5 ± 2.9 mmol mol^{-1} (2SD). Although an opposing behaviour is visible in Fig. 2.7a, the point-to-point correlation between Mg and S concentration is weak. The best fit using a nonpolynomial equation can be found by using a power law relationship (R^2 = 0.26, Fig. 2.7b).

Ba/Ca distribution

LA-ICP-MS mapping shows concentric Ba/Ca banding over the whole sample section (Fig. 2.8). Following the growth direction on the sample section from the central axis to the outer rim, no secular trend for Ba/Ca is observed. Unlike S/Ca and Mg/Ca, Ba/Ca does not show distinct behaviour surrounding the central axis and Ba/ Ca is banded both in the inner and outer increments of the internode. A possible covariation between S/Ca, Mg/Ca and Ba/Ca was investigated using actual or interpolated data points positioned at equal distances from the rim. No similarities between the Ba/Ca and Mg/Ca or S/Ca spatial distribution on the sample section can be found (R^2 < 0.01 and 0.15 respectively). Ba/Ca is elevated in the outer 250 μm of the internode, with Ba/Ca values as high as 15.7 μmol mol^{-1}, while the mean Ba/ Ca mean in the remaining part is 8.2 ± 1.9 μmol mol^{-1} (2SD). We applied a 40-point running mean to the Mg/ Ca and S/Ca data before comparison, since Ca, Mg and S were measured with a spot size of 1 μm while Ba/Ca was measured with 35 μm spot size. In addition, we also considered signal smoothing by sample mixing in the laser ablation cell given by its wash out time. We evaluated this for Ba by

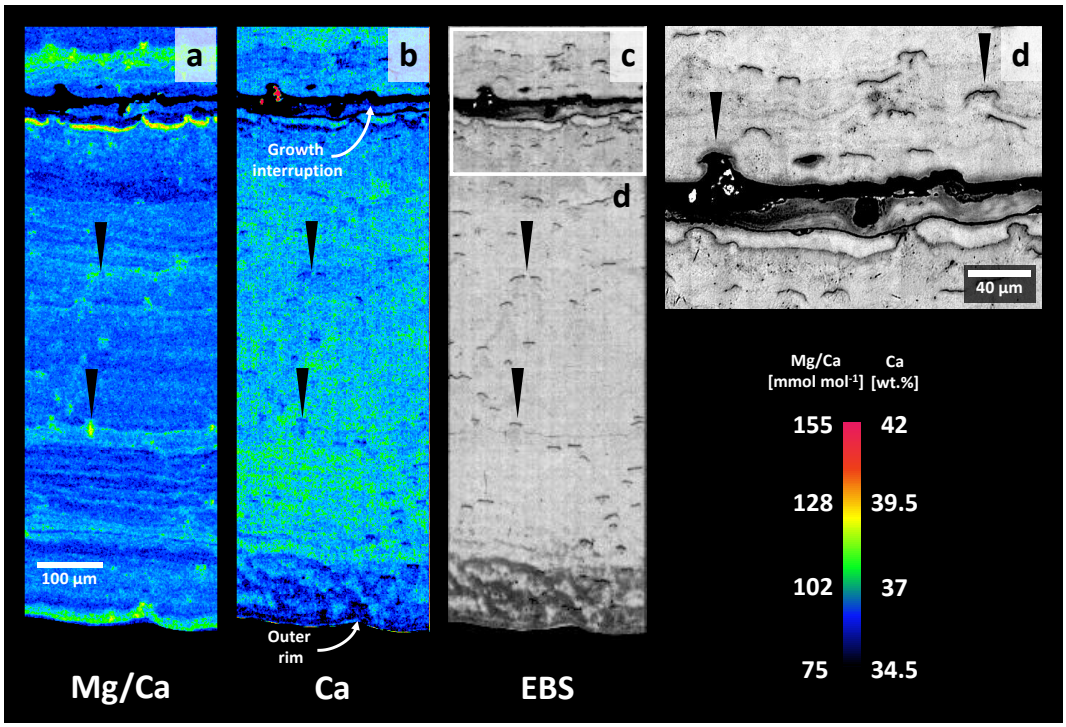

FIGURE 2.6: High resolution EMPA scans of the outermost 1 mm of a section of bamboo coral USNM 10496 from the Blake Plateau. The outer rim is towards the bottom of each figure. (a–c) Growth rings in Mg/Ca are interspersed with spots of high Mg/Ca starting at bands of low Ca concentrations and low density, which appear darker in the EBS figure (black arrowheads). (c) and (d) Low density bands are located at the base of fanlike structures that extend in growth direction. The left arrowhead in (d) shows an empty fanlike structure next to a growth interruption. (For interpretation of the references to colour in this figure legend, the reader is referred to the web version of this article.)

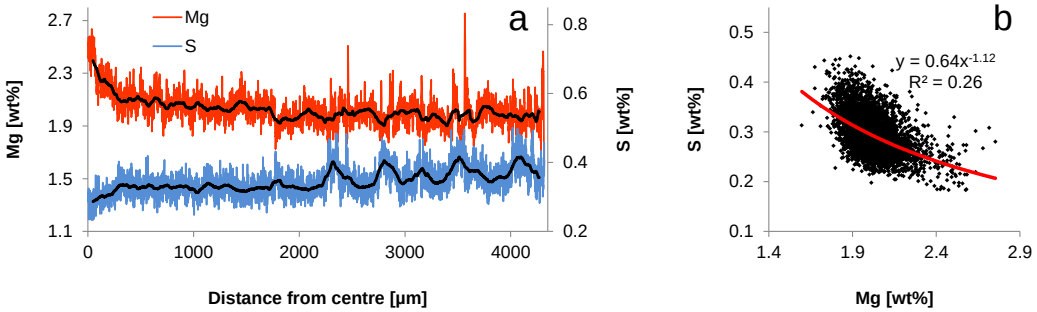

FIGURE 2.7: EMPA measurements of bamboo coral USNM 10496 from the Blake Plateau display an inverse distribution of Mg and S in the sample. The spatial covariation of the two elements (red and blue lines) and respective running means of 100 µm (black lines) are displayed in (a). (b) The cross plot of the Mg and S concentrations describes a weak inverse correlation using a power function for fitting. (For interpretation of the references to colour in this figure legend, the reader is referred to the web version of this article.)

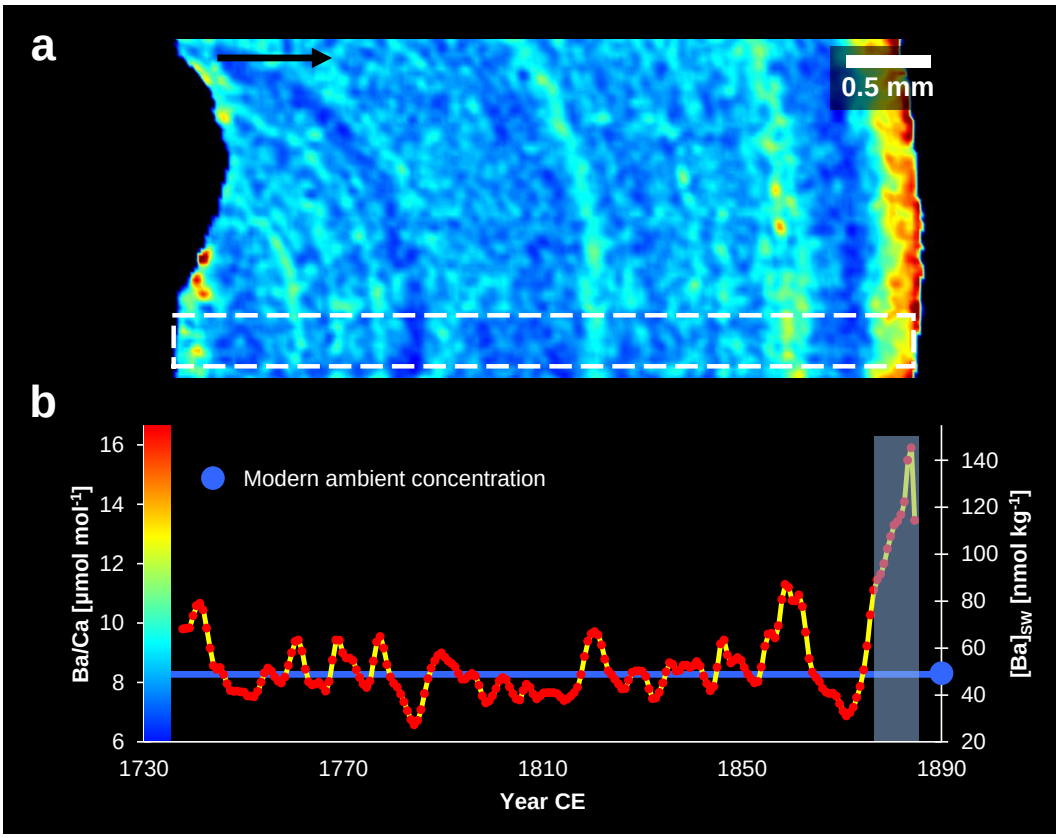

FIGURE 2.8: (a) Ba/Ca LA-ICP-MS mapping of bamboo coral USNM 10496 from the Blake Plateau of the same region where high resolution EMPA was done. (b) The mean of the 20 parallel Ba/Ca lines enclosed by the dashed rectangle was used to reconstruct the average seawater barium concentration during internode growth, using the calibration of LaVigne et al. (2011). The statistical error of the data in (b) is smaller than the symbol size. The blue line and blue dot in (b) show the recent $[Ba]_{SW}$ at the sampling site. The shaded bar in (b) denotes the region which was excluded from the reconstruction due to being a potential storage artefact. The black arrow in (a) shows growth direction. (For interpretation of the references to colour in this figure legend, the reader is referred to the web version of this article.)

measuring the time dropping from mean full signal intensity of ^{138}Ba on NIST 610 to one percent of it after laser shut off. This drop happened in less than 1.8 s; which corresponds to a distance the laser moved of about 45 µm.

2.5 Discussion

In the following we will discuss the use of Mg/Ca as a potential high-resolution temperature proxy, the capability of Ba/Ca to reliably record $[Ba]_{SW}$, and the limitations of both proxies in the bamboo coral we investigated. We will present a recommendation which part of the skeleton should be included in an environmental reconstruction. Finally, a schematic model for the ontogenetic origin of the observed micro-fan structures will be provided.

2.5.1 Calcification temperature reconstruction

Assuming that bamboo coral internode Mg/Ca reflects growth temperature, we estimate bottom water temperatures using the calibration of Thresher et al. (2016):

$$T\,(C) = -23.9\,(\pm 2.46) + 0.34\,(\pm 0.25) * \frac{Mg}{Ca}\left(mmol\ mol^{-1}\right) \tag{2.2}$$

The reconstructed bottom water temperatures (Fig. 2.5c) result in a mean of 7.5 °C ± 5.5 °C (2SD) while exhibiting a generally decreasing trend from the central axis outwards within the inner increment, around a mean of 8.4 ± 2.8 °C (2SD). The mean reconstructed temperature represented by the outer increment is 6.6 ± 3.6 °C (2SD), where no trend can be observed. Based on the ^{14}C age model (Section 2.7), the pronounced steplike shift in the mean reconstructed temperature occurred around 1800 (between 1755 and 1820) (Fig. 2.5). In addition to the broad patterns between the outer and inner increment, short-interval total Mg/Ca variability corresponds to reconstructed temperatures ranging between 2 and 20 °C. This unrealistically large temperature range indicates the need for a detailed analysis of the investigated material before high-resolution reconstructions can be attempted.

Before further statistical analysis of the reconstruction, two points must be addressed. First, we again note that the collection age of our specimen (1885) greatly predates any available hydrographic data. Thus, our comparison between these

reconstructed temperatures and modern hydrographic data is necessarily speculative. However, this comparison is still useful for illustrating how potential ontogenetic influences on Mg/Ca are manifest in temperature reconstructions. Second, some sections of the Mg/Ca data were excluded as shown in Fig. 2.5c. Similar to our observation, Thresher et al. (2007, 2010) and Sinclair et al. (2011) observed elevated Mg/Ca towards the centre of bamboo coral internodes. While anomalous geochemical behaviour near the central axis may relate to previous observations of amorphous calcium carbonate surrounding the central axis (Noé and Dullo, 2006; see Thresher et al., 2016), our specimen shows no amorphous calcium carbonate in the innermost part. This is indicated by the etched crystalline surface structure (Fig. 2.3a & b) and the absence of a peak typical for this calcium carbonate polymorph in the CRM spectra, while an amorphous precursor of the skeletal HMC can neither be verified nor excluded with our measurements. We nevertheless exclude this portion of the skeleton from the temperature reconstruction because of the absence of fanlike structures suggesting a change in calcification mode in that part of the skeleton (see also Noé and Dullo, 2006). This distinct central part with elevated Mg/Ca will be discussed separately below in Section 4.4. In addition to the central part, we excluded the band that showed a change in skeletal crystal structure (Fig. 2.3d), the material surrounding the growth interruption, the outermost rim and the high Mg/Ca fanlike structures (Fig. 2.6). All excluded regions showed anomalously elevated reconstructed temperatures of more than 15 °C. Peak temperatures of up to 20 °C were recorded close to the central axis and in proximity to a concentric crack in the sample, which are unlikely to represent true ambient temperatures given modern temperatures of 8 °C (Section 2.2). Despite the exclusion of these four regions, we emphasise that these sub-sections comprise only a small fraction of the specimen and the vast majority of the coral section (88 %) was considered (Fig. 2.5c). The mean Mg/Ca of the outer increment does not significantly change (α= 0.05, t-test) when removing the mentioned regions.

The mean reconstructed temperatures from the sample transect shown in Fig. 2.5c is 7 ± 3 °C (2SD). Although this is within uncertainty of the modern mean

bottom water temperature at our sampling site of about 8 °C (Lee and Waddell, 1983), a 1.5 °C warming of Florida Straits bottom water from 1900–2000 has been detected by Nagihara and Wang (2000) using borehole temperature measurements at the western margin of the Great Bahama Bank (Ocean Drilling Program Leg 166). If this warming trend is applicable to our coral specimen, then its Mg/Ca record appears slightly more favourable as a temperature proxy.

Taken at face value, Mg/Ca in our bamboo coral specimen suggests a total temperature variability of up to 8 °C. This exceeds the total temperature variability documented for the Blake Plateau (Lee and Waddell, 1983) by 4.1 °C, and from DWBC CTD casts spanning the years 2001–2017 off Abaco Island by 3.0 °C. One option is that the calibration of Thresher et al. (2016), which utilised bamboo coral specimens primarily originating from the southern hemisphere and included species other than *Keratoisis grayi*, is not appropriate for our specimen and/or for the high-resolution Mg/Ca mapping approach. Alternatively, the enhanced reconstructed temperature variability of our coral may not reflect calibration issues and instead may reflect physiological processes associated with octocoral growth. Aranha et al. (2014) documented similarly greater temperature variability recorded by skeletal Mg/Ca than in proximal instrumental measurements for Primnoa, another calcitic octocoral genus. A role for octocoral physiology in Mg/Ca is to some extent supported by findings from foraminifera despite expected differences in calcification, which for example leads to differential pH-regulation at the site of calcification in octocorals (e.g. Le Goff et al., 2017) and foraminifera (e.g. Nooijer et al., 2009). Similar to bamboo corals, foraminifera build a calcite skeleton and do not exhibit distinct centres of calcification, as are observed in aragonitic scleractinian coral skeletons (Adkins et al., 2003). Large Mg/Ca variations have been observed by LA-ICP-MS investigations in foraminifera (Eggins et al., 2003; Hathorne et al., 2003; Reichart et al., 2003; Hathorne et al., 2009; Sadekov et al., 2010; Nooijer et al., 2014; Spero et al., 2015), which may reflect light intensity (day/night cycles), calcifying reservoir depletion, the structural form of calcite, growth rate, authigenic surface coatings, and surficial as well as intra-shell organic matter. Although the majority of these

factors cannot yet be considered for bamboo corals given the paucity of information on bamboo coral physiology, our fluorescence and S/Ca data provides some constraints on whether organic matter contributes to bamboo coral Mg/Ca variations.

Our EMPA analysis for Mg/Ca was performed without pre-treatment for organic matter removal (such as dissolution in ethylenediaminetetraacetic acid (EDTA) and centrifugation; Thresher et al., 2016). Thus, our measurements cannot distinguish between calcitic and organically bound Mg. However, we discount a significant organic matter Mg contribution to this specimen because areas of enhanced fluorescence, which presumably represent increased organic matter contents, do not correspond to increased Mg; in fact, Mg and fluorescence appear to vary inversely (Appendix Fig. 2.10). The inverse variation of Mg and S will be discussed in detail in a separate section below (see section 4.3).

While our data suggest that organic matter content does not principally drive Mg/Ca variations in this bamboo coral specimen, given the high variability of reconstructed temperatures found above we recommend to further evaluate the comparability of bulk skeletal Mg/Ca calibrations with high-resolution reconstructions from single specimens. Ideally, modern high-resolution bamboo coral Mg/Ca records should be compared to modern oceanographic temperature records; this would reduce uncertainty from our comparison of Mg/Ca in a $\approx$ 140 year old coral with modern temperatures. Another option would be to compare reconstructed temperature records of other local calcifiers for which well-established temperature proxies exist with a bamboo coral Mg/Ca record grown in proximity to the sampling site. The reconstruction could be done with, e.g., Li/Mg (Montagna et al., 2014) or $\delta^{88/86}$Sr (Rüggeberg et al., 2008) in scleractinian corals or $\delta^{18}O$ shell in bivalves (e.g. Schöne et al., 2005). In addition, a comparison with another bamboo coral specimen of the same species and location is recommended to investigate the internal variability of the chemical composition (e.g. Thresher et al., 2007; 2010). Without any of these measures, a specimen-specific physiological non-linear response to temperature variation cannot be ruled out. Because of the low radial growth rate of bamboo corals, "core top" studies on live-collected coral skeletons as done by e.g. Thresher

et al. (2016) may offer a more practical option than long time culturing experiments. An improvement of the existing calibration might be realised by restricting the sampling area to the most recently grown material.

2.5.2 Potential infilling

The innermost 440 μm of the Mg/Ca data were excluded from the temperature considerations due to their high ratios leading to unrealistic bottom water temperatures. Several investigations mentioned a potential secondary infilling around the central axis in bamboo corals as an explanation for observed geochemical features in this region. Noé and Dullo (2006) found what they called amorphous calcite. Further, Sinclair et al. (2011) and Thresher et al. (2010) found a central increase in Mg/Ca. Radiocarbon (Farmer et al., 2015b; Thresher et al., 2016) and ^{210}Pb-based (Tracey et al., 2007; Andrews et al., 2009) investigations of growth rate report dates that are younger by the central axis than the surrounding, presumably ontogenetically younger calcite. The combination of anomalous dates and geochemical signatures led Farmer et al. (2015b) and Thresher et al. (2016) to conclude that the material surrounding the central axis may be precipitated after the initial internodal skeleton was built in some specimens, although it should be noted that this feature is not shared among all bamboo coral specimens (Thresher et al., 2004; Andrews et al., 2009; Thresher et al., 2010; Farmer et al., 2015b).

In addition to the infilling hypothesis, theoretical considerations and our experimental findings allow another explanation. We suggest that the observed feature might be a growth rate artefact. This is based on the gradual rather than abrupt shift in Mg/Ca around the central axis (Fig. 2.5c) accompanied with no major change in the crystallite structure in that part (Fig. 2.3b). If secondary infilling were present, we would rather expect a sharp contrast in composition and crystallite structure between the infilled and the primary material, which is not the case. In order to create the observed pattern of gradual change, the precipitation would have to start at exactly the same Mg/Ca as the skeleton and then successively change towards a

different composition, which seems unreasonable. Further, to the best of our knowledge there is no study published that describes living tissue in the central axis, while Alderslade and McFadden (2012) reported it to be filled with a transparent gelatinous material in a specimen of the bamboo coral subfamily *Keratoisidinae*. Given that no living coral tissue occupies the central axis, the infilling is highly unlikely to be actively produced by coral tissue. In that case the ions required for the precipitation of infilled calcite would need to be transported to the precipitation site through pores or channels in the nodes or internodes of this species, which were also not reported. To our knowledge, it has not yet been studied whether nodes seal the internodal axis or allow fluids to be exchanged. A strong argument against potential infilling is given by the observed chamber-forming walls across the central axis of the Isidid sub-family *Keratoisididae* (Tracey et al., 2007; Alderslade and McFadden, 2012). These walls would prevent mass transfer between chambers along the central axis and with that the supply of ions for precipitation of the secondary infilling.

Another way to test whether infilling occurs during specimen growth is to investigate the diameter of the internodes' central axis at different life stages of the animal. Tracey et al. (2007) observed an increase in diameter of the central axis towards the younger internodes for the bamboo coral genera *Keratoisis* and *Lepidisis*, which supports potential infilling with time. However, Alderslade and McFadden (2012) observe a progressive decrease in central axis diameter towards the younger internodes in the genus of Isidella. One explanation given by Tracey et al. (2007) for the increase was that it allows the growing coral to sway in the current to catch food particles. This does not necessarily imply that the diameter is changed after the internode was formed. It might be possible that new internodes are already initially built with a larger diameter of the central axis. To summarise, divergent observations of trends for central axis diameter along the main growth axis does not conclusively support or refute the infilling hypothesis.

A higher growth rate around the central axis would favour higher Mg/Ca through enhanced Mg partitioning at higher calcite precipitation rates. For example, such an effect was observed in bamboo corals in a subset of the investigated samples of

Thresher et al. (2016), and by measurements on coralline red algae conducted by Sletten et al. (2017), which contrasts with discrimination against Mg incorporation at higher precipitation rates in inorganic precipitation experiments (e.g. Gabitov et al., 2014a). Further, high precipitation rates surrounding the central axis may explain patterns of reduced $\delta^{18}O$ and $\delta^{13}C$ in the calcite surrounding the central axis of bamboo corals (Hill et al., 2011) through kinetic fractionation. We note that Hill et al. (2011) could not relate ^{14}C-derived growth rates to $\delta^{18}O$ and $\delta^{13}C$ fractionation; however these growth rates are constrained by relatively few data points and do not necessarily preclude higher growth rates in a small skeletal domain surrounding the central axis. Higher growth rates during early growth explain the anomalously young ^{14}C dates found near the central axis by Farmer et al., 2015b and Thresher et al. (2016) through two mechanisms. First, it should be noted that central axis ^{14}C dates are typically not significantly younger than surrounding dates (given the uncertainty of several decades on ^{14}C measurements), but rather fall within uncertainty of surrounding dates (Thresher, 2009; Farmer et al., 2015b) and thus do not exclude high growth rates near the central axis. According to the available ^{14}C data a linear growth rate was assumed but the uncertainty and resolution of the data can obviously not exclude small-scale nonlinear growth rates. Second, the ^{14}C deviations near the central axis could reflect increased incorporation of respired CO_2 during rapid skeletal formation, which is presumably younger than ambient seawater DIC that is otherwise used for bamboo coral calcification (Farmer et al., 2015b; Roark, 2005 and others). Although we cannot yet fully resolve whether the cause of the central anomaly is secondary infilling or a physiological process during early skeletal formation, we favour a physiological explanation given the gradual change in Mg/Ca alongside the distinct microstructural texture (Fig. 2.3) in the innermost part of our studied bamboo coral specimen. Further investigations on a larger set of adjacently grown bamboo corals and from multiple internodes of the same specimen would allow to shed more light on the observed feature.

2.5.3 Mg- and Ba-S relationship

Our EMPA results reveal a weak inverse relation of Mg to the distribution of S (Fig. 2.7), in agreement with earlier reports for the calcitic octocoral genus Corallium (Vielzeuf et al., 2013; Nguyen et al., 2014). Although we initially aimed to use S as an indicator of organic matter, its distribution turned out not to be related to organic content as indicated by comparison with CRM data. Instead, the S concentration seems to be inversely connected to processes driving the incorporation of Mg into the skeleton. Although elemental abundances show an inverse relation, the apparent correlation is not linear. The observed Mg/S relationship could be related to temperature or skeletal growth rate effects. We propose a temperature effect, since the skeletal Mg content seems to be mainly influenced by ambient seawater temperature and a growth rate effect, since the innermost part showing a Mg anomaly is assumed to grow faster. Furthermore, the incorporation of S has been linked to additional parameters. Based on infrared spectroscopy studies, it was found that S appears to substitute as sulfate for carbonate in the calcite lattice in bamboo coral internodes (Balan et al., 2017). These authors therefore postulated the ability of S in bamboo corals to record the sulfate concentrations in seawater. Also, an interaction between skeletal growth rate, carbonate ion concentration in the calcifying fluid and its reducing impact on the activity of sulfate ions was suggested by Nguyen et al. (2014) for the octocoral species Paracorallium japonicum. These authors found lower sulfur concentrations in skeletal portions secreted during warm seasons when the coral was growing fast. We speculate that the observed inverse correlation of Mg and S is related to growth rate; however this suggestion requires higher-resolution growth rate estimates than are currently available from ^{14}C.

The different spatial distributions of Ba/Ca and S/Ca in the sample transect suggest that the incorporation of Ba and S may not be coupled. A dominant control on Ba/S by barite ($BaSO_4$) can be excluded for stoichiometric reasons, given the large difference in mean skeletal concentration of Ba ($\approx$ 8 μmol mol^{-1}) and S ($\approx$ 9000 μmol mol^{-1}). However, since the cause(s) of elemental variation in bamboo coral skeletons (especially for S) are poorly studied, further investigations on the

environmental and physiological factors influencing Mg, Ba, and S incorporation into the skeleton are needed.

2.5.4 $[Ba]_{SW}$ reconstruction from Ba/Ca mapping

Ba concentrations in seawater can be estimated by applying the equation of LaVigne et al. (2011):

$$[Ba]_{SW}\left(nmol\,kg^{-1}\right) = \frac{\frac{Ba}{Ca}\left(\mu mol\,mol^{-1}\right) - 4.205\,(\pm 0.870)}{0.079\,(\pm 0.008)} \tag{2.3}$$

The reconstruction of $[Ba]_{SW}$ (Fig. 2.8b) is linearly related to Ba/Ca. $[Ba]_{SW}$ exhibits a mean value of 54 ± 37 nmol kg^{-1} (2SD) with a maximum 145.3 nmol kg^{-1} close to the rim.

For further detailed discussion on the reconstructed concentrations we restricted the dataset. LaVigne et al. (2011) used only the youngest outermost part of the skeleton for their calibration, allowing a comparison with recent instrumental $[Ba]_{SW}$ measurements. Our Ba/Ca data should be directly comparable to LaVigne et al. (2011) since both studies used unbleached bulk carbonate. In contrast, Thresher et al. (2016) excluded the innermost juvenile skeletal part from their calibration due to significantly elevated values, which were also found by Sinclair et al. (2011). However, we could not find any unusual values within this region but instead exclude the elevated values in the outer 250 μm (Fig. 2.8). Although the high Ba/Ca ratio found close to the rim might be a primary signal, these ratios are more likely an artefact of long-time storage in ethanol. For instance, Strzepek et al. (2014) found that 13 months of storage in ethanol elevated the Ba/Ca ratio of bamboo coral samples by 8 %, though the influence found was small and might have been related to a simple offset caused by the applied LA-ICP-MS method. Nevertheless, Strzepek et al. (2014) proposed that Ba had leached from the nodes and subsequently deposited on the internodes. The authors, however, provided no measure for the identification of potentially contaminated or altered material except by a higher Ba/Ca itself. LaVigne et al., 2011 did not mention whether their samples were stored in a preservative after sampling as our sample was. Since we cannot exclude a storage artefact as

suggested by the latter we refrain from interpreting the elevated Ba/Ca data of the outer 250 μm. From the remaining data we estimate a mean $[Ba]_{SW}$ for the coral's habitat of 50 ± 24 nmol kg^{-1} (2SD).

Evaluating our reconstructed $[Ba]_{SW}$ value with modern hydrographic data is hampered by the lack of data availability at the sampling region and water depth. However, we can approximate modern $[Ba]_{SW}$ with data from GEOTRACES section GA03 at around 800 m at 38.7° N and 69.1° W (Mawji et al., 2015). Though this is about 1300 km northeast of our sampling site, given the residence time of Ba in seawater on the order of about 10,000 years (Chan et al., 1976), the reported concentration of 48 nmol kg^{-1} is assumed to be representative for a broad region, including the sampling site. Our reconstructed mean estimate of 50 ± 24 nmol kg^{-1} (2SD), is in good agreement with the modern regional concentration. Since short term temporal variability of $[Ba]_{SW}$ is unknown from hydrographic data, we compare the variance with $[Ba]_{SW}$ from other oceanic regions. The total variability of our sample of $[Ba]_{SW}$ (27–89 nmol kg^{-1}) is larger than the range observed available in the GEOTRACES dataset between 80 and 60 °W in the upper 2000 m of the North Atlantic (i.e. $[Ba]_{SW}$ = 42–58 nmol kg^{-1})(Mawji et al., 2015). Since the reconstructed values exceed the range of recent oceanic concentrations, an influence of factors other than $[Ba]_{SW}$ on the skeletal Ba/Ca composition cannot be excluded.

We compared our Ba/Ca data with a record reported by Sinclair et al. (2011) from a bamboo coral sample from the Jacksonville Lithoherms, collected at 549 m depth about 40 km west of our sample location (Fig. 2.1b). While the reconstructed nutrient concentrations of our Florida Strait coral agree better with ambient $[Ba]_{SW}$ than Sinclair's Jacksonville Lithoherms sample, both data sets display a similar degree of variability. Sinclair et al. (2011) measured a mean skeletal Ba/Ca ratio of 12 ± 2 μmol mol^{-1} (2SD), which, using equations 2.3, translates to 102 ± 51 nmol kg^{-1} (2SD) $[Ba]_{SW}$. Our values are with a mean of about 8 μmol mol^{-1} nearly 30 % lower than the values reported for the Jacksonville Lithoherms specimen. A reason for the offset could be related to the growth of their coral closer to the shelf break, and some 250 m shallower than our specimen. At the eastern continental margin of Florida,

ground water is in contact with seawater until a water depth of at least 500 m (e.g. Hathaway et al., 1979; Kohout, 1965; Manheim and Paull, 1982). It is known that groundwater aquifers are enriched in adsorbed Ba which can be released by salt water intrusions (Shaw et al., 1998). We therefore speculate that the Sinclair sample may have been influenced by Ba leached from the Floridan limestone aquifer, leading to higher skeletal Ba/Ca values in their sample. The growth site of our sample might not have been affected by Baenriched seawater from this aquifer because of its greater depth of 805 m. Another reason for the observed offset could be that Sinclair et al. (2011) focused on the reproducibility of the measured Ba/Ca trends and not on their accuracy. Further could differing instrumental set ups and operational conditions have led to differing matrix effects. Hence, although the difference in mean Ba/Ca values of the samples may be due to a systematic measurement offset, the relative difference in estimated ambient water $[Ba]_{SW}$ could equally represent an environmental signal.

Our data show that skeletal Ba/Ca relates to mean ambient $[Ba]_{SW}$ levels. Our estimates are in good agreement with recent ambient instrumental values, supporting the use of bamboo corals as potential archives of ambient $[Ba]_{SW}$ levels over timescales of decades. The observed concentric Ba/Ca variation in our octocoral allows us to verify that the chosen sample transect for reconstruction is a representative selection on the sample section. This also resulted in an increase of statistical precision of the reconstructed $[Ba]_{SW}$ by being able to pool several data points for reconstruction. For a better understanding of the duration and timing of past concentration changes, a highresolution chronology is important. The variation of our $[Ba]_{SW}$ estimates cannot currently be evaluated in the light of actual environmental changes due to the age of our specimen and a lack of hydrographic $[Ba]_{SW}$ time series. Though high-resolution LA-ICP-MS sampling of skeletal Ba/Ca is a promising tool to understand short term variability in $[Ba]_{SW}$, further work on the potential impact of physiological processes on the Ba incorporation into bamboo corals is required. A future comparison of modern hydrographic $[Ba]_{SW}$ and Ba/Ca reconstructions from modern bamboo corals may better elucidate these potential

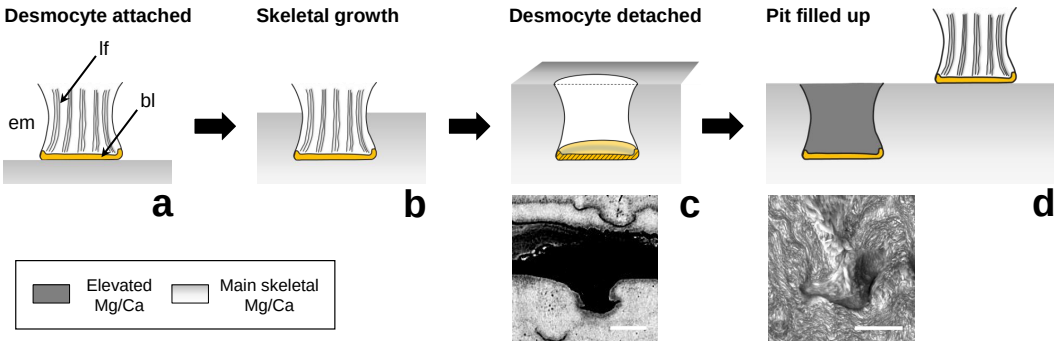

FIGURE 2.9: Possible explanation for the fan-shaped Mg/Ca anomalies seen after sample etching. (a) Desmocyte attached to the skeleton. (b) Calcite mineralisation around the desmocyte. (c) After detachment of the desmocyte, an empty fan-shaped pit remains with the organic basal lamina at its base. BSE picture in the lower half of (c) displays an empty fan next to a growth interruption (white bar = 20 μm). (d) The pit now fills with elevated Mg/Ca calcite meanwhile the tissue is connected to the skeleton by a desmocyte at a different site. The SE image in the lower panel shows the etched sample surface with an infilled fan (white bar = 10 μm). em = extracellular matrix, lf = long fibres, bl = basal organic layer.

impacts.

2.5.5 Ontogenetic limitations and growth model

One potential cause of variation expressed in isolated high-Mg/Ca features might be growth rate effects similar to those seen near the central axis, where Mg/Ca is most elevated. As shown by CRM- and EBS-imaging, high-Mg/Ca features always initiate at a short organic band from which a fan- or rivet-shaped feature develops (Figs. 2.3, 2.4, and 2.6). Fan-shaped or spherical arrangement of needlelike crystals so-called spherulitic structures which are typically associated with fast crystallite growth are ubiquitous in biogenic carbonates (e.g. Barnes, 1970; Cohen and McConnaughey, 2003). It must be pointed out that we use the term "fan-shaped" here as reference to the external shape only, not the internal crystallite arrangement which could not be investigated with the applied techniques.

Noé et al. (2007) describe fanlike crystallite arrangements in isidid skeletons which they call interfingering fascicles. We want to emphasise that these structures describe the bulk material around the here described fan-shapes but not the fans

themselves. Calcite fans called loculi have been found e.g. in the octoral genus *Plexaurella* (e.g. Bond et al., 2005; Lewis et al., 1992). Loculi are the only calcified parts of Plexaurella's otherwise organic skeleton which together with the shape of loculi seem to be a weak match to the features discussed here. More similar fan-shaped structures regarding surrounding skeletal material and shape are those embedded in the spherulitic crystal bundles described in calcitic sea fans (Ledger and Franc, 1978), but their origin has not yet been determined. Here we suggest a bamboo coral growth model that focuses on desmocytes, which are special cells observed in all three classes of cnidarian, and which connect the coral tissue to its calcareous skeleton (Muscatine et al., 1997). While Chapman (1969) suggested a development model of a desmocyte during growth in cnidarians, the authors did not focus on the carbonate skeleton in their model. Following these earlier observations, we propose a growth mechanism (Fig. 2.9) capable of explaining the observed chemical and morphological features of these fans.

Desmocytes link the coral tissue with the organic matrix of the skeleton via rod-like structures called fibrils and a basal lamina (Muscatine et al., 1997). While being attached to the skeletal surface, we infer that calcification occurs around the attached desmocyte. The surface of (dead) Isidid coral skeletons of the genus *Orstomisis* shows pits with diameters of about 50 μm (Bayer, 1990). Similar pits have also been shown for several genera like e.g. *Mopsea* or *Oparinisis* in the family of Isididae (Alderslade, 1998). Although similar features have not yet been reported in Isidids of genus *Keratoisis*, the basal diameters of these pits are within the length range of the observed low-Ca and high-fluorescence bands of the analysed *Keratoisis* sample (Figs. 2.4 and 2.6d). We propose that the observed bands are remains of the basal lamina and therefore represent sections of a three-dimensional cup-shaped structure. These structures could be left behind after calcification around the desmocyte reached a certain height (Fig. 2.9b) and the desmocyte is then detached by lowering the adhesion (Fig. 2.9c) (Muscatine et al., 1997). After detachment of the desmocyte the pit needs to be filled (Fig. 2.9d). As suggested by our fluorescence data (Fig.

2.4) and also by transmission electron microscopy images of stained and decalcified thin sections of a scleractinian coral (Goldberg, 2001), calcareous infilling of the attachment scar appears to incorporate remains of the organic basal lamina at its base. Alternatively, it was also suggested that desmocytes as a whole become mineralised into the skeleton (Muscatine et al., 1997). However, since fluorescence mapping shows only a thin bright band instead of a bright fanlike structure (Fig. 2.4), our geochemical data do not indicate the presence of an organic structure at this site and instead support the concept of desmocyte detachment proposed by Muscatine et al., 1997 for the scleractinian coral *Stylophora pistillata*. While we observed fanlike features in the majority of the skeleton, these are absent in the central-most part around the central axis. This is consistent with independent observations of fewer and less ordered desmocytes in fast growing areas of the scleractinian coral *Stylophora pistillata* (Tambutte et al., 2007). Also, Clode and Marshall (2002) suggest that since scleractinian desmocytes are not involved in the calcification process, they would not be present in high density in regions of fast calcification. Importantly, fanlike features are absent from the central region of elevated Mg/Ca ratios in our specimen (Fig. 2.3b), and we suggest that elevated growth rates in this area may cause elevated Mg/Ca.

As already mentioned by others (e.g. Thresher et al. (2010), see also Section 4.2), specimens were found in which the central growth axis of bamboo corals seems to be mineralised in a different way than the remaining part of the skeleton. For example, Farmer et al. (2015a) found an elevated boron isotopic composition and related it to ontogenetic variability in calcification rate. A different mode of growth was suggested by Sinclair et al. (2011) based on Ba and Mg anomalies around the central axis of a bamboo coral. Our sample does not show a Ba/ Ca anomaly in this region, although we found the lowest S concentrations of the sample there. Whatever the cause of the change in mineralisation is, our geochemical data suggest that the absence of fanlike structures (Fig. 2.3b) serves as one indicator for which parts of a bamboo coral should be avoided for Mg/Ca-temperature reconstructions. It has to be emphasised that in skeletal parts containing these structures only the material

surrounding the fanlike structures should be used since the structures themselves show an elevated Mg/Ca. In addition, we suggest that the fanlike structures may reflect desmocyte attachment throughout individual sample sections. Further investigations of the fan ultrastructure using scanning electron microscopy (SEM) with gold coated etched samples, ion microprobe (NanoSIMS) for elemental mapping or polarised microscopy of thin sections would be helpful to gain a more detailed view on their internal structure and formation mechanism.

2.6 Conclusion

Our data suggest that integrated Mg/Ca ratios in bamboo corals faithfully record mean growth temperature, whereas integrated Ba/Ca ratios reflect $[Ba]_{SW}$. However, we advise caution in interpreting high-resolution time series until reliable long-term time series information of these parameters becomes available for comparison to skeletal bamboo coral records. The reconstructed variability for all environmental parameters is larger than predicted from known recent environmental variations. This geochemical variability is most clearly expressed in isolated high-Mg/Ca skeletal features, which appear to be formed by rapid infilling of detached desmocyte spaces during biomineralisation, and a high Mg/Ca feature surrounding the central axis. The latter was not associated with anomalous Ba/Ca values. There is evidence that at least the Mg/Ca anomalies are related to locally elevated growth rates. To further improve existing calibrations for temperature and nutrient levels, we suggest to investigate the influence of growth rate and organic content on the incorporation of Mg and Ba into the skeleton of bamboo corals. In concert with a finely resolved chronology, this could lead to establish bamboo corals as high-resolution archives of ambient temperature and $[Ba]_{SW}$. The presented data emphasise the advantage of elemental mapping compared to point or line scans by allowing for choosing representative sections on the sample and improving statistical precision by pooling data. Further we show that bamboo coral skeletons exhibit isolated ontogenetic features that are geochemically distinct and can therefore be excluded for paleoenvironmental reconstructions. Although we found potential limitations for

highresolution environmental reconstruction on bamboo corals, these marine calcifiers remain promising candidates to serve as paleoenvironmental archives in the deeper ocean. Future studies on further specimens are needed to generalise our findings.

Acknowledgements

We thank Mario Thöner for help with the EMPA, Philip Alderslade, Jean-Pierre Cuif, Christopher Meinen, Dirk Nürnberg, and Rainer Zantopp for helpful discussions. The CTD data from east of the Bahamas are made freely available on the Atlantic Oceanographic and Meteorological Laboratory web page (`www.aoml.noaa.gov/phod/wbts/`) and are funded by the DOC-NOAA Climate Program Office-Ocean Observing and Monitoring Division, U.S.A. Funding was provided through the Helmholtz Research School on Ocean System Science and Technology (HOSST) and GEOMAR Helmholtz Centre for Ocean Research Kiel, Germany to S.F. Insightful and constructive reviews from three anonymous reviewers improved an earlier version of the manuscript. The associate editor Tom Marchitto is acknowledged for editorial handling and further constructive criticism. The data presented in this study are also available in digital format at `www.pangaea.de`.

2.7 Appendix

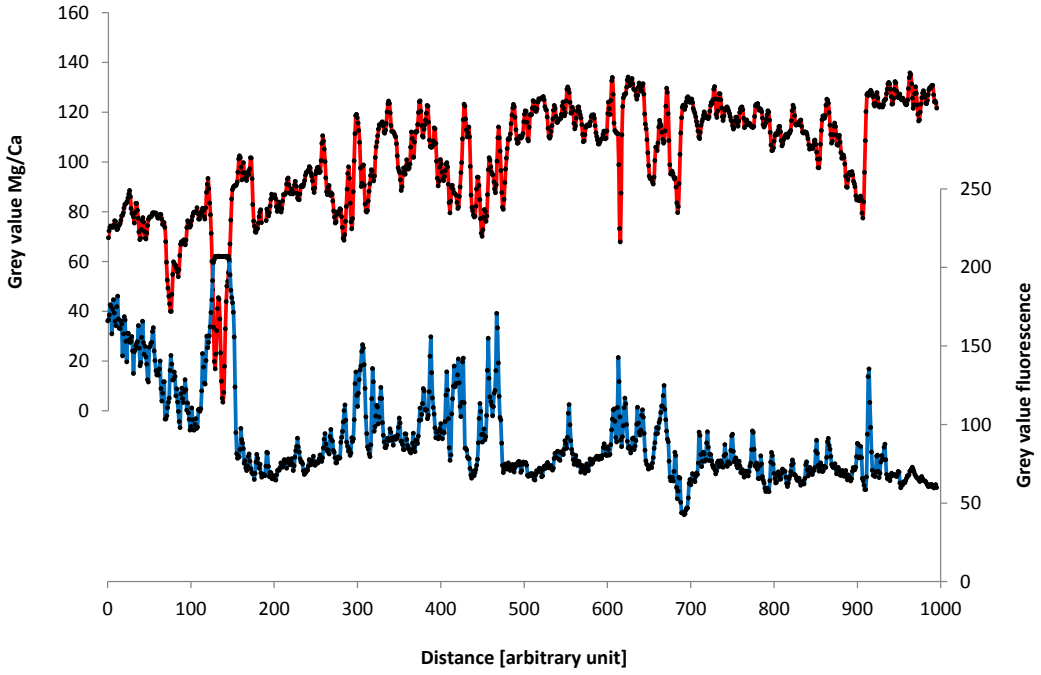

FIGURE 2.10: Fluorescence and Mg/Ca distribution on approximately the same bamboo coral sample section of USNM 10496 from the Blake Plateau indicate that Mg is not mainly contained in organic material compared to calcite indicated by a weak opposing variation. The signals shown are grey values obtained from Mg/Ca and fluorescence maps using ImageJ software (Schneider et al., 2012).

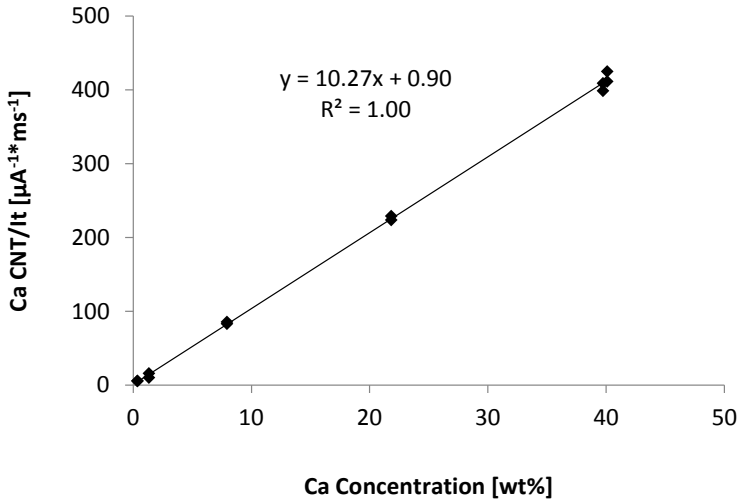

FIGURE 2.11: EMPA calibration for Ca with three silicate, two carbonate and one phosphate standard.

References

Adkins, J. F., E. A. Boyle, W. B. Curry, and A. Lutringer (2003). "Stable isotopes in deep-sea corals and a new mechanism for "vital effects"". In: *Geochimica Et Cosmochimica Acta* 67.6, pp. 1129–1143.

Alderslade, P. (1998). "Revisionary systematics in the gorgonian family Isididae, with descriptions of numerous new taxa (Coelenterata: Octocorallia)". In: *Records of the Western Australian Museum, supplement* 55.

Alderslade, P. and C. S. McFadden (2012). "A new genus and species of the family Isididae (Coelenterata: Octocorallia) from a CMAR Biodiversity study, and a discussion on the subfamilial placement of some nominal isidid genera". In: *Zootaxa* 3154, pp. 21–39.

Andrews, A. H., R. P. Stone, C. C. Lundstrom, and A. P. DeVogelaere (2009). "Growth rate and age determination of bamboo corals from the northeastern Pacific Ocean using refined 210Pb dating". In: *Marine Ecology Progress Series* 397, pp. 173–185.

Aranha, R., E. Edinger, G. Layne, and G. Piercey (2014). "Growth rate variation and potential paleoceanographic proxies in Primnoa pacifica: Insights from high-resolution trace element microanalysis". In: *Deep-Sea Research Part Ii-Topical Studies in Oceanography* 99, pp. 213–226.

Atkinson, L. P. (1983). "Distribution of Antarctic Intermediate Water over the Blake Plateau". In: *Journal of Geophysical Research-Oceans and Atmospheres* 88.Nc8, pp. 4699–4704.

Balan, E., J. Aufort, S. Pouillé, M. Dabos, M. Blanchard, M. Lazzeri, C. Rollion-Bard, and D. Blamart (2017). "Infrared spectroscopic study of sulfate-bearing calcite from deep-sea bamboo coral". In: *European Journal of Mineralogy* 29.3, pp. 397–408.

Barnes, D. J. (1970). "Coral skeletons: an explanation of their growth and structure". In: *Science* 170.3964, pp. 1305–1308.

Bayer, F. M. (1990). "A New Isidid Octocoral (Anthozoa, Gorgonacea) from New-Caledonia, with Descriptions of Other New Species from Elsewhere in the Pacific-Ocean". In: *Proceedings of the Biological Society of Washington* 103.1, pp. 205–228.

Bond, Z. A., A. L. Cohen, S. R. Smith, and W. J. Jenkins (2005). "Growth and composition of high-Mg calcite in the skeleton of a Bermudian gorgonian (Plexaurella dichotoma): Potential for paleothermometry". In: *Geochemistry Geophysics Geosystems* 6.8.

Bostock, H. C., D. M. Tracey, K. I. Currie, G. B. Dunbar, M. R. Handler, S. E. M. Fletcher, A. M. Smith, and M. J. M. Williams (2015). "The carbonate mineralogy and distribution of habitat-forming deep-sea corals in the southwest pacific region". In: *Deep-Sea Research Part I-Oceanographic Research Papers* 100, pp. 88–104.

Cairns, S. D. (2007). "Deep-water corals: An overview with special reference to diversity and distribution of deep-water Scleractinian corals". In: *Bulletin of Marine Science* 81.3, pp. 311–322.

Chan, L. H., J. M. Edmond, R. F. Stallard, W. S. Broecker, Y. C. Chung, R. F. Weiss, and T. L. Ku (1976). "Radium and barium at GEOSECS stations in the Atlantic and Pacific". In: *Earth and Planetary Science Letters* 32.2, pp. 258–267.

Chapman, D. M. (1969). "The nature of cnidarian desmocytes". In: *Tissue & Cell* 1.4, pp. 619–32.

Clode, P. L. and A. T. Marshall (2002). "Low temperature FESEM of the calcifying interface of a scleractinian coral". In: *Tissue Cell* 34.3, pp. 187–198.

Cohen, A. L. and T. A. McConnaughey (2003). "Geochemical perspectives on coral mineralization". In: *Biomineralization* 54.1, pp. 151–187.

Cuif, J. P., Y. Dauphin, J. Doucet, M. Salome, and J. Susini (2003). "XANES mapping of organic sulfate in three scleractinian coral skeletons". In: *Geochimica Et Cosmochimica Acta* 67.1, pp. 75–83.

Edinger, E. N., O. A. Sherwood, D. J. W. Piper, V. E. Wareham, K. D. Baker, K. D. Gilkinson, and D. B. Scott (2011). "Geological features supporting deep-sea coral habitat in Atlantic Canada". In: *Continental Shelf Research* 31.2, S69–S84.

Eggins, S., P. De Deckker, and J. Marshall (2003). "Mg/Ca variation in planktonic foraminifera tests: implications for reconstructing palaeo-seawater temperature and habitat migration". In: *Earth and Planetary Science Letters* 212.3, pp. 291–306.

Evans, D. and W. Müller (2013). "LA-ICPMS elemental imaging of complex discontinuous carbonates: An example using large benthic foraminifera". In: *Journal of Analytical Atomic Spectrometry* 28.7, pp. 1039–1044.

Farmer, J. R., B. Hönisch, L. F. Robinson, and T. M. Hill (2015a). "Effects of seawater-pH and biomineralization on the boron isotopic composition of deep-sea bamboo corals". In: *Geochimica Et Cosmochimica Acta* 155, pp. 86–106.

Farmer, J. R., L. F. Robinson, and B. Hönisch (2015b). "Growth rate determinations from radiocarbon in bamboo corals (genus Keratoisis)". In: *Deep-Sea Research Part I-Oceanographic Research Papers* 105, pp. 26–40.

Fietzke, J. and M. Frische (2016). "Experimental evaluation of elemental behavior during LA-ICP-MS: influences of plasma conditions and limits of plasma robustness". In: *Journal of Analytical Atomic Spectrometry* 31.1, pp. 234–244.

Fietzke, J., F. Ragazzola, J. Halfar, H. Dietze, L. C. Foster, T. H. Hansteen, A. Eisenhauer, and R. S. Steneck (2015). "Century-scale trends and seasonality in pH and temperature for shallow zones of the Bering Sea". In: *Proc Natl Acad Sci U S A* 112.10, pp. 2960–2965.

Filippelli, G. M. (2011). "Phosphate rock formation and marine phosphorus geochemistry: the deep time perspective". In: *Chemosphere* 84.6, pp. 759–66.

Frenkel, M. M., M. LaVigne, H. R. Miller, T. M. Hill, A. McNichol, and M. L. Gaylord (2017). "Quantifying bamboo coral growth rate nonlinearity with the radiocarbon bomb spike: A new model for paleoceanographic chronology development". In: *Deep-Sea Research Part I-Oceanographic Research Papers* 125, pp. 26–39.

Gabitov, R. I., A. Sadekov, and A. Leinweber (2014a). "Crystal growth rate effect on Mg/Ca and Sr/Ca partitioning between calcite and fluid: An in situ approach". In: *Chemical Geology* 367, pp. 70–82.

Goldberg, W. M. (2001). "Desmocytes in the calicoblastic epithelium of the stony coral Mycetophyllia reesi and their attachment to the skeleton". In: *Tissue Cell* 33.4, pp. 388–94.

Guinotte, J. M., J. Orr, S. Cairns, A. Freiwald, L. Morgan, and R. George (2006). "Will human-induced changes in seawater chemistry alter the distribution of deep-sea scleractinian corals?" In: *Frontiers in Ecology and the Environment* 4.3, pp. 141–146.

Hathaway, J. C., C. W. Poag, P. C. Valentine, F. T. Manheim, F. A. Kohout, M. H. Bothner, R. E. Miller, D. M. Schultz, and D. A. Sangrey (1979). "U.S. Geological survey core drilling on the atlantic shelf". In: *Science* 206.4418, pp. 515–27.

Hathorne, E. C., O. Alard, R. H. James, and N. W. Rogers (2003). "Determination of intratest variability of trace elements in foraminifera by laser ablation inductively coupled plasma-mass spectrometry". In: *Geochemistry Geophysics Geosystems* 4.12, pp. 1–14.

Hathorne, E. C., R. H. James, and R. S. Lampitt (2009). "Environmental versus biomineralization controls on the intratest variation in the trace element composition of the planktonic foraminifera G. inflata and G. scitula". In: *Paleoceanography* 24.

Hill, T. M., H. J. Spero, T. Guilderson, M. LaVigne, D. Clague, S. Macalello, and N. Jang (2011). "Temperature and vital effect controls on bamboo coral (Isididae) isotope geochemistry: A test of the "lines method"". In: *Geochemistry Geophysics Geosystems* 12.4.

Hill, T. M., C. R. Myrvold, H. J. Spero, and T. P. Guilderson (2014). "Evidence for benthic-pelagic food web coupling and carbon export from California margin bamboo coral archives". In: *Biogeosciences* 11.14, pp. 3845–3854.

Jahnke, R. and J. Blanton (2010). "The Gulf Stream". In: *Carbon and Nutrient Fluxes in Continental Margins: A Global Synthesis*. Ed. by K. Liu, L. Atkinson, R. Quinones, and L. Talaue-McManus. Springer.

Kashgarian, M. and N. Tanaka (1991). "Antarctic Intermediate Water Intrusion into South-Atlantic Bight Shelf Waters". In: *Continental Shelf Research* 11.2, pp. 197–201.

Kimball, J. B., R. B. Dunbar, and T. P. Guilderson (2014). "Oxygen and carbon isotope fractionation in calcitic deep-sea corals: Implications for paleotemperature reconstruction". In: *Chemical Geology* 381, pp. 223–233.

Kohout, F. A. (1965). "Section of Geological Sciences: A Hypothesis Concerning Cyclic Flow of Salt Water Related to Geothermal Heating in the Floridan aquifer". In: *Transactions of the New York Academy of Sciences* 28.2 Series II, pp. 249–271.

LaVigne, M., T. M. Hill, H. J. Spero, and T. P. Guilderson (2011). "Bamboo coral Ba/Ca: Calibration of a new deep ocean refractory nutrient proxy". In: *Earth and Planetary Science Letters* 312.3-4, pp. 506–515.

Le Goff, C., E. Tambutte, A. A. Venn, N. Techer, D. Allemand, and S. Tambutte (2017). "In vivo pH measurement at the site of calcification in an octocoral". In: *Sci Rep* 7.1, p. 11210.

Ledger, P. W. and S. Franc (1978). "Calcification of the collagenous axial skeleton of Veretillum cynomorium pall. (Cnidaria: Pennatulacea)". In: *Cell Tissue Res* 192.2, pp. 249–66.

Lee, T. N. and E. Waddell (1983). "On Gulf-Stream Variability and Meanders over the Blake Plateau at 30-Degrees-N". In: *Journal of Geophysical Research-Oceans and Atmospheres* 88.Nc8, pp. 4617–4631.

Levin, L. A. and N. Le Bris (2015). "The deep ocean under climate change". In: *Science* 350.6262, pp. 766–768.

Lewis, J. C., T. F. Barnowski, and G. J. Telesnicki (1992). "Characteristics of Carbonates of Gorgonian Axes (Coelenterata, Octocorallia)". In: *Biological Bulletin* 183.2, pp. 278–296.

Locarnini, R., A. Mishonov, J. I. Antonov, T. P. Boyer, H. E. Garcia, O. K. Baranova, M. M. Zweng, C. R. Paver, J. R. Reagan, D. R. Johnson, M. Hamilton, and D. Seidov (2013). "World Ocean Atlas 2013, Volume 1: Temperature". In: *NOAA Atlas NESDIS*. Ed. by S. Levitus and A. Mishonov. Vol. 73, p. 40.

Manheim, F. T. and C. K. Paull (1982). "Patterns of Groundwater Salinity Changes in A Deep Continental-Oceanic Transect off the Southeastern Atlantic Coast of

the U.S.A". In: *Symposium on Geochemistry of Groundwater - 26th International Geological Congress, Paris, 1980*. Ed. by W. Back and R. Létolle. Vol. 16. Developments in Water Science. Elsevier, pp. 95–105.

Mawji, E. et al. (2015). "The GEOTRACES Intermediate Data Product 2014". In: *Marine Chemistry* 177, pp. 1–8.

Milliman, J. D., O. H. Pilkey, and D. A. Ross (1972). "Sediments of the Continental Margin off the Eastern United States". In: *Geological Society of America Bulletin* 83.5, p. 1315.

Montagna, P., M. McCulloch, E. Douville, M. Lopez Correa, J. Trotter, R. Rodolfo-Metalpa, D. Dissard, C. Ferrier-Pages, N. Frank, A. Freiwald, S. Goldstein, C. Mazzoli, S. Reynaud, A. Ruggeberg, S. Russo, and M. Taviani (2014). "Li/Mg systematics in scleractinian corals: Calibration of the thermometer". In: *Geochimica Et Cosmochimica Acta* 132.0, pp. 288–310.

Muscatine, L., E. Tambutte, and D. Allemand (1997). "Morphology of coral desmocytes, cells that anchor the calicoblastic epithelium to the skeleton". In: *Coral Reefs* 16.4, pp. 205–213.

Nagihara, S. and K. Wang (2000). "Century-scale variation of seafloor temperatures inferred from offshore borehole geothermal data". In: *Proceedings of the Ocean Drilling Program, Scientific Results* 166.

Nguyen, L. T., M. A. Rahman, T. Maki, Y. Tamenori, T. Yoshimura, A. Suzuki, N. Iwasaki, and H. Hasegawa (2014). "Distribution of trace element in Japanese red coral Paracorallium japonicum by mu-XRF and sulfur speciation by XANES: Linkage between trace element distribution and growth ring formation". In: *Geochimica Et Cosmochimica Acta* 127, pp. 1–9.

Noé, S. U. and W. C. Dullo (2006). "Skeletal morphogenesis and growth mode of modern and fossil deep-water isidid gorgonians (Octocorallia) in the West Pacific (New Zealand and Sea of Okhotsk)". In: *Coral Reefs* 25.3, pp. 303–320.

Noé, S. U., L. Lembke-Jene, and W. C. Dullo (2007). "Varying growth rates in bamboo corals: sclerochronology and radiocarbon dating of a mid-Holocene deep-water gorgonian skeleton (Keratoisis sp.: Octocorallia) from Chatham Rise (New Zealand)". In: *Facies* 54.2, pp. 151–166.

Nooijer, L. J. de, T. Toyofuku, and H. Kitazato (2009). "Foraminifera promote calcification by elevating their intracellular pH". In: *Proc Natl Acad Sci U S A* 106.36, pp. 15374–8.

Nooijer, L. J. de, E. C. Hathorne, G. J. Reichart, G. Langer, and J. Bijma (2014). "Variability in calcitic Mg/Ca and Sr/Ca ratios in clones of the benthic foraminifer Ammonia tepida". In: *Marine Micropaleontology* 107, pp. 32–43.

Oppelt, A., M. López Correa, and C. Rocha (2017). "Biogeochemical analysis of the calcification patterns of cold-water corals Madrepora oculata and Lophelia pertusa along contact surfaces with calcified tubes of the symbiotic polychaete Eunice norvegica: Evaluation of a 'mucus' calcification hypothesis". In: *Deep Sea Research Part I: Oceanographic Research Papers* 127, pp. 90–104.

Palter, J. B. (2015). "The role of the Gulf Stream in European climate". In: *Ann Rev Mar Sci* 7, pp. 113–37.

Pratt, R. M. (1963). "Bottom Currents on the Blake-Plateau". In: *Deep-Sea Research* 10.3, pp. 245–249.

Pratt, R. M. and P. F. McFarlin (1966). "Manganese pavements on the blake plateau". In: *Science* 151.3714, pp. 1080–1082.

Prouty, N. G., E. B. Roark, N. A. Buster, and S. W. Ross (2011). "Growth rate and age distribution of deep-sea black corals in the Gulf of Mexico". In: *Marine Ecology Progress Series* 423, pp. 101–115.

Reed, J. K., D. C. Weaver, and S. A. Pomponi (2006). "Habitat and fauna of deep-water Lophelia pertusa coral reefs off the southeastern U.S.: Blake plateau, Straits of Florida, and Gulf of Mexico". In: *Bulletin of Marine Science* 78.2, pp. 343–375.

Reichart, G.-J., F. Jorissen, P. Anschutz, and P. R. Mason (2003). "Single foraminiferal test chemistry records the marine environment". In: *Geology* 31.4, pp. 355–358.

Rüggeberg, A., J. Fietzke, V. Liebetrau, A. Eisenhauer, W. C. Dullo, and A. Freiwald (2008). "Stable strontium isotopes (δ88/86Sr) in cold-water corals — A new proxy for reconstruction of intermediate ocean water temperatures". In: *Earth and Planetary Science Letters* 269.3-4, pp. 570–575.

Roark, E. B. (2005). "Radiocarbon-based ages and growth rates of bamboo corals from the Gulf of Alaska". In: *Geophysical Research Letters* 32.4.

Robinson, L. F., J. F. Adkins, N. Frank, A. C. Gagnon, N. G. Prouty, E. B. Roark, and T. van de Flierdt (2014). "The geochemistry of deep-sea coral skeletons: A review of vital effects and applications for palaeoceanography". In: *Deep-Sea Research Part Ii-Topical Studies in Oceanography* 99, pp. 184–198.

Ruhl, H. A. and J. Smith K. L. (2004). "Shifts in deep-sea community structure linked to climate and food supply". In: *Science* 305.5683, pp. 513–515.

Sadekov, A. Y., S. M. Eggins, G. P. Klinkhammer, and Y. Rosenthal (2010). "Effects of seafloor and laboratory dissolution on the Mg/Ca composition of Globigerinoides sacculifer and Orbulina universa tests — A laser ablation ICPMS microanalysis perspective". In: *Earth and Planetary Science Letters* 292.3, pp. 312–324.

Saenger, C., R. I. Gabitov, J. Farmer, J. M. Watkins, and R. Stone (2017). "Linear correlations in bamboo coral $\delta^{13}C$ and $\delta^{18}O$ sampled by SIMS and micromill: Evaluating paleoceanographic potential and biomineralization mechanisms using $\delta^{11}B$ and Δ_{47} composition". In: *Chemical Geology* 454, pp. 1–14.

Schiff, J. T., F. C. Batista, O. A. Sherwood, T. P. Guilderson, T. M. Hill, A. C. Ravelo, K. W. McMahon, and M. D. McCarthy (2014). "Compound specific amino acid δ13C patterns in a deep-sea proteinaceous coral: Implications for reconstructing detailed δ13C records of exported primary production". In: *Marine Chemistry* 166, pp. 82–91.

Schlitzer, R. (2018). "Ocean Data View, https://odv.awi.de". In:

Schöne, B. R., M. Pfeiffer, T. Pohlmann, and F. Siegismund (2005). "A seasonally resolved bottom-water temperature record for the period AD 1866-2002 based on shells ofArctica islandica (Mollusca, North Sea)". In: *International Journal of Climatology* 25.7, pp. 947–962.

Schneider, C. A., W. S. Rasband, and K. W. Eliceiri (2012). "NIH Image to ImageJ: 25 years of image analysis". In: *Nat Methods* 9.7, pp. 671–675.

Serrato Marks, G., M. LaVigne, T. M. Hill, W. Sauthoff, T. P. Guilderson, E. B. Roark, R. B. Dunbar, and T. J. Horner (2017). "Reproducibility of Ba/Ca variations recorded by northeast Pacific bamboo corals". In: *Paleoceanography* 32.9, pp. 966–979.

Shaw, T. J., W. S. Moore, J. Kloepfer, and M. A. Sochaski (1998). "The flux of barium to the coastal waters of the southeastern USA: The importance of submarine groundwater discharge". In: *Geochimica et Cosmochimica Acta* 62.18, pp. 3047–3054.

Sherwood, O. A. and M. J. Risk (2007). "Chapter Twelve Deep-Sea Corals: New Insights to Paleoceanography". In: *Developments in Marine Geology*. Ed. by H. Claude and V. Anne De. Vol. Volume 1. Elsevier, pp. 491–522.

Sherwood, O. A., R. E. Thresher, S. J. Fallon, D. M. Davies, and T. W. Trull (2009). "Multi-century time-series of 15N and 14C in bamboo corals from deep Tasmanian seamounts: evidence for stable oceanographic conditions". In: *Marine Ecology Progress Series* 397, pp. 209–218.

Sinclair, D. J., B. Williams, G. Allard, B. Ghaleb, S. Fallon, S. W. Ross, and M. Risk (2011). "Reproducibility of trace element profiles in a specimen of the deep-water bamboo coral Keratoisis sp." In: *Geochimica Et Cosmochimica Acta* 75.18, pp. 5101–5121.

Sletten, H. R., D. P. Gillikin, J. Halfar, C. F. T. Andrus, and H. M. Guzman (2017). "Skeletal growth controls on Mg/Ca and P/Ca ratios in tropical Eastern Pacific rhodoliths (coralline red algae)". In: *Chemical Geology* 465, pp. 1–10.

Spero, H. J., S. M. Eggins, A. D. Russell, L. Vetter, M. R. Kilburn, and B. Honisch (2015). "Timing and mechanism for intratest Mg/Ca variability in a living planktic foraminifer". In: *Earth and Planetary Science Letters* 409, pp. 32–42.

Strzepek, K. M., R. E. Thresher, A. T. Revill, C. I. Smith, A. F. Komugabe, and S. F. Fallon (2014). "Preservation effects on the isotopic and elemental composition

of skeletal structures in the deep-sea bamboo coral Lepidisis spp. (Isididae)". In: *Deep-Sea Research Part Ii-Topical Studies in Oceanography* 99, pp. 199–206.

Tambutte, E., D. Allemand, D. Zoccola, A. Meibom, S. Lotto, N. Caminiti, and S. Tambutte (2007). "Observations of the tissue-skeleton interface in the scleractinian coral Stylophora pistillata". In: *Coral Reefs* 26.3, pp. 517–529.

Thresher, R., S. R. Rintoul, J. A. Koslow, C. Weidman, J. Adkins, and C. Proctor (2004). "Oceanic evidence of climate change in southern Australia over the last three centuries". In: *Geophysical Research Letters* 31.7, pp. 1–4.

Thresher, R. E. (2009). "Environmental and compositional correlates of growth rate in deep-water bamboo corals (Gorgonacea; Isididae)". In: *Marine Ecology Progress Series* 397, pp. 187–196.

Thresher, R. E. and H. Neil (2016). "Scale dependence of environmental and physiological correlates of δ18O and δ13C in the magnesium calcite skeletons of bamboo corals (Gorgonacea; Isididae)". In: *Geochimica et Cosmochimica Acta* 187, pp. 260–278.

Thresher, R. E., C. M. MacRae, N. C. Wilson, and R. Gurney (2007). "Environmental effects on the skeletal composition of deep-water Gorgonians (Keratoisis spp.; Isididae)". In: *Bulletin of Marine Science* 81.3, pp. 409–422.

Thresher, R. E., N. C. Wilson, C. M. MacRae, and H. Neil (2010). "Temperature effects on the calcite skeletal composition of deep-water gorgonians (Isididae)". In: *Geochimica Et Cosmochimica Acta* 74.16, pp. 4655–4670.

Thresher, R. E., S. J. Fallon, and A. T. Townsend (2016). "A "core-top" screen for trace element proxies of environmental conditions and growth rates in the calcite skeletons of bamboo corals (Isididae)". In: *Geochimica Et Cosmochimica Acta* 193, pp. 75–99.

Tracey, D. M., H. Neil, P. Marriott, A. H. Andrews, G. M. Cailliet, and J. A. Sanchez (2007). "Age and growth of two genera of deep-sea bamboo corals (family Isididae) in New Zealand waters". In: *Bulletin of Marine Science* 81.3, pp. 393–408.

Vielzeuf, D., J. Garrabou, A. Gagnon, A. Ricolleau, J. Adkins, D. Gunther, K. Hametner, J. L. Devidal, E. Reusser, J. Perrin, and N. Floquet (2013). "Distribution of sulphur and magnesium in the red coral". In: *Chemical Geology* 355, pp. 13–27.

Wall, M. and G. Nehrke (2012). "Reconstructing skeletal fiber arrangement and growth mode in the coral Porites lutea (Cnidaria, Scleractinia): a confocal Raman microscopy study". In: *Biogeosciences* 9.11, pp. 4885–4895.

3 Incorporation of Na and S in calcitic octocoral skeletons

3.1 Abstract

Ocean environmental conditions might be reflected in the skeletal composition of bamboo corals. The high magnesium calcite internodes of these long living octocorals may therefore represent a potential archive for seawater properties such as salinity or temperature where instrumental time series are absent. To extend these time series into the past using a natural archive the influences on the skeletal composition has to be investigated. Since skeletal Na and S concentrations have been proposed as environmental proxies, we mapped the spatial distribution and concentration of these elements in two Atlantic specimens of *Keratoisis grayi* (family Isididae) with a resolution of four micrometre. The mean distribution coefficient of Na for the two Atlantic samples was within 2.5 and 2.8*10^{-4}, while that of S shows a similar depletion with 2.2 and 2.3*10^{-4}, hence in the range of inorganic calcite precipitation experiments. The two elements show an inverse correlation in bamboo coral skeletons. Based on the spatial variations along growth rings an exclusive control of environmental factors on the element distribution can be discarded. We further exclude Rayleigh fractionation, ion specific pumping and Ca-proton exchange as the driver of Na and S distribution in bamboo corals. Instead, we propose a calcification model based on Ca pumping and bicarbonate active transport. This model is able to explain the observed distribution of Na and S in the skeleton without the involvement of skeletal organic matter. Nevertheless, organic matter might play a minor role especially for the microscale patterns along growth rings. Although

the skeletal Na and S composition is seemingly largely driven by the coral physiology, the distribution coefficient similar to inorganic calcites indicate the potential for bamboo corals to record environmental conditions.

3.2 Introduction

The elemental composition incorporated into the skeletons of deep sea corals may hold vital information about deep water environmental conditions over decadal to centennial timescales and depth where instrumental records are missing (Robinson et al., 2014). It is key to assess if and how sensitively a reconstructed geochemical signature responds to external environmental conditions, whether it is merely controlled by internal physiological processes, or a combination of both internal and external controls. For this purpose, the calcification process of the skeleton and its influence on the elemental composition needs to be fully understood. The advantage of using bamboo corals as environmental proxy recorders are their long life span of up to 300 years (Andrews et al., 2009; Hill et al., 2011), their fixed growth location on hardgrounds and the wide habitat depth range of less than 10 to over 3000 m (Bostock et al., 2015; Thresher et al., 2016). Closer investigation of the geochemical controls over cold-water coral growth is not only important for further developing deep water corals as environmental proxy archives. Knowledge of their calcification mechanism with regard to environmental demands is important in view of likely future changes to evaluate their susceptibility to ocean acidification, warming or deoxygenation (Roberts et al., 2016b).

Sodium as the most abundant cation in the ocean has a concentration of 0.486 mol kg^{-1} at a salinity of 35 (Millero, 2014) and a mean residence time of $44*10^6$ years (Lecuyer, 2016), while sulfur is the second most abundant anion with a concentration of 0.03 mol kg^{-1} (Millero, 2014) and a mean residence time of $9*10^6$ years (Lecuyer, 2016). The incorporation of Na and S into biogenic and abiogenic calcite was found to be dependent on several factors. Studies on biogenic calcite reported a relationship of skeletal Na/Ca to seawater salinity for several recent calcifying species. The clearest indication into this direction comes from recent studies

on foraminifera. A positive salinity-Na/Ca correlation was observed by Wit et al. (2013), Allen et al. (2016), and Mezger et al. (2016), as well as Bertlich et al. (2018), and Geerken et al. (2018). Apart from foraminifera, other species were also found to show a positive Na/Ca correlation with salinity. Gordon et al. (1970) presented similar findings from barnacle shells, while brachiopods may also hold potential for recording seawater salinity (Rollion-Bard et al., 2019.

Skeletal sodium concentrations were also explained by a variety of other factors than salinity. According to Hauzer et al. (2018), the Na/Ca ratio in tests of the foraminifera Operculina ammonoides is positively correlated with Na/Ca ratio of seawater which does not vary with salinity. Iglikowska et al. (2018) found an inverse correlation between Na/Ca ratios and barnacle size. Also, acidification was found to raise the shell Na/Ca ratio of the bivalve Mytilus edulis by Zhao et al. (2017), while Ballesta-Artero et al. (2018) suggested that the Na/Ca ratio is influenced by growth rate for the same species.

Inorganic precipitation experiments on the incorporation of Na into calcite were conducted by Kitano et al. (1975) and Okumura and Kitano (1986), who found the Na/Ca ratio to be influenced by Na content of the parent solution. Similarly to these studies, Ishikawa and Ichikuni (1984) found the Na/Ca ratio of the precipitate to rise with increased Na content in the parent solution. Nevertheless, the Na/Ca ratio reaches saturation in the calcite phase at about 0.2 mol L^{-1} aqueous Na, hence below seawater concentrations. Crystal growth rate was found to be the driver of Na incorporation in the experimental setup of Busenberg and Niel Plummer (1985) resulting in a positive correlation.

Although representing a different mineralogy, studies on Na/Ca in biogenic aragonite (e.g. Mitsuguchi and Kawakami, 2012; Mitsuguchi et al., 2010; Rollion-Bard and Blamart, 2015) found incorporation by lattice defects or ion adsorption, and kinetic effects as possible explanations for increased Na incorporation.

The incorporation of S into biogenic calcite is less well understood to date. The amount of sulfur incorporated in biogenic calcite appears to be influenced by the carbonate chemistry of the calcifying solution (Dijk et al., 2019; Dijk et al., 2017) and

organic matrix association (e.g. Dauphin, 2006; Geerken et al., 2019; Glock et al., 2019; Nguyen et al., 2014; Vielzeuf et al., 2013; Yoshimura et al., 2019). Although sulfur can be associated with organic compounds in biogenic calcite, it has equally been suggested to be present in inorganic form as so-called structurally substituted sulfur (e.g. Balan et al., 2017; Cusack et al., 2008; Fichtner et al., 2018; Nguyen et al., 2014; Perrin et al., 2017; Pingitore et al., 1995; Takano, 1985; Tamenori et al., 2014).

Precipitation experiments on inorganic calcite formation found less sulfur to be incorporated with rising sodium in precipitation solution (Kitano et al., 1975), but a rising sulfur content with higher solution sulfate concentration until a saturation level in calcite on the order of four to five % given as the S/Ca atomic ratio was reached (Okumura et al., 2018). Calcite crystal growth rate was found to be one driver of sulfate incorporation in the precipitation experiments of Busenberg and Niel Plummer (1985). Conversely, Wynn et al. (2018) reported that pH is the main driver of sulfate incorporation followed by increased incorporation with rising precipitation rates due to defect site incorporation.

In this study, we investigate the Na/Ca and S/Ca spatial distribution in the skeleton of two bamboo corals of the genus *Keratoisis*. We used high-resolution element mapping techniques (LA-ICPMS and EMPA) combined with Raman spectroscopy to gain insight to potential processes that control the incorporation of Na and S into the skeleton.

3.3 Oceanographic setting, material and methods

3.3.1 Specimen and sample

We used two specimens of *Keratoisis grayi* (family Isididae) collected in the North Atlantic (Fig. 3.1). Sample YPM 37031 was dredged 2006 on Bear Seamount (40.257 °N, 67.691°W) from about 950 m depth during R/V Delaware cruise DE 04-08. After collection it was frozen, treated with 70 % alcohol and stored dried. The second sample (USNM 10496) was collected in 1885 on the Blake Plateau (30.733 °N, 79.433 °W) in approximately 805 m water depth. This sample was collected during

a cruise of the United States Fish Commission and stored in ethanol. For both samples the mean growth rate was previously determined using radiocarbon (Farmer et al., 2015b). Both samples were covered with coral tissue at collection and thus are assumed to have been alive at the time of collection. No signs of bioerosion or diagenetic alteration can be found in the samples.

3.3.2 Oceanographic setting (Blake Plateau and Bear Seamount)

The Blake Plateau in the South Atlantic Bight is overflown by the Florida Current and represents a highly variable environment. The bottom water temperature at the sampling site shows a total variability of 3.9 °C around an annual mean of about 7.9 °C at the nearest long-time mooring station (Lee and Waddell, 1983), while frequent CTD casts carried out between 2001 until 2017 show a total variability of 2.0 °C at 725 m (n=64). The salinity variability in the Florida Straits given as 2SD was measured to be about 0.05 with a total range of 0.21 PSU around an annual mean of 34.93 PSU (data were collected as part of NOAA's Deep Western Boundary Current Time Series (DWBC) and are available at `www.aoml.noaa.gov/phod/wbts/data`).

Bear Seamount is part of the New England Seamount Chain and is located 50 km off the shelf break of Georges Bank. It is occupied by the Gulf Stream and exhibits a more stable environment in comparison to the Blake Plateau. Temperature data were taken at 1000 m depth at mooring station W1 (39.601 °N, 69.717 °W) from 2008 to 2013 and is a part of the long-time observing system Line W south of New England carried out by Woods Hole Oceanographic Institution (`www.whoi.edu/science/PO/linew/index.htm`). The total recorded temperature variability at this location is 0.9 °C and with a mean of 4.3 ± 0.2 °C (2SD) and the salinity variability is 0.02 (2SD) (total range of 0.13) around a mean of 34.96 PSU. Mean temperature is therefore higher on the Blake Plateau than on Bear Seamount with a smaller variability at the latter location. The same trend in variability is observed for salinity at the sampling sites but with only marginally different mean salinities.

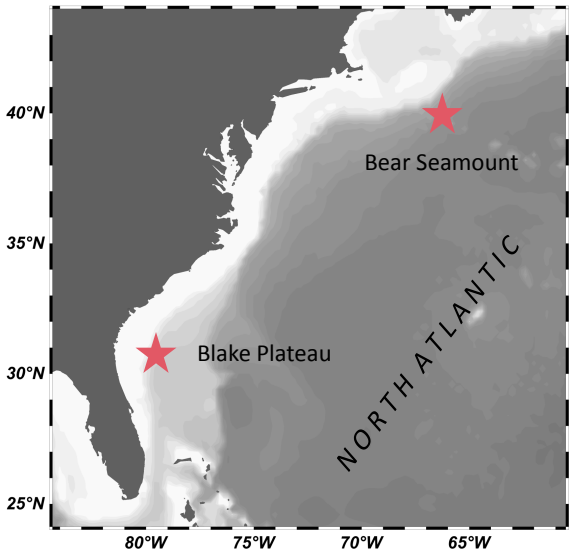

FIGURE 3.1: Sampling sites (red stars) of the two investigated bamboo corals from the North Atlantic.

3.3.3 EMPA (Na, S, Ca mapping)

The samples were embedded in Araldite resin and polished in a graded series with Struers Dia Pro polishing emulsions (9, 3 and 1 µm) with a Struers TegraPol polishing machine. The embedded sample was rinsed after each polishing step with demineralised water and dried with pressured air. After final polishing it was stored until measurement in a bolted vial.

Sodium, S and Ca were mapped by electron microprobe (EMPA) using a JEOL JXA 8200. Prior to analysis the sample was sputtered with carbon to avoid sample charging. Desired elements were measured simultaneously by wavelength-dispersive spectrometers. Na was measured using TAPH (thallium acid phthalate, high intensity) and TAP (thallium acid phthalate), Ca using PETJ (pentaerythritol) and S using two times PETH (pentaerythritol, high intensity) as diffraction crystals, respectively. A high-resolution transect across the sample radius was performed with an electron beam diameter of 4 µm, a dwell time of 50 ms and a current of 50 nA at 15 kV accelerator voltage. All the investigated areas were scanned five times. This, together with multiple simultaneous measurements of Na and S, was done to increase the count rates and with that to minimise the statistical uncertainty to receive a spatially better resolved map. The dwell time and current were chosen

to assure high signal intensity without damaging the carbon coating or significant loss of Na during mapping. Concentrations were calculated by mapping different carbonate and silicate reference materials under the same conditions as the samples (see Appendix Fig. 3.6, 3.7 and 3.8). The mapped area for the Blake Plateau sample is 2.00 ×4.44 mm, while on the Bear Seamount sample an area of 2.00 ×6.50 mm was mapped.

3.3.4 LA-ICP-MS (Na and Ca mapping)

Besides following the EMPA elemental mapping approach, the distribution of ^{23}Na and ^{44}Ca was also mapped on the embedded and polished sample of the Bear Seamount sample by laser ablation inductively coupled mass spectrometer (LA-ICP-MS). The additional mapping by laser ablation was carried out in order to exclude potential surface contamination. Ablation was carried out using a Nu AttoM sector field ICP-MS coupled to an Electro Scientific Industries NWR 193 nm excimer laser. Plasma conditions were tuned for hot plasma conditions according to Fietzke and Frische (2016). The data were acquired with a scan speed of 25 µm s^{-1}, a laser pulse rate of 20 Hz, a fluence of about 3 J cm^{-1} and a laser beam diameter of 32 µm. Each laser line overlapped with the neighbouring line by two µm. Prior to the acquisition of the two maps a pre-ablation was carried out on the same sample area. Pre-ablation was performed with a scan speed of 200 µm s^{-1}, a laser pulse rate of 15 Hz, a fluence of 3 J cm^{-1} and a beam diameter of 44 µm. The sample transects comprised three neighbouring maps recorded subsequently. Before and after each of these three maps a NIST SRM 610 glass standard was measured under the same ablation conditions.

The data reduction was performed in accordance to Flöter et al. (2019). ^{44}Ca was used as an internal standard and NIST SRM 610 as an external calibration. The three separate sections of each map were stitched together after background correction of the raw counts. Subsequently, both maps of the Bear Seamount sample were added to each other and drift-corrected. The offset between individual lines was removed by averaging representative regions on the map and subsequent application of a

factor (Na 0.94 to 1.07, Ca 0.98 to 1.03 on Bear Seamount sample) to match the mean value. After drift correction the maps were smoothed with a three times three cells Gaussian filter and finally the molar concentration calculated.

3.3.5 Confocal Raman microscopy

The polished sample was mapped with confocal Raman microscopy for their organic material distribution and for their crystallite orientation. The measurements were performed using WITec alpha 300 R instrument equipped with a diode laser having an excitation wavelength of 488 nm. The spectrometer had a grating of 600 mm^{-1} blazed at 50 nm. We used enhanced fluorescence in the spectral range of 2000 to 2400 cm^{-1} to map the distribution of organic matter. This was done in accordance to Wall and Nehrke (2012) who found that enhanced fluorescence correlated with organic matter content in the skeleton of corals. Overview maps were recorded with an integration time of 0.2 s every 10 μm using a Zeiss 20x Epiplan lens (NA 0.4). For the higher resolved maps an integration time of 0.2 s every 1.2 μm was used with a Zeiss 60x Lens Epiplan-NEOFLUAR Pol lens (NA 0.8).

3.4 Results

3.4.1 Spatial distribution and concentration of Na (EMPA and LA-ICP-MS)

The concentrations of Na in the Bear Seamount sample were calculated based on LA-ICPMS and EMPA measurements. For that we assumed that the sample consists only out of calcium carbonate and one mole Ca is represented by one mole of skeletal material. EMPA maps show a mean Na concentration of 12.9 ± 3.3 mmol mol^{-1} (2SD), which matches concentrations determined via LA-ICPMS of 14.4 ± 2.9 mmol mol^{-1} (2SD) from two overlaying maps. In comparison to LA-ICPMS the EMPA results show a finer resolved but similar spatial Na distribution. Both methods integrated over approximately the same depth range of 2 μm. The LA-ICPMS penetration depth was approximated based on average ablation yields according to

Eggins et al. (1998) and for EMPA based on Kanaya and Okayama, 1972. Based on the acquisition of Na/Ca with LA and EMPA we can exclude any surface contamination. This exclusion can be done since LA revealed the same mean Na/Ca ratios for both mappings and a similar spatial distribution of Na as the EMPA measurements (see Appendix Fig. 3.10).

The sample from the Blake Plateau, on which exclusively microprobe measurements were conducted, shows a mean Na concentration of 11.5 ± 3.9 mmol mol^{-1} (2SD). To relate the skeletal Na concentration to that of the calcifying fluid the apparent distribution coefficient can be determined. The calculation of the mean apparent distribution coefficient K_D was done using equation 1 where E is the molar concentration of a given trace element of interest in the skeleton (*Sk*) and seawater (*SW*), respectively. Based on the microprobe measurements we found a mean K_D of $2.5*10^{-4}$ and $2.8*10^{-4}$ for the Blake Plateau and Bear Seamount sample, respectively. For the calculation we used a molar Na to Ca ratio in seawater of 45.6 mol mol^{-1} with concentrations from Millero et al. (2008).

$$K_D = \frac{\left(\frac{E}{Ca}\right)_{Sk}}{\left(\frac{E}{Ca}\right)_{SW}} \tag{3.1}$$

Within the Bear Seamount sample (Fig. 3.2b) a high Na concentration ($\approx$ 20 mmol mol^{-1}) ring at about 5 mm from the rim can be observed while the lowest values ($\approx$ 7 mmol mol^{-1}) were found in the outer 1.5 mm of the section. The zig zag pattern recorded from 5.2 to 1.3 mm from the rim can only be seen in the high-resolution map from EMPA measurements. Growth rings and ring parallel patterns can also be observed on the Blake Plateau sample (Fig. 3.2a). The highest values were measured around the central channel with $\approx$ 22 mmol mol^{-1} while the lowest of $\approx$ 5 mmol mol^{-1} are found in ring structures from 2.1 mm from the rim to the rim itself.

Sodium and Ca are highly significantly ($p < 0.001$) inversely correlated suggesting a linear relationship with an R^2 of 0.46 and 0.47 on the Blake Plateau sample and the Bear Seamount sample, respectively (see Fig. 3.9 in the appendix). The relative variation of Ca (EMPA) calculated from the 5 and 95 % percentile is much smaller

than the corresponding variability in Na, accounting to 2.4 % on the Bear Seamount sample and 2.6 % on the Blake Plateau. In turn, the Na content in these specimens varies with 41 % and 45 %, respectively. The absolute variation for Na is 4.9 mmol mol^{-1} on Bear Seamount sample and 4.5 mmol mol^{-1} on Blake Plateau sample and therefore smaller than that of Ca (22.1 and 23.4 mmol mol^{-1}, respectively).

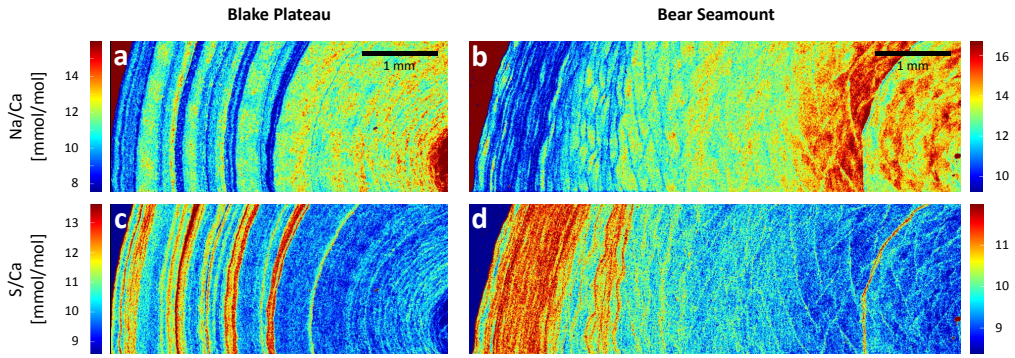

FIGURE 3.2: EMPA maps of Na/Ca and S/Ca on the bamboo coral samples from the Blake Plateau (a and c) and Bear Seamount (b and d).

3.4.2 Spatial distribution of fluorescence and S

The concentration of S measured by EMPA revealed a mean of 9.8 ± 1.9 mmol mol^{-1} (2SD) for the Bear Seamount coral and 10.3 ± 2.1 mmol mol^{-1} (2SD) for Blake Plateau sample (Fig. 3.2c and d). The highest concentrations on the Bear Seamount sample of about 12 mmol mol^{-1} are mostly found in a broad band in the outer 0.9 mm from the rim and a less broader band about 1.7 mm from the rim. An additional single thin band of increased S concentrations can also be found about 1.3 mm from the centre. Lower concentrations down to about 7 mmol mol^{-1} can be observed between these features on the sample from the Bear Seamount. The Blake Plateau sample shows lowest values in a region of about 0.2 mm around the central channel containing ≈ 7 mmol mol^{-1}. The highest concentrations were observed within thin bands in the outer 2.6 cm with up to ≈ 13 mmol mol^{-1}.

The apparent distribution coefficient was calculated to be $2.3*10^{-4}$ for the Blake Plateau sample and $2.2*10^{-4}$ for the Bear Seamount sample based on a S to Ca ratio

of 2.75 mol mol^{-1} in seawater according to Millero (2014).

The distribution patterns are mirrored by CRM fluorescence maps (Fig. 3.3). Fluorescence and S generally show a positive correlation, while the fluorescence maps provide a better resolved picture of the distribution. For example, banded structures of about 15 ± 9 μm (2SD, n=38) length can be resolved that form the rings and zig zag structures (Fig. 3.3c). Broad low-S zig zags mostly in the right half of Fig. 3.3a are surrounded by thin borders of higher S concentrations. This is clearly mirrored in the CRM mappings with a higher fluorescence.

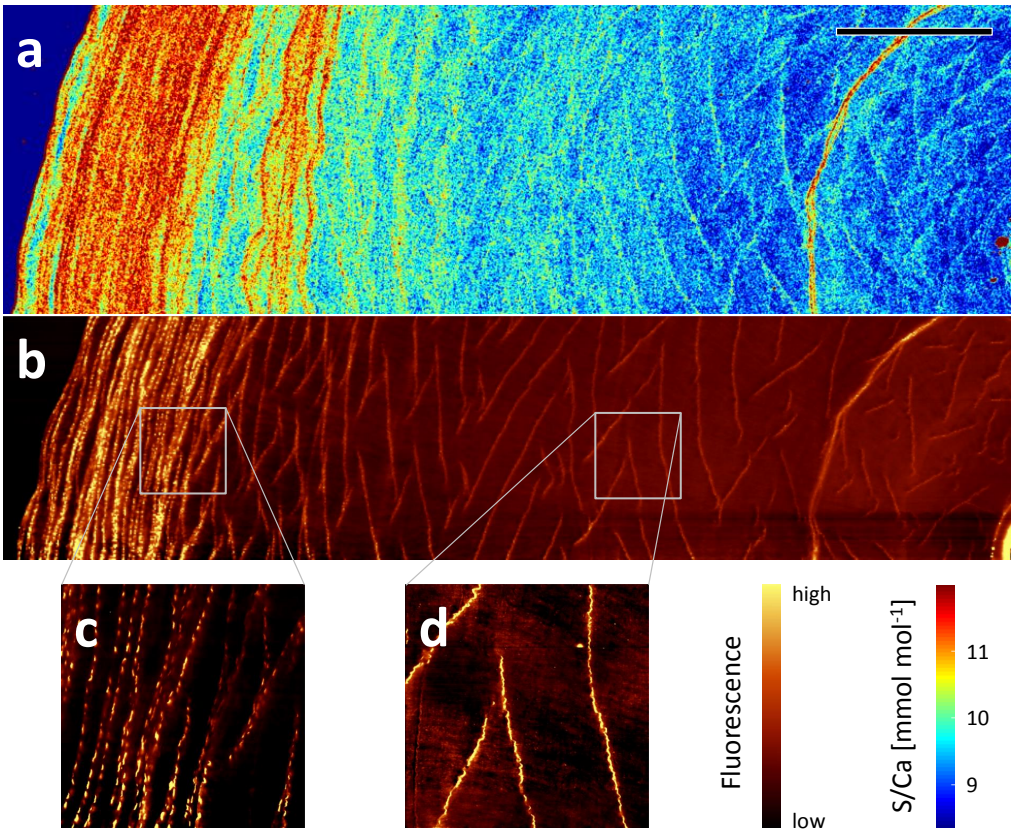

FIGURE 3.3: S/Ca and fluorescence of approximately the same area on the bamboo coral sample from Bear Seamount. The comparison shows the similarity in distribution indicating a spatial relationship of S and organic matter (a and b). Insets (c) and (d) provide a cl closer look into the small scale structure of the high-fluorescent bands. The bar in (a) denotes the length of 1 mm.

3.4.3 Na to S ratio

The mean ratio of Na to S in the Blake Plateau sample is 1.13 ± 0.47 and in the Bear Seamount sample 1.34 ± 0.50 mol mol^{-1}. As evident from Fig. 3.2, S is inversely correlated with Na with a slight sigmoidal distribution (Fig. 3.4). The frequency distribution was created with an integration interval of 0.1 mmol mol^{-1} for S/Ca and Na/Ca and a minimum of ten displayed counts for each interval.

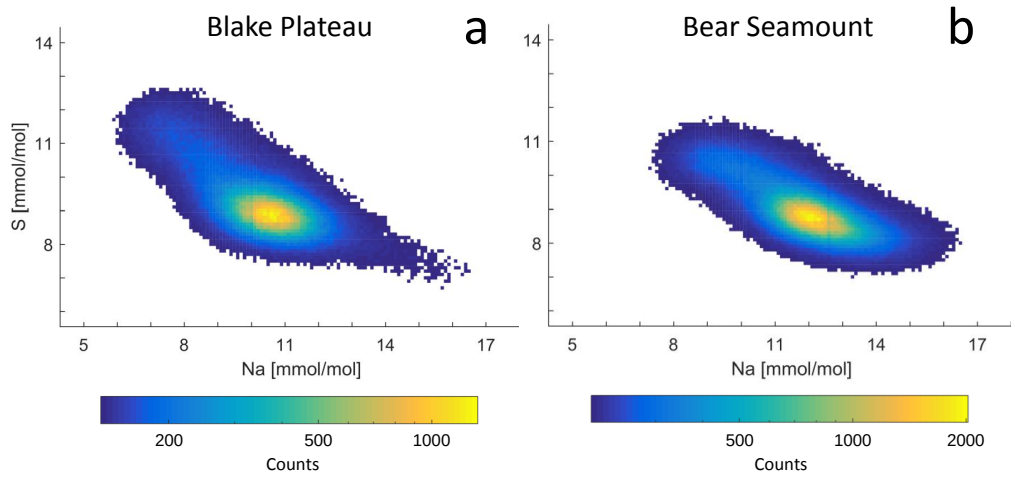

FIGURE 3.4: Sodium to Ca and S/Ca are inversely correlated in bamboo coral samples from the Blake Plateau and the Bear Seamount. The distribution suggests an inverse correlation following a sigmoidal relationship which can be inferred from the frequency distribution.

3.5 Discussion

3.5.1 Apparent distribution coefficients

The partitioning of Na and S into carbonates was investigated in several previous studies that included biotic (e.g. Rollion-Bard and Blamart (2015) for Na and Dijk et al. (2017) for S) and abiotic calcite (e.g. Ishikawa and Ichikuni (1984) for Na and Kitano et al. (1975) for S). Comparing the apparent distribution coefficients with previously reported values might give information on the hypothetical composition of the calcifying fluid (CF), and provide hints towards how this composition is

changed. A comparison with distribution coefficients from abiotic precipitation appears to be more useful in this regard rather than using values from other calcifying organisms where the processes behind the change are more complex.

The mean apparent distribution coefficient for Na in our two NW Atlantic samples (2.5 and 2.8*10^{-4}) fall within the range of values from precipitation experiments for inorganic calcite. Kitano et al. (1975) found apparent distribution coefficients of 0.7 – 0.9*10^{-4}, Busenberg and Niel Plummer (1985) 13.1*10^{-4} and Okumura and Kitano (1986) 0.6*10^{-4}. The literature values chosen for comparison are the ones closest to seawater conditions although only the experimental conditions of Kitano et al. (1975) were matching that of seawater. Busenberg and Niel Plummer (1985) explained the range of different reported distribution coefficients in the different studies by varying numbers of defects sites where Na is incorporated, which can for example be driven by precipitation rate.

The mean S apparent distribution coefficients found in this study are with 2.2 and 2.3*10^{-4} in the range of observed values for synthetic calcite presented by Wynn et al., 2018. These authors reported values of about 0.5 to 10*10^{-4} which is similar to the range of 0.1 to 8*10^{-4} by Busenberg and Niel Plummer (1985). Both studies found a strong positive correlation with precipitation rate. Further rising sulfate concentration of the precipitation solution is reported to increase the S content of precipitated calcite (e.g. Kitano et al., 1975; Kontrec et al., 2004; Okumura et al., 2018). We assume that the S concentration in the CF is approximately kept constant. This assumption is valid since only minor S quantities are consumed during the calcification process and excludes the concentration variation as a potential source of S variability in the skeleton. Since Na and S distribution coefficients seem to be similarly driven by precipitation rate this cannot explain the observed inverse correlation in bamboo corals.

Although the skeletal Na and S composition is seemingly largely driven by the coral physiology, the distribution coefficient similar to inorganic calcites indicate the potential for bamboo corals to record environmental conditions.

It has to be mentioned that for interstudy comparisons uniform calculation of

the mean apparent distribution coefficient are needed. For that the activity and not the concentration should be used. This is since ion couples with an unequal activity coefficient but the same concentration behave differently during precipitation. Nevertheless, the activity in the CF is not known due to its unknown composition and with that e.g. organic complex formation. This might result in uncertainties when comparing different carbonates and prevent us from drawing conclusions from these on the underlying calcification mechanism.

3.5.2 Potential drivers of the elemental composition

Recent seawater variability for temperature and salinity on the Blake Plateau (3.9 °C and 0.21 PSU) is higher than that on Bear Seamount (0.9 °C and 0.13 PSU). Similarly, we observe a stronger pronounced banding pattern (Fig. 3.2) and a higher variability in the Na/Ca composition of the Blake Plateau sample (± 3.9 2SD) compared to the Bear Seamount sample (± 3.3 2SD) . This could indicate a response of skeletal Na/Ca and S/Ca to environmental factors, although a long list of possible factors besides temperature and salinity could equally be responsible. These include ambient nutrient availability, predation, and dynamics of the associated microbiome, oxygen concentration or pH. Although information towards these additional parameters are not available, observable chemical patterns distributed along intraskeletal regions of presumed simultaneous growth found in both samples suggest that Na/Ca and S/Ca in bamboo corals are not governed by environmental factors. Therefore most likely an internal driver seems to be responsible to create the observed element distribution. In the following we will describe a possible mechanism that could explain the observed elemental distribution in context with the distribution of the organic matter in the skeleton.

Several mechanisms have been tested to explain the distribution of Na in comparison with other metal ions and S in biogenic calcium carbonates. Besides precipitation rate effects, which we already ruled out in the previous section, Rayleigh fractionation, pH change in the CF, ion specific pumping, and carrier phase mixing have previously been considered (e.g. Allen et al., 2016; Rollion-Bard and Blamart,

2015; Vielzeuf et al., 2018.

One possible internal influence is Rayleigh fractionation with and without Ca-pumping which was considered by Gagnon et al. (2012) and Rollion-Bard and Blamart (2015). In this model Na and S are regarded as conservative elements in the semi enclosed CF, while Ca as well as carbonate is successively removed from the CF by precipitation. The absolute concentration of Na and S in the CF does not change due to physiological processes. The explanation by Rayleigh fractionation falls short since the Ca removal by precipitation would cause an enrichment of both, Na and S, and therefore a positive correlation. For an inverse correlation the distribution coefficients had to be smaller and greater one for the investigated elements respectively. Based on the skeletal and SW concentrations of Na, S and Ca both D's are significantly smaller than one.

Another model we tested to explain the Na/S distribution in the corals was the Ca/proton exchange model which was recently suggested by Giri and Swart (2019). In this model Ca is pumped into the CF in exchange of two protons. This raises the pH and accelerates CO_2 flux into the CF which in presence of carbonic anhydrases reacts to bicarbonate. As a result the S/C and the Na/Ca ratio in the CF would be lowered causing a positive correlation in the elemental composition of the skeleton. Given that such elemental trends are not seen in our specimens this model also cannot explain the observed patterns.

Finally, ion specific pumping of Na and S that results in an enrichment of sulfur in the CF while depleting Na seems unlikely. Since S does not seem to play an essential role during calcification we propose that ion specific transport of S to the CF does not take place. Even if Na is involved in Ca pumping by Na/Ca exchange (Barron et al., 2018; Marshall, 1996) this would not result in the observed inverse correlation.

3.5.3 Constraints for bamboo coral calcification

The observed Na/S inverse correlation might involve two separate mechanisms. The first is calcite built from a reservoir and the second involves the formation of

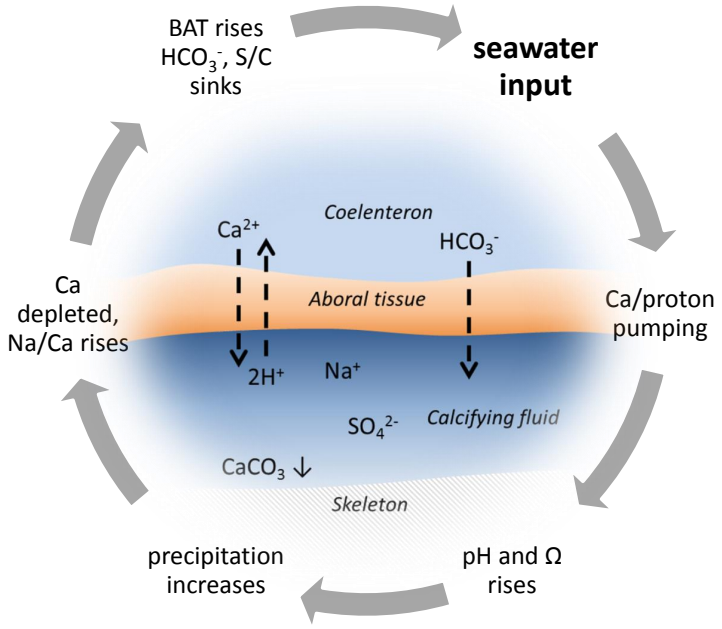

FIGURE 3.5: Proposed calcification mechanism for bamboo corals. This model adopts an earlier model for scleractinian corals from McCulloch et al. (2017). Bicarbonate active transport is abbreviated BAT and Ωdenotes the calcite saturation state.

organic matter in the skeletal matrix.

We suggest that skeletal calcite formation takes place in a finite reservoir confined by a tissue layer and the skeleton such as proposed earlier (e.g. Barnes, 1970; Clode and Marshall, 2002; Cohen and McConnaughey, 2003); and that this space has an initial composition of seawater (e.g. Cohen et al., 2006; Erez and Braun, 2007; Rollion-Bard et al., 2010)(Fig. 3.5). Further, Na and S are only removed by precipitation with calcite and these elements are not actively enriched in the CF.

Through the activity of Ca/H-pumps the Ca concentration and the pH rises in the CF (Cohen and McConnaughey, 2003). This leads to a higher calcite saturation which favours a faster growth rate (e.g. Teng et al., 2000; Weijden and Weijden, 2014). This might have two implications for Na. The first is the enhanced formation of defect sites during elevated calcification, which leads to a higher rate of Na incorporation (Füger et al., 2019). The second one is the successive depletion of Ca in the CF. If delivery of new Ca ions to the CF is slower than removal by precipitation the reservoir gets depleted for Ca and the ratio of Na/Ca rises. Based on the findings

of Wynn et al. (2018) one could assume that the rate-dependent formation of defect sites also leads to the increased incorporation of S. Since Na and S are inversely correlated we suggest that this at most plays only a minor role during S incorporation. Instead we favour a different explanation.

To keep the Ωhigh and the buffer capacity of the CF stable, bicarbonate active transport (BAT) delivers bicarbonate to the CF (Zoccola et al., 2015). BAT therefore leads to a lowered S/C ratio in the CF. The skeletal S/Ca ratio was found to decrease with rising pH and therefore with carbonate concentration in the precipitation solution similar to the solution S/Carbonate ratio but at a lower rate (Wynn et al., 2018). Therefore the sulfur composition of the CF is positively correlated with the sulfur composition of the skeleton. During times of lowered calcification more Ca will be left in the CF lowering the Na/Ca ratio and kinetic incorporation effects in combination with a low BAT activity ultimately raising the S/C. Since Ca and C as carbonate are equimolar in the calcite lattice the changes in skeletal Na/Ca and S/C ratios are in agreement with the observed inverse correlation of Na and S.

The second mechanism for the explanation of the inverse correlation involves the formation of a collagen-like substance in the skeleton and the admixture of inorganic calcite and organic material. Several studies suggested that metal ions might be enriched in organic matter using Mg in aragonitic coral skeletons as an example (Cuif et al., 2003; Finch and Allison, 2008; Meibom et al., 2008).

Most organically bound sulfate is contained in the acidic polysaccharide chondroitin sulfate (e.g. Dauphin, 2006; Perrin et al., 2017). The formation of organic matter-rich growth layers will therefore enrich sulfate in the skeleton. This is in line with our observation that high S-regions correlate with high fluorescence, an indicator for organic matter content. Contrary to the findings for Mg in hexacorals, however, Na is depleted in regions of higher S concentrations and potential organic matter enrichment. Nevertheless, most S in calcitic octocorals is found to be present as inorganic sulfate (e.g. Balan et al., 2017; Nguyen et al., 2014; Perrin et al., 2017). Nguyen et al. (2014) reported a ratio of one part organic S to 20 parts inorganic S

for the calcitic octocorals *Paracorallium japonicum*. This exceeds the ratio of S variability calculated as the difference of the 99 and 1 % quantile of S concentrations on the samples in both samples relative to their mean concentration. Therefore the S variability in the skeleton is not mainly driven by organic S. The Blake Plateau coral shows a mean S concentration of 0.50 wt% and a variability of 0.15 wt% while the Bear Seamount sample a mean concentration 0.49 wt% and a variability of 0.12 wt%. For a comparison the S concentration has to be given in wt% and not as a ratio of S to Ca. This is since a relative depletion of Ca by dilution through a non-calcitic phase in the sample would lead to an increase of the S/Ca ratio. Therefore, a change of S/Ca is possible without any contribution of S from the diluting phase. This comparison indicates that the main driver of the observed inverse correlation in Na/S is unlikely to be represented by mixing calcitic and organic phases. Furthermore, the depletion of Na in potentially organic-rich matter may be specific to bamboo corals since in foraminifera the primary organic sheet and high Na/Ca are reported to be positively correlated (Bonnin et al., 2019).

Given the above line of reasoning, we suggest that both mechanisms, the first including dilution and kinetic effects and the second based on organic matter build-up, are deemed to influence the Na and S composition of bamboo coral skeletons. The first one likely dominates during times of high growth rates while the latter one requires more energy and takes place during times of high energy supply.

3.6 Conclusion

This study investigated the elemental distribution of Na and S in the internodes of two Atlantic bamboo corals at the microscale to evaluate the proxy potential of these elements and the drivers of their incorporation. Sodium and S were found to be incorporated into the calcitic skeleton with partitioning coefficients that fall in the range of inorganically precipitated calcite. The relative variability of salinity at the sampling sites is reflected in the skeletal variability of Na/Ca while a coincidence cannot be excluded. Strikingly, chemical variability along growth rings excludes an environmental impact on these small-scale patterns. We found Rayleigh

fractionation, ion specific pumping of Na and S and Ca/proton exchange not to be responsible for the observed Na/S inverse correlation. We rather suggest a model that involves active Ca regulation and bicarbonate active transport based on the conservative behaviour of Na and S in the CF. Although this model is capable to successfully describe the observed inverse correlation by not involving organic matter. Yet organic matter might play a minor role especially in the microscale patterns along the growth rings. We summarise that visible and elemental patterns can be mainly explained by physiological processes. This indicates that skeletal Na/Ca and S/Ca are dominated by physiological processes within bamboo corals rather than by environmental salinity or temperature. Nevertheless, the physiological impact on skeletal formation might be driven by environmental factors such as food availability, stress through predators, infections, departure from temperature, pH, oxygen or salinity optimum or energy demanding gametogenesis for spawning. It has to be shown in future studies which factors influence to which extant the calcification of bamboo corals to use their skeletons as environmental archives.

3.7 Appendix

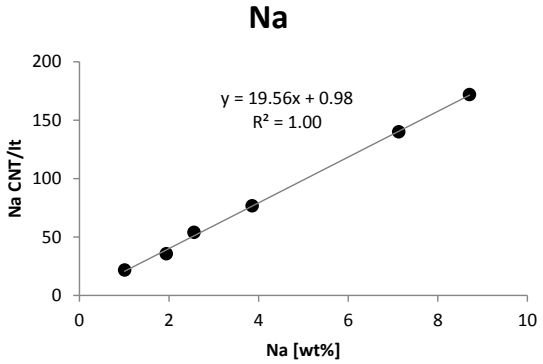

FIGURE 3.6: EMPA calibration of Na.

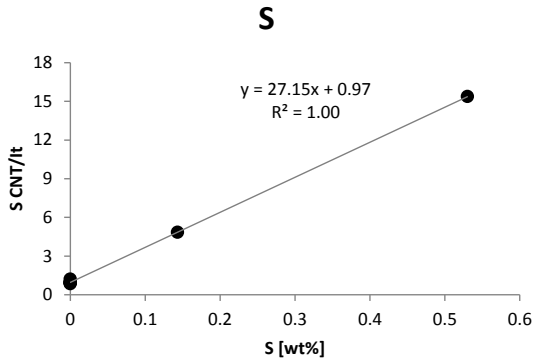

FIGURE 3.7: EMPA calibration of S.

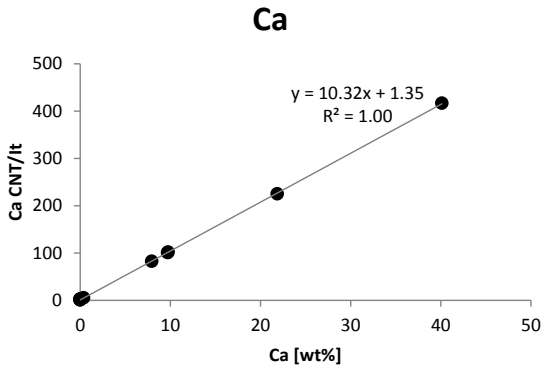

FIGURE 3.8: EMPA calibration of Ca.

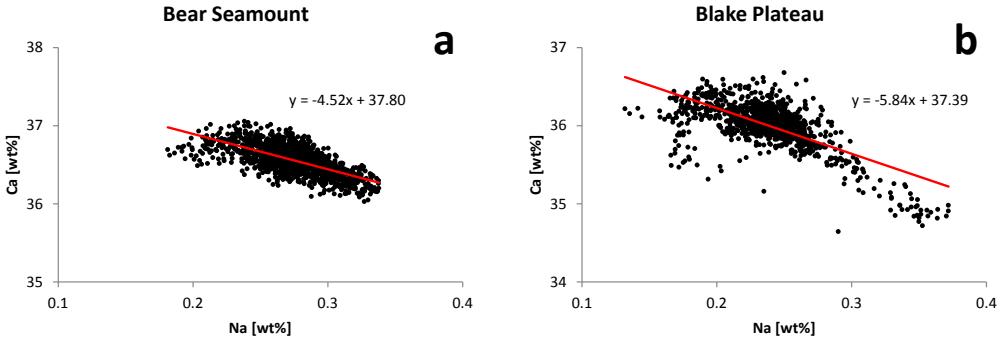

FIGURE 3.9: Correlation of Na and Ca in the Bear Seamount and the Blake Plateau bamboo coral samples.

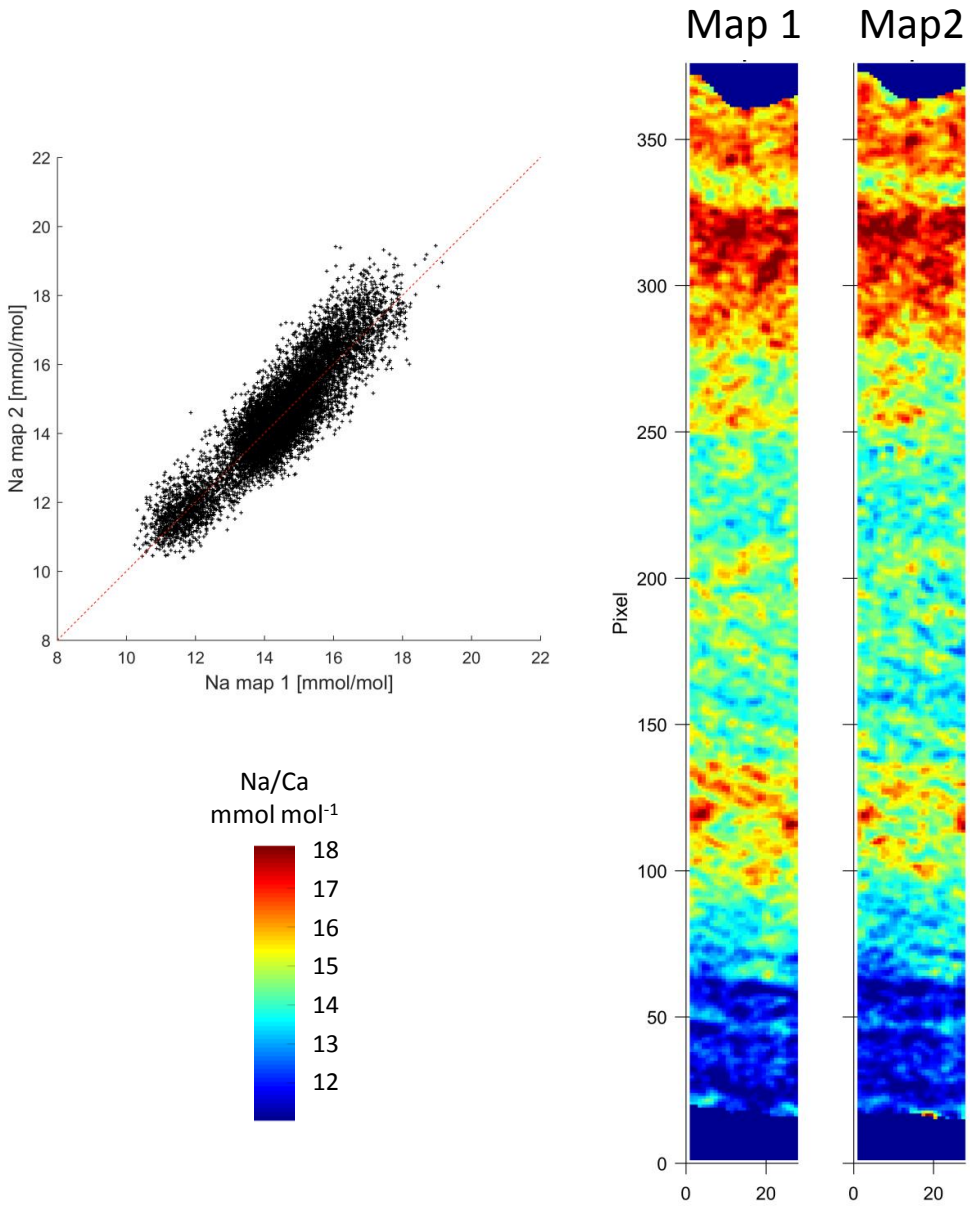

FIGURE 3.10: Comparison of the laser ablation ICPMS measurements of Na on the Bear Seamount bamboo coral sample. Both runs on the same area show similar concentrations and spatial distribution of Na indicating the absence of surface contamination. Red dotted line in the scatter plot denotes the 1:1 line.

References

Allen, K. A., B. Hönisch, S. M. Eggins, L. L. Haynes, Y. Rosenthal, and J. M. Yu (2016). "Trace element proxies for surface ocean conditions: A synthesis of culture calibrations with planktic foraminifera". In: *Geochimica Et Cosmochimica Acta* 193, pp. 197–221.

Andrews, A. H., R. P. Stone, C. C. Lundstrom, and A. P. DeVogelaere (2009). "Growth rate and age determination of bamboo corals from the northeastern Pacific Ocean using refined 210Pb dating". In: *Marine Ecology Progress Series* 397, pp. 173–185.

Balan, E., J. Aufort, S. Pouillé, M. Dabos, M. Blanchard, M. Lazzeri, C. Rollion-Bard, and D. Blamart (2017). "Infrared spectroscopic study of sulfate-bearing calcite from deep-sea bamboo coral". In: *European Journal of Mineralogy* 29.3, pp. 397–408.

Ballesta-Artero, I., L. Zhao, S. Milano, R. Mertz-Kraus, B. R. Schone, J. van der Meer, and R. Witbaard (2018). "Environmental and biological factors influencing trace elemental and microstructural properties of Arctica islandica shells". In: *Sci Total Environ* 645, pp. 913–923.

Barnes, D. J. (1970). "Coral skeletons: an explanation of their growth and structure". In: *Science* 170.3964, pp. 1305–1308.

Barron, M. E., A. B. Thies, J. A. Espinoza, K. L. Barott, A. Hamdoun, and M. Tresguerres (2018). "A vesicular Na+/Ca2+ exchanger in coral calcifying cells". In: *PLoS One* 13.10, e0205367.

Bertlich, J., D. Nürnberg, E. C. Hathorne, L. J. de Nooijer, E. M. Mezger, M. Kienast, S. Nordhausen, G.-J. Reichart, J. Schönfeld, and J. Bijma (2018). "Salinity control on Na incorporation into calcite tests of the planktonic foraminifera Trilobatus sacculifer – evidence from culture experiments and surface sediments". In: *Biogeosciences Discussions*, pp. 1–38.

Bonnin, E. A., Z. Zhu, J. S. Fehrenbacher, A. D. Russell, B. Hönisch, H. J. Spero, and A. C. Gagnon (2019). "Submicron sodium banding in cultured planktic foraminifera shells". In: *Geochimica et Cosmochimica Acta* 253, pp. 127–141.

Bostock, H. C., D. M. Tracey, K. I. Currie, G. B. Dunbar, M. R. Handler, S. E. M. Fletcher, A. M. Smith, and M. J. M. Williams (2015). "The carbonate mineralogy and distribution of habitat-forming deep-sea corals in the southwest pacific region". In: *Deep-Sea Research Part I-Oceanographic Research Papers* 100, pp. 88–104.

Busenberg, E. and L. Niel Plummer (1985). "Kinetic and thermodynamic factors controlling the distribution of SO32- and Na+ in calcites and selected aragonites". In: *Geochimica et Cosmochimica Acta* 49.3, pp. 713–725.

Clode, P. L. and A. T. Marshall (2002). "Low temperature FESEM of the calcifying interface of a scleractinian coral". In: *Tissue Cell* 34.3, pp. 187–198.

Cohen, A. L. and T. A. McConnaughey (2003). "Geochemical perspectives on coral mineralization". In: *Biomineralization* 54.1, pp. 151–187.

Cohen, A. L., G. A. Gaetani, T. Lundalv, B. H. Corliss, and R. Y. George (2006). "Compositional variability in a cold-water scleractinian, Lophelia pertusa: New insights into "vital effects"". In: *Geochemistry Geophysics Geosystems* 7.12, pp. 1–10.

Cuif, J. P., Y. Dauphin, J. Doucet, M. Salome, and J. Susini (2003). "XANES mapping of organic sulfate in three scleractinian coral skeletons". In: *Geochimica Et Cosmochimica Acta* 67.1, pp. 75–83.

Cusack, M., Y. Dauphin, J. P. Cuif, M. Salome, A. Freer, and H. Yin (2008). "Micro-XANES mapping of sulphur and its association with magnesium and phosphorus in the shell of the brachiopod, Terebratulina retusa". In: *Chemical Geology* 253.3-4, pp. 172–179.

Dauphin, Y. (2006). "Mineralizing matrices in the skeletal axes of two Corallium species (Alcyonacea)". In: *Comparative Biochemistry and Physiology Part A: Molecular & Integrative Physiology* 145.1, pp. 54–64.

Dijk, I. van, L. J. de Nooijer, W. Boer, and G. J. Reichart (2017). "Sulfur in foraminiferal calcite as a potential proxy for seawater carbonate ion concentration". In: *Earth and Planetary Science Letters* 470, pp. 64–72.

Dijk, I. van, C. Barras, L. J. de Nooijer, A. Mouret, E. Geerken, S. Oron, and G.-J. Reichart (2019). "Coupled calcium and inorganic carbon uptake suggested by magnesium and sulfur incorporation in foraminiferal calcite". In: *Biogeosciences* 16.10, pp. 2115–2130.

Eggins, S. M., L. P. J. Kinsley, and J. M. G. Shelley (1998). "Deposition and element fractionation processes during atmospheric pressure laser sampling for analysis by ICP-MS". In: *Applied Surface Science* 127-129, pp. 278–286.

Erez, J. and A. Braun (2007). "Calcification in hermatypic corals is based on direct seawater supply to the biomineralization site". In: *Geochimica Et Cosmochimica Acta* 71.15, A260.

Farmer, J. R., L. F. Robinson, and B. Hönisch (2015b). "Growth rate determinations from radiocarbon in bamboo corals (genus Keratoisis)". In: *Deep-Sea Research Part I-Oceanographic Research Papers* 105, pp. 26–40.

Füger, A., F. Konrad, A. Leis, M. Dietzel, and V. Mavromatis (2019). "Effect of growth rate and pH on lithium incorporation in calcite". In: *Geochimica Et Cosmochimica Acta* 248, pp. 14–24.

Fichtner, V., H. Strauss, V. Mavromatis, M. Dietzel, T. Huthwelker, C. N. Borca, P. Guagliardo, M. R. Kilburn, J. Gottlicher, C. L. Pederson, E. Griesshaber, W. W. Schmahl, and A. Immenhauser (2018). "Incorporation and subsequent diagenetic alteration of sulfur in Arctica islandica". In: *Chemical Geology* 482, pp. 72–90.

Fietzke, J. and M. Frische (2016). "Experimental evaluation of elemental behavior during LA-ICP-MS: influences of plasma conditions and limits of plasma robustness". In: *Journal of Analytical Atomic Spectrometry* 31.1, pp. 234–244.

Finch, A. A. and N. Allison (2008). "Mg structural state in coral aragonite and implications for the paleoenvironmental proxy". In: *Geophysical Research Letters* 35.8.

Flöter, S., J. Fietzke, M. Gutjahr, J. Farmer, B. Hönisch, G. Nehrke, and A. Eisenhauer (2019). "The influence of skeletal micro-structures on potential proxy records in a bamboo coral". In: *Geochimica Et Cosmochimica Acta* 248, pp. 43–60.

Gagnon, A. C., J. F. Adkins, and J. Erez (2012). "Seawater transport during coral biomineralization". In: *Earth and Planetary Science Letters* 329-330, pp. 150–161.

Geerken, E., L. J. de Nooijer, I. van Dijk, and G. J. Reichart (2018). "Impact of salinity on element incorporation in two benthic foraminiferal species with contrasting magnesium contents". In: *Biogeosciences* 15.7, pp. 2205–2218.

Geerken, E., L. J. de Nooijer, A. Roepert, L. Polerecky, H. E. King, and G. J. Reichart (2019). "Element banding and organic linings within chamber walls of two benthic foraminifera". In: *Sci Rep* 9.1, p. 3598.

Giri, S. J. and P. K. Swart (2019). "The influence of seawater chemistry on carbonate-associated sulfate derived from coral skeletons". In: *Palaeogeography Palaeoclimatology Palaeoecology* 521, pp. 72–81.

Glock, N., V. Liebetrau, A. Vogts, and A. Eisenhauer (2019). "Organic Heterogeneities in Foraminiferal Calcite Traced Through the Distribution of N, S, and I Measured With NanoSIMS: A New Challenge for Element-Ratio-Based Paleoproxies?" In: *Frontiers in Earth Science* 7.175.

Gordon, C. M., R. A. Carr, and R. E. Larson (1970). "The Influence of Environmental Factors on the Sodium and Manganese Content of Barnacle Shells". In: *Limnology and Oceanography* 15.3, pp. 461–466.

Hauzer, H., D. Evans, W. Muller, Y. Rosenthal, and J. Erez (2018). "Calibration of Na partitioning in the calcitic foraminifer Operculina ammonoides under variable Ca concentration: Toward reconstructing past seawater composition". In: *Earth and Planetary Science Letters* 497, pp. 80–91.

Hill, T. M., H. J. Spero, T. Guilderson, M. LaVigne, D. Clague, S. Macalello, and N. Jang (2011). "Temperature and vital effect controls on bamboo coral (Isididae) isotope geochemistry: A test of the "lines method"". In: *Geochemistry Geophysics Geosystems* 12.4.

Iglikowska, A., M. Ronowicz, E. Humphreys-Williams, and P. Kuklinski (2018). "Trace element accumulation in the shell of the Arctic cirriped Balanus balanus". In: *Hydrobiologia* 818.1, pp. 43–56.

Ishikawa, M. and M. Ichikuni (1984). "Uptake of Sodium and Potassium by Calcite". In: *Chemical Geology* 42.1-4, pp. 137–146.

Kanaya, K. and S. Okayama (1972). "Penetration and Energy-Loss Theory of Electrons in Solid Targets". In: *Journal of Physics D-Applied Physics* 5.1, pp. 43–58.

Kitano, Y., M. Okumura, and M. Idogaki (1975). "Incorporation of sodium, chloride and sulfate with calcium carbonate". In: *Geochemical Journal* 9.2, pp. 75 –84.

Kontrec, J., D. Kralj, L. Brecevic, G. Falini, S. Fermani, V. Noethig-Laslo, and K. Mirosavljevic (2004). "Incorporation of inorganic anions in calcite". In: *European Journal of Inorganic Chemistry* 2004.23, pp. 4579–4585.

Lecuyer, C. (2016). "Seawater residence times of some elements of geochemical interest and the salinity of the oceans". In: *Bulletin De La Societe Geologique De France* 187.6, pp. 245–259.

Lee, T. N. and E. Waddell (1983). "On Gulf-Stream Variability and Meanders over the Blake Plateau at 30-Degrees-N". In: *Journal of Geophysical Research-Oceans and Atmospheres* 88.Nc8, pp. 4617–4631.

Marshall, A. T. (1996). "Calcification in hermatypic and ahermatypic corals". In: *Science* 271.5249, pp. 637–639.

McCulloch, M. T., J. P. D'Olivo, J. Falter, M. Holcomb, and J. A. Trotter (2017). "Coral calcification in a changing World and the interactive dynamics of pH and DIC upregulation". In: *Nat Commun* 8, p. 15686.

Meibom, A., J. P. Cuif, F. Houlbreque, S. Mostefaoui, Y. Dauphin, K. L. Meibom, and R. Dunbar (2008). "Compositional variations at ultra-structure length scales in coral skeleton". In: *Geochimica et Cosmochimica Acta* 72.6, pp. 1555–1569.

Mezger, E. M., L. J. de Nooijer, W. Boer, G. J. A. Brummer, and G. J. Reichart (2016). "Salinity controls on Na incorporation in Red Sea planktonic foraminifera". In: *Paleoceanography* 31.12, pp. 1562–1582.

Millero, F. J. (2014). "8.1 - Physico-Chemical Controls on Seawater". In: *Treatise on Geochemistry (Second Edition)*. Ed. by H. D.H. K. Turekian. Oxford: Elsevier, pp. 1–18.

Millero, F. J., R. Feistel, D. G. Wright, and T. J. McDougall (2008). "The composition of Standard Seawater and the definition of the Reference-Composition Salinity Scale". In: *Deep-Sea Research Part I-Oceanographic Research Papers* 55.1, pp. 50–72.

Mitsuguchi, T. and T. Kawakami (2012). "Potassium and other minor elements in Porites corals: implications for skeletal geochemistry and paleoenvironmental reconstruction". In: *Coral Reefs* 31.3, pp. 671–681.

Mitsuguchi, T., T. Uchida, and E. Matsumoto (2010). "Na/Ca variability in coral skeletons". In: *Geochemical Journal* 44.4, pp. 261–273.

Nguyen, L. T., M. A. Rahman, T. Maki, Y. Tamenori, T. Yoshimura, A. Suzuki, N. Iwasaki, and H. Hasegawa (2014). "Distribution of trace element in Japanese red coral Paracorallium japonicum by mu-XRF and sulfur speciation by XANES: Linkage between trace element distribution and growth ring formation". In: *Geochimica Et Cosmochimica Acta* 127, pp. 1–9.

Okumura, M. and Y. Kitano (1986). "Coprecipitation of Alkali-Metal Ions with Calcium-Carbonate". In: *Geochimica Et Cosmochimica Acta* 50.1, pp. 49–58.

Okumura, T., H. J. Kim, J. W. Kim, and T. Kogure (2018). "Sulfate-containing calcite: crystallographic characterization of natural and synthetic materials". In: *European Journal of Mineralogy* 30.5, pp. 929–937.

Perrin, J., C. Rivard, D. Vielzeuf, D. Laporte, C. Fonquernie, A. Ricolleau, M. Cotte, and N. Floquet (2017). "The coordination of sulfur in synthetic and biogenic Mg calcites: The red coral case". In: *Geochimica Et Cosmochimica Acta* 197, pp. 226–244.

Pingitore, N. E., G. Meitzner, and K. M. Love (1995). "Identification of Sulfate in Natural Carbonates by X-Ray-Absorption Spectroscopy". In: *Geochimica Et Cosmochimica Acta* 59.12, pp. 2477–2483.

Roberts, J. M., F. Murray, E. Anagnostou, S. Hennige, A. Gori, L.-A. Henry, A. Fox, N. Kamenos, and G. L. Foster (2016b). "Cold-Water Corals in an Era of Rapid

Global Change: Are These the Deep Ocean's Most Vulnerable Ecosystems?" In: *The Cnidaria, Past, Present and Future: The world of Medusa and her sisters*. Ed. by S. Goffredo and Z. Dubinsky. Cham: Springer International Publishing, pp. 593–606.

Robinson, L. F., J. F. Adkins, N. Frank, A. C. Gagnon, N. G. Prouty, E. B. Roark, and T. van de Flierdt (2014). "The geochemistry of deep-sea coral skeletons: A review of vital effects and applications for palaeoceanography". In: *Deep-Sea Research Part Ii-Topical Studies in Oceanography* 99, pp. 184–198.

Rollion-Bard, C. and D. Blamart (2015). "Possible controls on Li, Na, and Mg incorporation into aragonite coral skeletons". In: *Chemical Geology* 396, pp. 98–111.

Rollion-Bard, C., D. Blamart, J. P. Cuif, and Y. Dauphin (2010). "In situ measurements of oxygen isotopic composition in deep-sea coral, Lophelia pertusa: Re-examination of the current geochemical models of biomineralization". In: *Geochimica Et Cosmochimica Acta* 74.4, pp. 1338–1349.

Rollion-Bard, C., S. Milner Garcia, P. Burckel, L. Angiolini, H. Jurikova, A. Tomašových, and D. Henkel (2019). "Assessing the biomineralization processes in the shell layers of modern brachiopods from oxygen isotopic composition and elemental ratios: Implications for their use as paleoenvironmental proxies". In: *Chemical Geology* 524, pp. 49–66.

Takano, B. (1985). "Geochemical Implications of Sulfate in Sedimentary Carbonates". In: *Chemical Geology* 49.4, pp. 393–403.

Tamenori, Y., T. Yoshimura, N. T. Luan, H. Hasegawa, A. Suzuki, H. Kawahata, and N. Iwasaki (2014). "Identification of the chemical form of sulfur compounds in the Japanese pink coral (Corallium elatius) skeleton using mu-XRF/XAS speciation mapping". In: *J Struct Biol* 186.2, pp. 214–23.

Teng, H. H., P. M. Dove, and J. J. De Yoreo (2000). "Kinetics of calcite growth: Surface processes and relationships to macroscopic rate laws". In: *Geochimica Et Cosmochimica Acta* 64.13, pp. 2255–2266.

Thresher, R. E., S. J. Fallon, and A. T. Townsend (2016). "A "core-top" screen for trace element proxies of environmental conditions and growth rates in the calcite

skeletons of bamboo corals (Isididae)". In: *Geochimica Et Cosmochimica Acta* 193, pp. 75–99.

Vielzeuf, D., J. Garrabou, A. Gagnon, A. Ricolleau, J. Adkins, D. Gunther, K. Hametner, J. L. Devidal, E. Reusser, J. Perrin, and N. Floquet (2013). "Distribution of sulphur and magnesium in the red coral". In: *Chemical Geology* 355, pp. 13–27.

Vielzeuf, D., A. C. Gagnon, A. Ricolleau, J. L. Devidal, C. Balme-Heuze, N. Yahiaoui, C. Fonquernie, J. Perrin, J. Garrabou, J. M. Montel, and N. Floquet (2018). "Growth Kinetics and Distribution of Trace Elements in Precious Corals". In: *Frontiers in Earth Science* 6.

Wall, M. and G. Nehrke (2012). "Reconstructing skeletal fiber arrangement and growth mode in the coral Porites lutea (Cnidaria, Scleractinia): a confocal Raman microscopy study". In: *Biogeosciences* 9.11, pp. 4885–4895.

Weijden, C. H. van der and R. D. van der Weijden (2014). "Calcite growth: Rate dependence on saturation, on ratios of dissolved calcium and (bi)carbonate and on their complexes". In: *Journal of Crystal Growth* 394, pp. 137–144.

Wit, J. C., L. J. de Nooijer, M. Wolthers, and G. J. Reichart (2013). "A novel salinity proxy based on Na incorporation into foraminiferal calcite". In: *Biogeosciences* 10.10, pp. 6375–6387.

Wynn, P. M., I. J. Fairchild, A. Borsato, C. Spotl, A. Hartland, A. Baker, S. Frisia, and J. U. L. Baldini (2018). "Sulphate partitioning into calcite: Experimental verification of pH control and application to seasonality in speleothems". In: *Geochimica Et Cosmochimica Acta* 226, pp. 69–83.

Yoshimura, T., A. Maeda, Y. Tamenori, A. Suzuki, K. Fujita, and H. Kawahata (2019). "Partitioning and Chemical Environments of Minor Elements in Individual Large Benthic Foraminifera Cultured in Temperature-Controlled Tanks". In: *Frontiers in Earth Science* 7.

Zhao, L., B. R. Schöne, R. Mertz-Kraus, and F. Yang (2017). "Insights from sodium into the impacts of elevated p CO 2 and temperature on bivalve shell formation". In: *Journal of Experimental Marine Biology and Ecology* 486, pp. 148–154.

Zoccola, D., P. Ganot, A. Bertucci, N. Caminiti-Segonds, N. Techer, C. R. Voolstra, M. Aranda, E. Tambutte, D. Allemand, J. R. Casey, and S. Tambutte (2015). "Bicarbonate transporters in corals point towards a key step in the evolution of cnidarian calcification". In: *Sci Rep* 5, p. 9983.

4 Boron isotopes in bamboo corals

4.1 Abstract

Bamboo corals show a cosmopolitan distribution in the world's oceans. Their long lifespans may allow a highly resolved reconstruction of environmental conditions at sites where instrumental time series are scarce. The key to use this potential is a detailed understanding of bamboo coral calcification. This would allow differentiating between environmental and physiological signals preserved in the skeleton. One important factor for calcification is the carbonate parameters in the calcifying fluid of the coral. In order to investigate these parameters we measured the boron isotopic composition in bamboo corals with two methods allowing us to look into the bulk and the calcite phase of the skeleton. We applied laser ablation MC-ICPMS mapping and solution-based MC-ICPMS analyses to an Atlantic and one Pacific specimen. Assuming the boron in the calcifying fluid resembles the isotopic composition of sea water, we can confirm the smaller pH upregulation of bamboo corals compared with scleractinians. Further, we found a statistically significant offset of about 2 ‰ between the mean lasered bulk δ^{11}B and the calcite phase δ^{11}B in the Atlantic coral and the Pacific sample. The observed range in boron isotopic composition revealed by laser ablation was 16 ‰ for the Atlantic and 13 ‰ for the Pacific sample, partly plotting below the theoretical borate fractionation curve of seawater. Therefore laser ablation mapping of δ^{11}B does not allow a direct reconstruction of the calcifying fluid carbonate parameters based in the established assumption of the B isotopes pH proxy. Possible controls on the B elemental and isotopic composition have been identified in this study as organic matter content, and other non-lattice bound B, kinetic effects and borate influx into the calcifying fluid. The B/C ratio and δ^{11}B values were spatially positively correlated which allows B/C to be used as

an indicator for $\delta^{11}B$ variation in bamboo corals. Before using bamboo corals temporal high-resolution records as environmental proxies, calcification processes and drivers of skeletal composition have to be further investigated.

4.2 Introduction

Bamboo corals (Isididae) are a genus of calcifying octocorals that are globally distributed in the world's ocean (e.g. Watling et al., 2011) and grow in a wide range of water depths from near surface (e.g. Thresher et al., 2016) down to 4000 m (e.g. Lapointe and Watling, 2015). They are reported to have long live spans sometimes over 300 years during which they build their high magnesium calcite skeleton (e.g. Noé and Dullo, 2006). This makes them promising high resolution archives for environmental conditions at sites where instrumental time series are scarce or even absent.

Physiological activity might have an important impact on the chemical composition of bamboo coral skeletons. The fine scale internal variations of Mg/Ca and Ba/Ca that have been found to be coupled to seawater temperature (Thresher et al., 2016) and Ba concentration (LaVigne et al., 2016; LaVigne et al., 2011), respectively, are higher than expected from natural variability at the growth site (Flöter et al., 2019). Further, scleractinian corals elevate their internal pH in comparison to the surrounding seawater by up to 1 pH unit (e.g. Anagnostou et al., 2012; McCulloch et al., 2017; Wall et al., 2016). In contrast, octocorals were reported to have a limited control on their calcifying fluid pH (e.g. Farmer et al., 2015a; Rollion-Bard et al., 2017; Saenger et al., 2017).

The boron isotopic composition of a sample can be expressed as $\delta^{11}B$ which normalises the 11B to ^{10}B ratio of a sample relative to a standard (Eq. 4.1). The pH of an aqueous solution determines the B isotopic composition in carbonates precipitating from these solutions. This is due the pH-dependent equilibrium between boric acid and borate (Fig. 4.1a) while the former preferentially incorporates heavy boron isotopes. This leads to an isotopic fractionation of B (Zeebe, 2005)(Fig. 4.1b).

Assuming that only borate is incorporated into calcium carbonate, this would allow reconstructing solution pH from its B isotopic composition (e.g. Hönisch and Hemming, 2004; Rollion-Bard et al., 2011; Spivack et al., 1993). Boron isotopes have been used in multiple studies to investigate the conditions under which calcification takes place (e.g. Cornwall et al., 2017; Holcomb et al., 2014; McCulloch et al., 2017). Nevertheless, there is an ongoing debate on factors influencing the isotopic composition through the species incorporated into calcite (Balan et al., 2016), whether fractionation takes place during incorporation (Farmer et al., 2019), or active borate concentration modulation of the calcifying fluid in corals (Rae, 2018).

$$\delta^{11}B = \left(\left(\frac{\left(\frac{^{11}B}{^{10}B}\right)_{sample}}{\left(\frac{^{11}B}{^{10}B}\right)_{NIST951}} \right) - 1 \right) * 1000 \tag{4.1}$$

This study investigates the boron isotopic composition of bamboo corals by laser ablation multi collector inductively coupled mass spectrometry (LA-ICPMS) and solution based MC-ICPMS. These techniques allow for a detailed insight into the spatial distribution of B isotopes in skeletal sections of this calcitic coral. This will reveal further information on the potential calcification mechanism and allow evaluation of the proxy potential of bamboo corals.

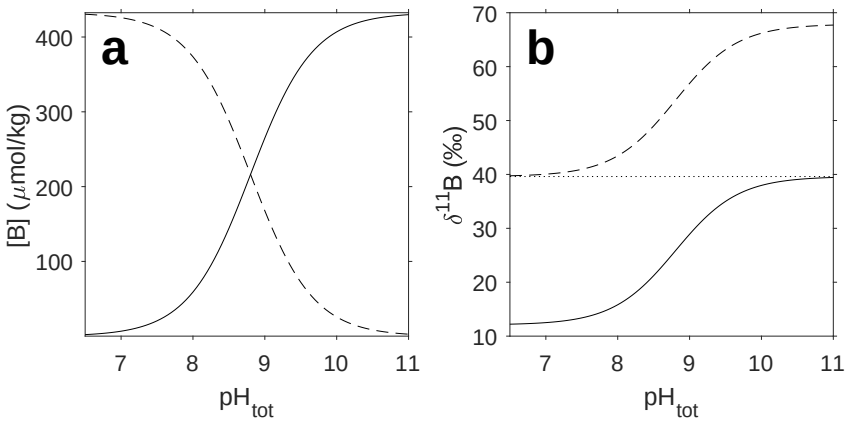

FIGURE 4.1: Equilibrium of borate and boric acid as a function of pH_{tot} (total scale) (a) and the isotope fractionation curves of boric acid and borate (b). The curves were calculated for a salinity of 35, a depth of 800 m and a temperature of 5 °C after (Rae, 2018). Fractionation factor used is 27.2 ‰ (Klochko et al., 2006) with $\delta^{11}B$ of seawater of 39.61 ‰ (Foster et al., 2010).

4.3 Oceanographic setting, material and methods

4.3.1 Samples

For the analysis, two samples of the species Keratoisis sp. from the North Atlantic and the North Pacific were chosen. The Pacific sample T1104 A7 (Fig. 4.3a) stems from the Monterey Canyon in the Californian margin (36.744 °N, 122.037 °W) (Fig. 4.2) and grew at 870 m depth. After collecting the living coral the polyp material was removed and the sample was stored dry. Sample YPM 37031 (Fig. 4.3b) from the North Atlantic was collected alive on Bear Seamount off Georges Bank (40.257 °N, 67.691 °W) (Fig. 4.2) between 847 and 1079 m depth. It was frozen, treated with alcohol and stored dry afterwards.

4.3.2 Oceanographic setting

Bear Seamount is part of the New England Seamount chain and influenced by the cold southward flowing Deep Water Boundary Current and the warm northward flowing Gulf Stream. The mean annual water temperature at 980 m depth measured by the long-time observation station W1 (39.601 °N, 69.717 °W) between 2008

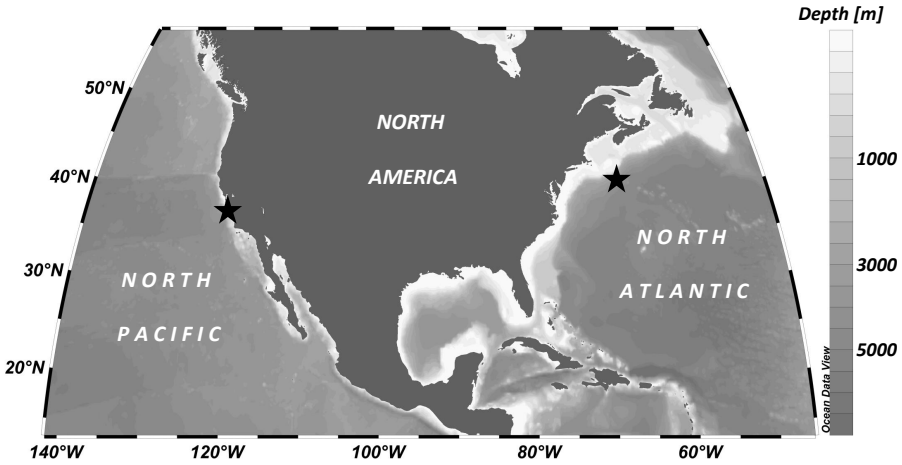

FIGURE 4.2: Samples were collected in the North Pacific in the Monterey Canyon and in the North Atlantic on Bear Seamount. The map was created using Ocean Data View (Schlitzer, 2019) and modified manually.

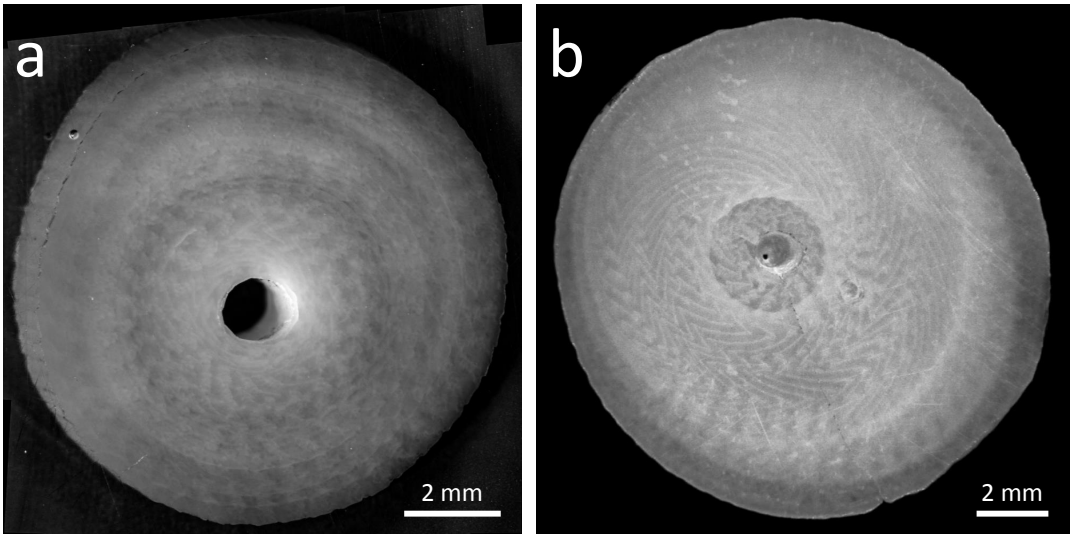

FIGURE 4.3: Micrographs of the bamboo coral Pacific sample T1104 A7 from the Monterey Canyon (a) and the Atlantic sample YPM 37031 from Bear Seamount (b).

and 2013 was 4.39 ± 2.19 °C (2SD) with a mean salinity of 34.97 ± 0.02 (2SD). This station is part of the long-time observing system Line W carried out by Woods Hole Oceanographic Institution (`www.whoi.edu/science/PO/linew/index.htm`). In situ pH_{tot} (total scale) is 8.01 under in situ conditions calculated with CO2sys v2.3.

The Pacific sample is influenced by the cold California Current. The nearest grid point of the 0.25° ×0.25° World Ocean Atlas 2013 (36.625 °N, 122.125 °W) reports a mean annual water temperature at 900 m depth is 4.21 °C (Locarnini et al., 2013) with a salinity of 34.42 (Zweng et al., 2013). The sampling site shows a mean pH_{tot} of 7.55 at in situ conditions calculated with CO2sys v2.3.

4.3.3 Laser ablation mapping

The samples were cut and embedded in Araldite and subsequently polished with a Stuers Tegrapol. Polishing was carried out using Struers Dia Pro water based diamond solutions starting with a grain size of 9, then 3, and finally 1 µm.

The laser ablation mapping was conducted using a Thermo Fisher AXIOM MC-ICPMS coupled to an UP193fx laser ablation system of New Wave Research which is equipped with an excimer laser (193 nm). The measurements were carried out following Fietzke et al. (2010) and Fietzke et al. (2015). Boron isotopes were measured on electron multipliers (MH and ML) while C was measured simultaneously with a Faraday cup (H5) as conducted by Wall et al. (2019). Plasma conditions were tuned for most accurate results to hot conditions (NAI of 11.5, according to Fietzke and Frische (2016)) to calibrate the sample results. Isotope mapping had been done under cold plasma conditions (NAI of 0.8 – 1.7 Fietzke and Frische (2016)) allowing for high sensitivity and most precise data collection. Standards used were NIST 610 (Wise and Watters, 2012), JCp-1 (Okai et al., 2002), JCt-1 (Okai et al., 2004) and NBS SRM 951 (Catanzaro et al., 1970) which revealed a B isotopic composition of 0.7 ± 0.5 ‰ (2SE), 24.0 ± 0.5 ‰ (2SE), 15.9 ± 1.1 ‰ (2SE) and -0.3 ± 0.9 ‰ (2SE) respectively. Typical background levels for ^{10}B, 11B, and 12C were about 100, 700, and 40*10^6 counts s^{-1} respectively while sample intensities were about 16*10^3, 80*10^3, and 70*10^6 counts s^{-1} respectively.

The mapping area on both samples was pre-ablated using a laser beam diameter of 35 μm, a laser pulse frequency of 20 Hz, a laser fluence of ≈ 4.1 J cm^{-2}, and the sample stage was moved under the laser with 200 μm s^{-1}. Both samples were mapped with the same settings as for the pre-ablation except the sample stage was moved with 25 μm s^{-1}. Eighty parallel lines overlapping by 10 μm were ablated on each sample, which resulted in a map width of 2 mm. To achieve better counting statistics, the sample area was mapped five times.

Data evaluation was performed in MATLAB. First all five maps of each sample were combined. Then a 3×3 Gaussian smoothing was carried out on the combined map and the background was subtracted. Afterwards a drift correction between the lines was applied. Finally the data were normalised based on the high NAI calibration on JCp-1 and JCt-1.

4.3.4 Solution based measurements

To distinguish between the bulk boron composition of the bamboo coral internodes and that of the carbonate phase a bleaching step was carried out. The isotopic composition of the bleached skeletal calcite was further determined with a Neptune plus MC-ICPMS. Sample material was collected using a Proxxon handrill with a 1 mm drill bit and further processed following Foster (2008) with modifications. The amount of sample needed was calculated based on mean skeletal boron concentrations given in Farmer et al. (2015a). The sample powders were transferred to precleaned Teflon vials. The sample was then rinsed with boron-free deionised water, centrifuged, and the supernatant solution was discarded. This step was repeated three times.

To remove non-lattice boron and the organic matrix of the sample, a fresh mixture of 0.3 % hydrogen peroxide and 0.1 M ammonia was added into the vial and heated in an ultra-sonicated water bath for 30 minutes at 80 °C. The sample was then centrifuged and the bleaching solution was discarded. The remaining sample was rinsed three times with boron-free deionised water. Next, the sample material

TABLE 4.1: Elution scheme for boron column chemistry

Elution scheme
Pre-cleaning Fill entire column reservoir with 0.5 M HNO3 Add 1 ml 0.5 M HNO3 Wait until reservoir is empty
Conditioning of resin add 2 times 1 ml of deionised water
Load samples in steps of max 300 µl to waste
Elute matrix with 10 times 200 µl deionised water to waste
Collect boron with 6 times 250 µl 0.5 M HNO_3 in Teflon vial
Collect 200 µl boron **tail** in separate Teflon vial

was dissolved in 0.25 ml distilled 0.5 M HNO_3 and the double amount of acetic acid acetate buffer solution was added to the sample to reach a pH of 5.

Boron was then separated from the sample solution by column chemistry using Amberlite resin IRA 743 with a volume of approximately 25 µl. The acid-cleaned columns were preconditioned with 2 ml deionised water and the sample solution was added in steps of a maximum of 300 µl. The matrix was then eluted to waste with ten times 200 µl B-free deionised water. The B fraction was subsequently collected in 5 ml Teflon vials by adding a total amount of 1.5 ml distilled 0.5 M HNO_3 in six steps. To ensure no significant loss of B during column chemistry the elution tail of 200 µl was collected in a separate vial, which confirmed a recovery of > 99 %. Samples were stored in sealed Teflon vials and measured within 24 h hours after separation (Table 4.1).

The measurement of the purified sample solution was performed on a Thermo Fisher Neptune Plus MC-ICPMS following with modification the procedure described by Foster (2008). The inlet system was equipped with a Teflon spray chamber with an ESA 50 µl min^{-1} PFA nebuliser. The mass spectrometer was tuned for signal stability and intensity with a 5 ppb NIST SRM 951 solution (Catanzaro et al., 1970). Faraday cups chosen for measuring ^{10}B were L4 and for ^{11}B H4 both using 10^{12} Ω resistors. A batch of not more than nine column separated samples and standards including 0.5 M HNO_3 blanks and 35 ppb NIST SRM 951 bracketing standards

were measured to achieve low B background values. Sample boron concentration was adjusted to the standard concentration by the amount of dissolved carbonate separated on the column. A column-separated procedural blank and the sample tails were measured in a separate session against 2 ppb NIST SRM 951 B standards matching the volume between tail and 2 ppb standards to account for boron fall-in during the analytical session. Accuracy was checked by measuring 35 ppb ERM AE 121 B standard solutions (Vogl and Rosner, 2012) together with column separated JCp-1 standard material (Okai et al., 2002). Five JCp-1 samples were column separated for each sample sessions resulting in a reproducibility of better than 0.23 ‰ (2SD) and an overall mean of 24.12 ‰ (n = 10). We assume the reproducibility of JCp-1 to be representative for that of the sample material. The average B isotopic composition and reproducibility is in good agreement with the reported value of 24.22 ± 0.20 ‰ (2SD) (n = 10) (Zhang et al., 2017). The long term in-house mean of AE121 is 19.72 ± 0.25‰ (2SD) (n = 215) and therefore in agreement with the certified value of 19.88 ± 0.60 (2SD) (Vogl and Rosner, 2012).

The data were evaluated by background value correction for ^{10}B and ^{11}B and calculating the sample $\delta^{11}B$ according to formula (1). On-peak background values were measured 85 seconds before every sample and standard after a wash time of 30 seconds without ammonia. The subtracted background signal for ^{10}B and ^{11}B were between about 0.5 to 5 and 2 to 30 mV respectively while the signal intensities rose during the sample sequence. The uncorrected ^{10}B and ^{11}B sample intensities were in the range of 150 to 200 and 700 to 1000 mV. The subtracted blank from the sample signal was therefore below 5 %.

4.4 Results

4.4.1 LA-MC-ICPMS bulk carbonate analyses

The ratio of B/C shows a mean of 161 μmol mol^{-1} on the Bear Seamount specimen and 167 μmol mol^{-1} on the Monterey Canyon sample. The internal variation for each coral specimen (given as 2SD was 66 μmol mol^{-1} and 55 μmol mol^{-1}, respectively. In

Fig. 4.3b banding patterns and zigzag structures become visible and resemble the optical properties of the sample section (Fig. 4.3a and b). A less pronounced pattern is present in the Monterey Canyon sample section (Fig. 4.3d). The younger part of the Bear Seamount sample shows higher values with 134 ± 25 μmol mol^{-1} (2SD) than the older more central part with 182 ± 42 μmol mol^{-1} (2SD). In contrast, the Monterey Canyon sample is enriched in B relative to C in the inner 1.5 mm with 182 ± 46 μmol mol^{-1} (2SD) compared to the younger part of about 157 ± 15 μmol mol^{-1} (2SD).

The mean B isotopic composition of the Bear Seamount sample was 15.07 ± 7.49 ‰ (2SD) while the Monterey Canyon sample shows a similar $\delta^{11}B$ value with significantly smaller internal variability of 15.41 ± 3.79 ‰ (2SD). The absolute range for the Bear Seamount sample is 6.59 to 22.74 ‰ ($\Delta\ \delta^{11}B$ = 16.15 ‰) while that of the Monterey Canyon sample is smaller with compositions between 9.93 and 22.08 ‰ ($\Delta\ \delta^{11}B$ = 12.15 ‰). The pattern found for B/C is reflected in the isotopic composition, although the distribution of the isotopic composition is more scattered. The granular structure of the $\delta^{11}B$ value maps (Fig. 4.5a and c) are caused by statistical noise in the data and are not real compositional patterns. Based on counting statistics, the best precision (1 SD) of a single pixel (5 times 1 s of data collection) of $\delta^{11}B$ values that can be achieved is about 3.5 ‰ based on the mean count rates ($80*10^3$ counts) for ^{10}B. This value improved for the transect due to integration over five parallel lines to about 1.6 ‰.

On the transect shown in Fig. 4.4 a positive linear correlation between the B isotopic and elemental composition on the Bear Seamount sample is more pronounced than on the Monterey Canyon sample(Fig 4.5). This is most likely due to the lower B/C and $\delta^{11}B$ variation that can be found along the chosen sample transect.

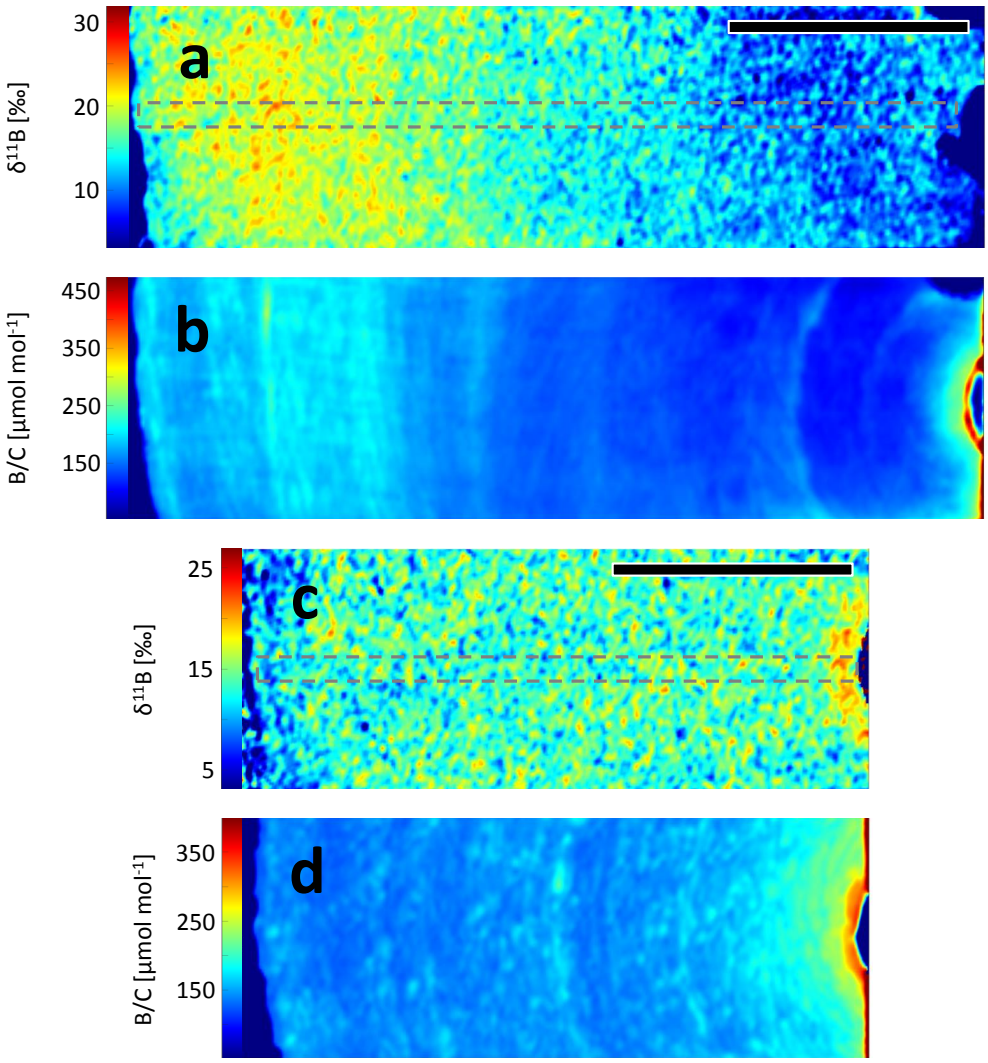

FIGURE 4.4: Internal δ^{11}B and B/C variability of the Bear Seamount sample (a and b) and the Monterey Canyon (c and d) respectively. The scale bar in a and c represents a length of 2 mm. The grey ticked box denote the area for the comparison of δ^{11}B and B/C shown in Fig. 4.5.

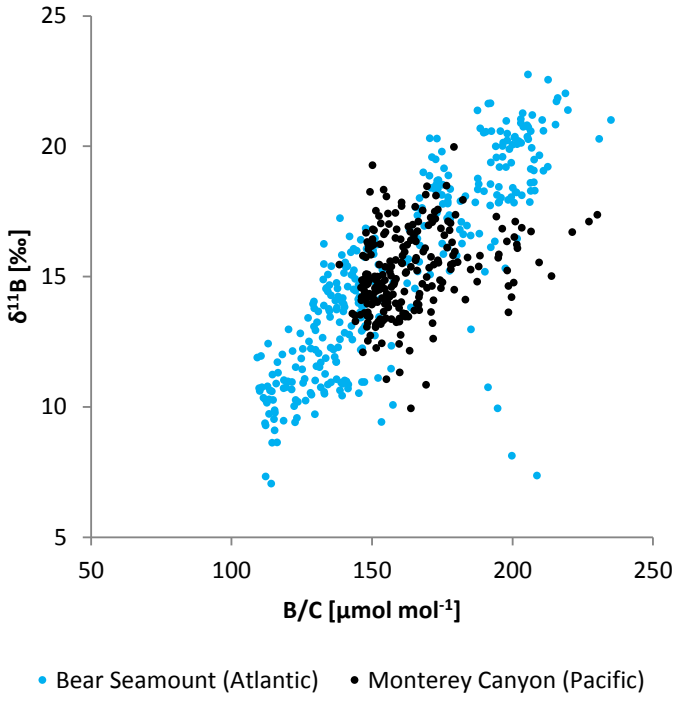

FIGURE 4.5: A linear positive correlation between $\delta^{11}B$ and B/C can be observed on the bamboo coral sample from the Bear Seamount while this is less pronounced on the Monterey Canyon sample.

4.4.2 Solution-based MC-ICPMS

The solution-based measurements on the bleached sample material revealed a mean $\delta^{11}B$ value of 13.06 ± 1.41 ‰ (2SD) (n = 4) for the Bear Seamount sample, falling between 12.63 to 14.12 ‰ (Fig. 4.6a). The B isotopic compositions change to heavier values from the core to the rim of the sample. The Monterey Canyon sample showed a mean B isotopic composition of 13.53 ± 1.37 ‰ (2SD) (n = 4) over a range of 12.74 to 14.14 ‰ (Fig. 4.6b). No general trend of the B isotopic composition can be observed across the growth radius for this sample.

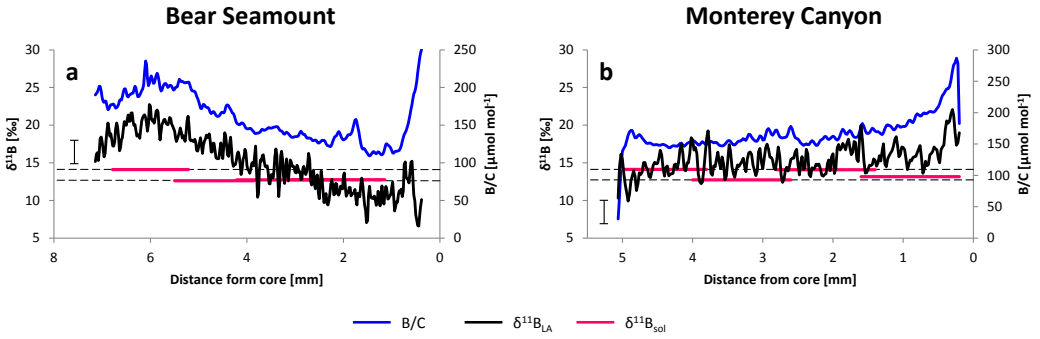

FIGURE 4.6: Transect of B/C (blue line) and laser ablation $\delta^{11}B$ values ($\delta^{11}B_{LA}$) (black line) across the centre of the mapped area of the Atlantic sample (a) and the Pacific sample (b). Red lines denote the drilled and bleached results ($\delta^{11}B_{sol}$). Uncertainties for B/C and $\delta^{11}B_{sol}$ values are smaller than line thickness. Uncertainty given as 2SD for $\delta^{11}B_{LA}$ values is denoted as the black bar left of the curve.

4.5 Discussion

4.5.1 Comparison with other species

A comparison of our solution-based $\delta^{11}B$ values with that of other studies on octocorals in the same pH range show that our data fall below these values (Fig. 4.7). Our Pacific sample grown under a local pH_{tot} value of about 7.55 was measured to have a $\delta^{11}B$ range from 12.74 to 14.14 ± 0.23 ‰ (2SD). This is lower than found by Saenger et al. (2017). They report for a local pH_{tot} of 7.54 $\delta^{11}B$ values of 15.52 ± 0.10 ‰ (2SD) for Keratoisis sp. and 14.37 ± 0.10 ‰ (2SD) for Isidella tentaculum. The drilled samples of our Atlantic bamboo coral show $\delta^{11}B$ values at a local pH_{tot} of 8.01 between 12.63 and 14.12 ± 0.23 ‰ (2SD). Therefore the isotopic composition of our Atlantic sample falls below the $\delta^{11}B$ values range of 14.84 ± 0.09 to 17.26 ± 0.10 ‰ (2SD) measured by Farmer et al. (2015a) on several *Keratoisis sp.* specimens grown in a pH_{tot} range from 7.99 to 8.02. If we assume the calcifying fluid to have a boron isotopic composition of seawater, our findings substantiate the finding of earlier studies that skeletal $\delta^{11}B$ of octocorals indicate a lower pH upregulation of lower than 0.4 (Farmer et al., 2015a; McCulloch et al., 2012). This finding is in contrast to the proposed up-regulation of about one pH unit for other deep sea hexacorals as proposed by e.g. Anagnostou et al. (2012), McCulloch et al. (2012), or Blamart et al.

(2007).

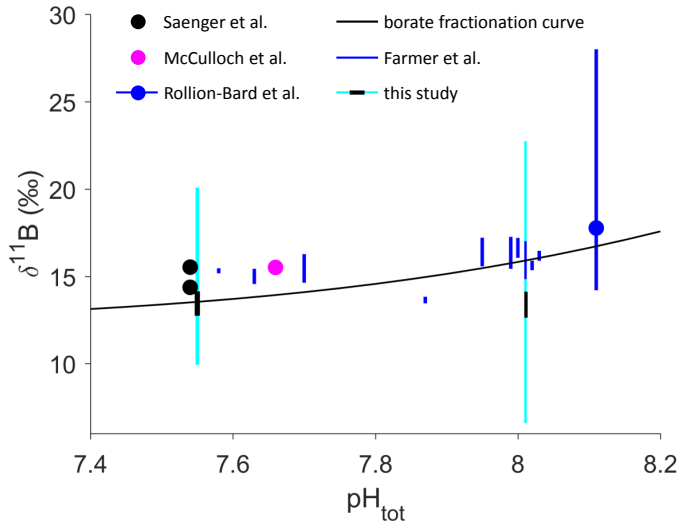

FIGURE 4.7: Boron isotopic composition of octocorals against pH (total scale). Black circles denote data from Saenger et al. (2017), magenta circle that of McCulloch et al. (2012) and the blue circle that of Rollion-Bard et al. (2017). Bars denote the observed range on the sample while the bars without the circle are data from Farmer et al. (2015a). Cyan and black coloured bars represent the range of the laser ablation and drilled δ^{11}B values measured in this study. Black curve describes the borate fractionation curve at 800 m water depth, 5 °C, a salinity of 35, $\delta^{11}B_{SW}$ of 39.61 ‰ (Foster et al., 2010) and a boron fractionation factor of 27.2 ‰ (Klochko et al., 2006).

4.5.2 Bulk vs. bleached carbonate

In this study the B isotopic composition of bamboo corals were measured with two different methods. The comparison of the mean $\delta^{11}B_{LA}$ and mean $\delta^{11}B_{sol}$ values of the Bear Seamount and the Monterey Canyon sample show a significant (α = 0.05, Welch-test) offset of about 2 ‰. Nevertheless, no consistent offset between the two methods across the sample transect can be observed (Fig. 4.6). Further, the internal δ^{11}B variability observed in the bulk measurements by laser ablation is much larger than the one derived from solution-based methods, especially in the case of the Bear Seamount sample (Fig. 4.6a). This difference results on the one hand from smoothing internal heterogeneity by drilling millimetre sized sample areas compared to micrometre scale sampling by the laser ablation measurement. On the other hand, the larger range of $\delta^{11}B_{LA}$ values compared to $\delta^{11}B_{sol}$ values will also be

controlled by the bulk sampling approach employed during laser ablation, targeting also fractions other than the pure carbonate phase in the sample. A strong indication for this assumption is, that the values of the bulk isotopic composition are not just the smoothed value over the integrated distance from a single drill sample (see Fig. 4.6). The laser ablation method measures the total δ^{11}B composition, which includes the calcite phase, the organic matrix, as well as other non-lattice bound skeletal components. The avoidance of the non-carbonate phase might partially explain the smaller range for the solution-based method and the spatially inconsistent δ^{11}B offset between the two approaches. The mean δ^{11}B value of the bleached material does not fall to one end of the δ^{11}B value range of the laser measurements. Therefore, concentration changes of isotopically from the calcite phase distinct non-lattice B cannot explain this observation, since this would shift the bulk δ^{11}B signal to lighter or heavier values. It is more likely, that isotopically variable B would have to be removed from the sample material in different parts of the sample. A loss of isotopically heavy B through the oxidative cleaning step in the outer part of the Bear Seamount sample would be accompanied by a loss of isotopically light B in the inner part. This indicates that B of different isotopic compositions is present as non-lattice bound component in different parts of the skeleton. Apart from compositional origins of the variation that can be investigated with the two applied approaches, other possible influences are discussed further below.

4.5.3 Comparison with other methods

The boron isotopic composition of the Bear Seamount sample has now been analysed using three different methods including thermal ionisation mass spectrometer in negative-ion mode (N-TIMS) (Farmer et al., 2015a), LA-MC-ICPMS and solution-based MC-ICPMS. This study compares for the first time δ^{11}B values of the same samples analysed by the three different methods. We observe that with an internal variability of about 1.5 ‰, the solution-based range of δ^{11}B values on the Bear Seamount sample is similar to the 2.2 ‰ reported by Farmer et al. (2015a). Nevertheless, the absolute δ^{11}B value of the solution-based method shows lower values

than reported by Farmer et al. (2015a) with a mean difference of 2.8 ‰. Systematic $\delta^{11}B$ offsets of 0.5 to 2.7 ‰ between N-TIMS and MC-ICPMS measurements have been reported by Farmer et al. (2016) which equally corresponds to the observed mean offset on the same sample in this study.

The range of observed $\delta^{11}B$ values from laser ablation measurements in the two bamboo corals partly falls below the theoretical borate fractionation curve. This is lower than any $\delta^{11}B$ value reported by Farmer et al. (2015a) for the same sample analysed using N-TIMS or our dissolved samples. A reconstruction of the pH in the calcifying fluid using the conventional seawater pH to borate ion relationship used for other biogenic carbonates (e.g. Martin et al., 2016; Trotter et al., 2011; Wall et al., 2016) by laser ablation MC-ICPMS therefore appears hardly feasible. In contrast, the values of the solution based method employing the inorganic borate ion to pH relationship would result in a pH_{tot} of 7.1 to 7.7 (see Fig. 4.8). The pH reconstruction in such a low pH range is less sensitive due to the slope of the borate fractionation curve. This will lead to an increased uncertainty in pH reconstructions at low $\delta^{11}B$ values. Precise reconstruction of the calcifying fluid conditions might be therefore hard to achieve.

4.5.4 Possible causes for skeletal boron isotope fractionation

The composition of the calcifying fluid is actively regulated by corals (e.g. Cohen and McConnaughey, 2003; Ross et al., 2017; Sevilgen et al., 2019). This might be another explanation for the observed low $\delta^{11}B$ values in our bamboo coral samples. Although active input of isotopically light borate during calcification by borate pumping would lower the skeletal $\delta^{11}B$ value, not much is known about borate transport across membranes in animals. Nevertheless, borate transport is indeed known from plants and fungi (e.g. Takano et al., 2008; Yoshinari and Takano, 2017). Borate pumping can help the coral to buffer the pH at a certain level since the buffer capacity of B in seawater with a pH of about 8 is one fifth of the total seawater buffer capacity (Middelburg, 2019). Borate transport would result in a calcifying fluid B isotopic composition lower than that of seawater. This would lead to a negative

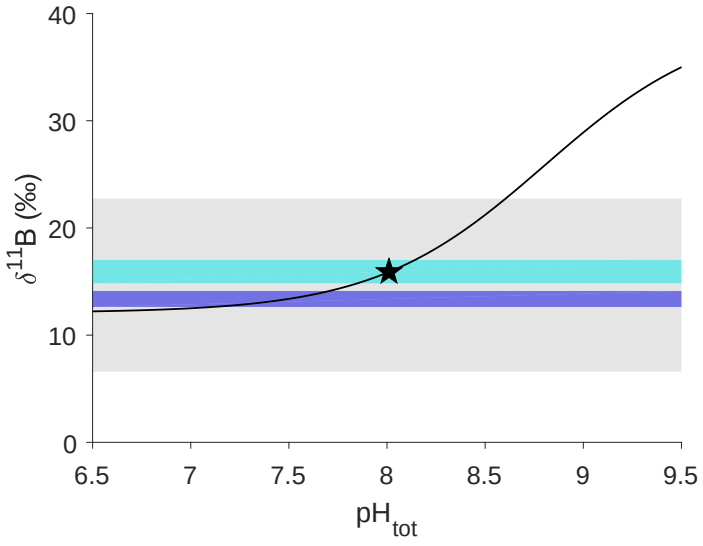

FIGURE 4.8: Range of the laser ablation MC-ICPMS $\delta^{11}B$ of the Bear Seamount sample (grey) in comparison to the borate fractionation curve (black line) at salinity of 35, 5 °C and a depth of 800 m. We used the fractionation factor α of 27.2 ‰ from Klochko et al. (2006) and the $\delta^{11}B_{SW}$ value of 39.61 ‰ from Foster et al. (2010). The isotopic range of the solution-based N-TIMS measurements from Farmer et al. (2015a) (cyan) is offset to the range found by MC-ICPMS measurements in this study (blue). The black star denotes environmental pH.

shift in the theoretical borate fractionation curve and subsequently to higher pH values from skeletal $\delta^{11}B$ values or to the possibility to calculate the pH at all based on skeletal $\delta^{11}B$ values.

Isotopic fractionation of B during incorporation has to be considered as an additional reason for the observed offset from the borate curve. Contrary to the findings of Zeebe et al. (2001), incorporation of B into the skeleton was found to cause an offset between calcifying fluid and skeletal $\delta^{11}B$ value under equilibrium conditions by an experimental (Saldi et al., 2018) and a computational study (Balan et al., 2018). Fractionation of B in bamboo corals might therefore also be driven by this process. Nevertheless, no equilibrium condition can be assumed for precipitation in calcifying organisms (DePaolo, 2011) as investigated by the two studies above. Impurity incorporation into calcite has been explained by the growth entrapment model (Gabitov et al., 2014b; Kaczmarek et al., 2016) and the surface kinetic model (DePaolo, 2011; Farmer et al., 2019). The growth entrapment model describes B incorporation as a relation of B diffusion rate out of the newly built crystal and the lattice to precipitation rate. The growth entrapment model seems to be less appropriate for B isotopic fractionation since B diffusivities in calcite are poorly constrained and previous studies (Gabitov et al., 2014b; Kaczmarek et al., 2016) focused on the bulk incorporation of B (Branson, 2018). Rising precipitation rates were found by Farmer et al. (2019) to lower the difference between the $\delta^{11}B$ value of precipitated calcite and solution borate. These authors could explain their findings by application of the surface kinetic model of DePaolo (2011). For their model, Farmer et al. (2019) assumed a preferential adsorption of charged borate on the crystal surface in comparison to boric acid. This attachment competes with the preferential uptake of trigonal (H_3BO_3 and $BO_2(OH)^{2-}$) species into the calcite crystal lattice. The B isotopic composition of the calcite is therefore a result of these competing fluxes. Further, Farmer et al. (2019) reported that the bulk B incorporation is also positively correlated to the precipitation rate and with that predictable by the surface kinetic model. These findings underpin the potential influence of precipitation rate on the B elemental and isotopic composition of bamboo corals. Therefore, the parts with

higher B might have been grown under conditions of higher precipitation rate. This seems to be contradicted by the observation of zigzag patterns in B/C on the Bear Seamount sample. Different precipitation rates would have to be assumed for skeleton mineralised at the same time, which seems to be unlikely.

In addition to the mentioned possible cause of B isotope fractionation organic matter was reported to fractionate B isotopes during adsorption (Lemarchand et al., 2005; Tossell, 2006). While Lemarchand et al. (2005) report a fractionation of B isotopes on humic acids of -18 to -47 ‰ less negative fractionation of -2 to -5 ‰ was calculated by Tossell (2006). If we assume humic acids as a representative for the organic matter in bamboo coral skeletons a shift to lighter B isotopic values seems to be possible. The preferential incorporation of ^{10}B in organic matter is in contrast to what can be observed by the comparison of the fluorescence map recorded on the Bear Seamount sample by Flöter et al. (2019). Note that the maps were not recorded at exactly the same sample transect. Figure 4.9 shows that the region of higher fluorescence, which indicate a higher organic matter concentration (Wall and Nehrke, 2012), occurs like the higher δ^{11}B values at the rim of the sample. The reported negative isotopic fractionation at humic acids and the observation of higher organic matter concentrations coincident with higher δ^{11}B values do not permit a conclusive statement about the role of organic matter in isotope fractionation in bamboo coral mineralisation.

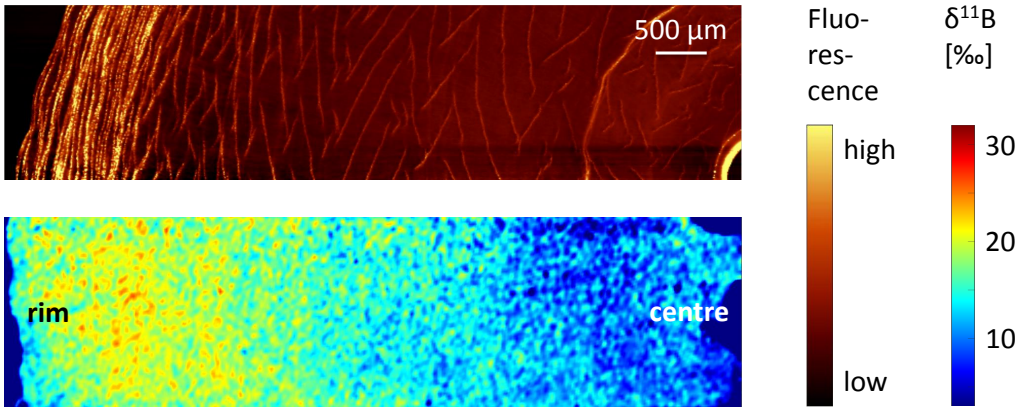

FIGURE 4.9: The comparison of the fluorescence (map from Flöter et al. (2019)) and the B isotopic composition of the bamboo coral sample from the Bear Seamount shows that high δ^{11}B values occur together with a higher fluorescence and therefore organic matter.

Based on our observations, the bulk B isotopic composition of bamboo corals cannot be ascribed to a single driving mechanism. It is more likely that a combination of borate transport to the CF, precipitations rate and isotopic fractionation on organic matter result in the observed patterns.

4.6 Conclusion

In this study the spatial distribution of B and its isotopes were mapped at the microscale to evaluate the calcification mechanism and proxy potential of bamboo corals. Under the assumption of conservative borate behaviour in the calcifying fluid, the range in B isotopic compositions found during this study confirms that bamboo corals – if at all – internally upregulate pH to a lower degree than found in hexacorals. Further, we found that both the mean bulk B isotopic composition but also its absolute range differs from that of the calcitic phase. This might be caused by organic and inorganic non-calcite lattice-bound B but also by kinetic effects or active borate pumping. The latter seems to be a process which can explain the apparent low pH upregulation. The similarity between the mapped B/C and δ^{11}B values suggest that B/C can be used as a first indicator for potential B isotopic variation in bamboo corals. Nevertheless, the large range of observed δ^{11}B values

by laser ablation MC-ICPMS mapping does not allow a valid reconstruction of the calcifying fluid pH. Faithful reconstructions of the calcifying fluid pH will require a more detailed knowledge of the calcification mechanism in bamboo corals.

References

Anagnostou, E., K. F. Huang, C. F. You, E. L. Sikes, and R. M. Sherrell (2012). "Evaluation of boron isotope ratio as a pH proxy in the deep sea coral Desmophyllum dianthus: Evidence of physiological pH adjustment". In: *Earth and Planetary Science Letters* 349–350.0, pp. 251–260.

Balan, E., F. Pietrucci, C. Gervais, M. Blanchard, J. Schott, and J. Gaillardet (2016). "First-principles study of boron speciation in calcite and aragonite". In: *Geochimica et Cosmochimica Acta* 193, pp. 119–131.

Balan, E., J. Noireaux, V. Mavromatis, G. D. Saldi, V. Montouillout, M. Blanchard, F. Pietrucci, C. Gervais, J. R. Rustad, J. Schott, and J. Gaillardet (2018). "Theoretical isotopic fractionation between structural boron in carbonates and aqueous boric acid and borate ion". In: *Geochimica Et Cosmochimica Acta* 222, pp. 117–129.

Blamart, D., C. Rollion-Bard, A. Meibom, J. P. Cuif, A. Juillet-Leclerc, and Y. Dauphin (2007). "Correlation of boron isotopic composition with ultrastructure in the deep-sea coralLophelia pertusa: Implications for biomineralization and paleo-pH". In: *Geochemistry, Geophysics, Geosystems* 8.12, pp. 1–11.

Branson, O. (2018). "Boron Incorporation into Marine CaCO3". In: *Boron Isotopes*. Ed. by H. Marschall and G. Foster. Advances in Isotope Geochemistry. Cham: Springer International Publishing. Chap. Chapter 4, pp. 71–105.

Catanzaro, E., C. E. Champion, E. L. Garner, G. Marinenko, K. M. Sappenfield, and W. R. Shields (1970). *Boric acid: isotopic and assay standard reference materials*. National Bureau of Standards, Institute for Materials Research.

Cohen, A. L. and T. A. McConnaughey (2003). "Geochemical perspectives on coral mineralization". In: *Biomineralization* 54.1, pp. 151–187.

Cornwall, C. E., S. Comeau, and M. T. McCulloch (2017). "Coralline algae elevate pH at the site of calcification under ocean acidification". In: *Glob Chang Biol* 23.10, pp. 4245–4256.

DePaolo, D. J. (2011). "Surface kinetic model for isotopic and trace element fractionation during precipitation of calcite from aqueous solutions". In: *Geochimica Et Cosmochimica Acta* 75.4, pp. 1039–1056.

Farmer, J. R., B. Hönisch, L. F. Robinson, and T. M. Hill (2015a). "Effects of seawater-pH and biomineralization on the boron isotopic composition of deep-sea bamboo corals". In: *Geochimica Et Cosmochimica Acta* 155, pp. 86–106.

Farmer, J. R., B. Hönisch, and J. Uchikawa (2016). "Single laboratory comparison of MC-ICP-MS and N-TIMS boron isotope analyses in marine carbonates". In: *Chemical Geology* 447, pp. 173–182.

Farmer, J. R., O. Branson, J. Uchikawa, D. E. Penman, B. Honisch, and R. E. Zeebe (2019). "Boric acid and borate incorporation in inorganic calcite inferred from B/Ca, boron isotopes and surface kinetic modeling". In: *Geochimica Et Cosmochimica Acta* 244, pp. 229–247.

Fietzke, J. and M. Frische (2016). "Experimental evaluation of elemental behavior during LA-ICP-MS: influences of plasma conditions and limits of plasma robustness". In: *Journal of Analytical Atomic Spectrometry* 31.1, pp. 234–244.

Fietzke, J., A. Heinemann, I. Taubner, F. Böhm, J. Erez, and A. Eisenhauer (2010). "Boron isotope ratio determination in carbonates via LA-MC-ICP-MS using soda-lime glass standards as reference material". In: *Journal of Analytical Atomic Spectrometry* 25.12, pp. 1953–1957.

Fietzke, J., F. Ragazzola, J. Halfar, H. Dietze, L. C. Foster, T. H. Hansteen, A. Eisenhauer, and R. S. Steneck (2015). "Century-scale trends and seasonality in pH and temperature for shallow zones of the Bering Sea". In: *Proc Natl Acad Sci U S A* 112.10, pp. 2960–2965.

Flöter, S., J. Fietzke, M. Gutjahr, J. Farmer, B. Hönisch, G. Nehrke, and A. Eisenhauer (2019). "The influence of skeletal micro-structures on potential proxy records in a bamboo coral". In: *Geochimica Et Cosmochimica Acta* 248, pp. 43–60.

Foster, G. L. (2008). "Seawater pH, pCO_2 and $[CO_3^{2-}]$ variations in the Caribbean Sea over the last 130 kyr: A boron isotope and B/Ca study of planktic forminifera". In: *Earth and Planetary Science Letters* 271.1-4, pp. 254–266.

Foster, G. L., P. A. E. Pogge von Strandmann, and J. W. B. Rae (2010). "Boron and magnesium isotopic composition of seawater". In: *Geochemistry Geophysics Geosystems* 11.

Gabitov, R. I., C. Rollion-Bard, A. Tripati, and A. Sadekov (2014b). "In situ study of boron partitioning between calcite and fluid at different crystal growth rates". In: *Geochimica et Cosmochimica Acta* 137, pp. 81–92.

Hönisch, B. and N. G. Hemming (2004). "Ground-truthing the boron isotope-paleo-pH proxy in planktonic foraminifera shells: Partial dissolution and shell size effects". In: *Paleoceanography* 19.4.

Holcomb, M., A. A. Venn, E. Tambutte, S. Tambutte, D. Allemand, J. Trotter, and M. McCulloch (2014). "Coral calcifying fluid pH dictates response to ocean acidification". In: *Sci Rep* 4, p. 5207.

Kaczmarek, K., G. Nehrke, S. Misra, J. Bijma, and H. Elderfield (2016). "Investigating the effects of growth rate and temperature on the B/Ca ratio and δ11B during inorganic calcite formation". In: *Chemical Geology* 421, pp. 81–92.

Klochko, K., A. J. Kaufman, W. S. Yao, R. H. Byrne, and J. A. Tossell (2006). "Experimental measurement of boron isotope fractionation in seawater". In: *Earth and Planetary Science Letters* 248.1-2, pp. 276–285.

Lapointe, A. and L. Watling (2015). "Bamboo corals from the abyssal Pacific: Bathygorgia". In: *Proceedings of the Biological Society of Washington* 128.2, pp. 125–136.

LaVigne, M., T. M. Hill, H. J. Spero, and T. P. Guilderson (2011). "Bamboo coral Ba/Ca: Calibration of a new deep ocean refractory nutrient proxy". In: *Earth and Planetary Science Letters* 312.3-4, pp. 506–515.

LaVigne, M., A. G. Grottoli, J. E. Palardy, and R. M. Sherrell (2016). "Multi-colony calibrations of coral Ba/Ca with a contemporaneous in situ seawater barium record". In: *Geochimica et Cosmochimica Acta* 179, pp. 203–216.

Lemarchand, E., J. Schott, and J. Gaillardet (2005). "Boron isotopic fractionation related to boron sorption on humic acid and the structure of surface complexes formed". In: *Geochimica Et Cosmochimica Acta* 69.14, pp. 3519–3534.

Locarnini, R., A. Mishonov, J. I. Antonov, T. P. Boyer, H. E. Garcia, O. K. Baranova, M. M. Zweng, C. R. Paver, J. R. Reagan, D. R. Johnson, M. Hamilton, and D. Seidov (2013). "World Ocean Atlas 2013, Volume 1: Temperature". In: *NOAA Atlas NESDIS*. Ed. by S. Levitus and A. Mishonov. Vol. 73, p. 40.

Martin, P., N. F. Goodkin, J. A. Stewart, G. L. Foster, E. L. Sikes, H. K. White, S. Hennige, and J. M. Roberts (2016). "Deep-sea coral δ13C: A tool to reconstruct the difference between seawater pH and δ11B-derived calcifying fluid pH". In: *Geophysical Research Letters* 43.1, pp. 299–308.

McCulloch, M., J. Trotter, P. Montagna, J. Falter, R. Dunbar, A. Freiwald, N. Forsterra, M. Lopez Correa, C. Maier, A. Ruggeberg, and M. Taviani (2012). "Resilience of cold-water scleractinian corals to ocean acidification: Boron isotopic systematics of pH and saturation state up-regulation". In: *Geochimica Et Cosmochimica Acta* 87, pp. 21–34.

McCulloch, M. T., J. P. D'Olivo, J. Falter, M. Holcomb, and J. A. Trotter (2017). "Coral calcification in a changing World and the interactive dynamics of pH and DIC upregulation". In: *Nat Commun* 8, p. 15686.

Middelburg, J. J. (2019). "Biogeochemical Processes and Inorganic Carbon Dynamics". In:

Noé, S. U. and W. C. Dullo (2006). "Skeletal morphogenesis and growth mode of modern and fossil deep-water isidid gorgonians (Octocorallia) in the West Pacific (New Zealand and Sea of Okhotsk)". In: *Coral Reefs* 25.3, pp. 303–320.

Okai, T., A. Suzuki, H. Kawahata, S. Terashima, and N. Imai (2002). "Preparation of a new Geological Survey of Japan geochemical reference material: Coral JCp-1". In: *Geostandards Newsletter-the Journal of Geostandards and Geoanalysis* 26.1, pp. 95–99.

Okai, T., A. Suzuki, S. Terashima, M. Inoue, M. Nohara, H. Kawahata, and N. Imai (2004). "Collaborative analysis of GSJ/AIST geochemical reference materials JCp-1 (Coral) and JCt-1 (Giant Clam)". In: *Chikyukagaku* 38.4, pp. 281–286.

Rae, J. W. B. (2018). "Boron Isotopes in Foraminifera: Systematics, Biomineralisation, and CO2 Reconstruction". In: *Boron Isotopes*. Ed. by H. Marschall and G. Foster.

Advances in Isotope Geochemistry. Cham: Springer International Publishing. Chap. Chapter 5, pp. 107–143.

Rollion-Bard, C., D. Blamart, J. Trebosc, G. Tricot, A. Mussi, and J.-P. Cuif (2011). "Boron isotopes as pH proxy: A new look at boron speciation in deep-sea corals using 11B MAS NMR and EELS". In: *Geochimica et Cosmochimica Acta* 75.4, pp. 1003–1012.

Rollion-Bard, C., J.-P. Cuif, and D. Blamart (2017). "Optical Observations and Geochemical Data in Deep-Sea Hexa- and Octo-Coralla Specimens". In: *Minerals* 7.9, p. 154.

Ross, C. L., J. L. Falter, and M. T. McCulloch (2017). "Active modulation of the calcifying fluid carbonate chemistry (δ11B, B/Ca) and seasonally invariant coral calcification at sub-Tropical limits". In: *Scientific Reports* 7.1.

Saenger, C., R. I. Gabitov, J. Farmer, J. M. Watkins, and R. Stone (2017). "Linear correlations in bamboo coral $\delta^{13}C$ and $\delta^{18}O$ sampled by SIMS and micromill: Evaluating paleoceanographic potential and biomineralization mechanisms using $\delta^{11}B$ and Δ_{47} composition". In: *Chemical Geology* 454, pp. 1–14.

Saldi, G. D., J. Noireaux, P. Louvat, L. Faure, E. Balan, J. Schott, and J. Gaillardet (2018). "Boron isotopic fractionation during adsorption by calcite – Implication for the seawater pH proxy". In: *Geochimica et Cosmochimica Acta* 240, pp. 255–273.

Schlitzer, R. (2019). "Ocean Data View, https://odv.awi.de". In:

Sevilgen, D. S., A. A. Venn, M. Y. Hu, E. Tambutte, D. de Beer, V. Planas-Bielsa, and S. Tambutte (2019). "Full in vivo characterization of carbonate chemistry at the site of calcification in corals". In: *Sci Adv* 5.1, eaau7447.

Spivack, A. J., C. F. You, and H. J. Smith (1993). "Foraminiferal Boron Isotope Ratios as a Proxy for Surface Ocean Ph over the Past 21-Myr". In: *Nature* 363.6425, pp. 149–151.

Takano, J., K. Miwa, and T. Fujiwara (2008). "Boron transport mechanisms: collaboration of channels and transporters". In: *Trends in Plant Science* 13.8, pp. 451–457.

Thresher, R. E., S. J. Fallon, and A. T. Townsend (2016). “A "core-top" screen for trace element proxies of environmental conditions and growth rates in the calcite skeletons of bamboo corals (Isididae)”. In: *Geochimica Et Cosmochimica Acta* 193, pp. 75–99.

Tossell, J. A. (2006). “Boric acid adsorption on humic acids: Ab initio calculation of structures, stabilities, 11B NMR and 11B,10B isotopic fractionations of surface complexes”. In: *Geochimica et Cosmochimica Acta* 70.20, pp. 5089–5103.

Trotter, J., P. Montagna, M. McCulloch, S. Silenzi, S. Reynaud, G. Mortimer, S. Martin, C. Ferrier-Pagès, J. P. Gattuso, and R. Rodolfo-Metalpa (2011). “Quantifying the pH ’vital effect’ in the temperate zooxanthellate coral Cladocora caespitosa: Validation of the boron seawater pH proxy”. In: *Earth and Planetary Science Letters* 303.3-4, pp. 163–173.

Vogl, J. and M. Rosner (2012). “Production and Certification of a Unique Set of Isotope and Delta Reference Materials for Boron Isotope Determination in Geochemical, Environmental and Industrial Materials”. In: *Geostandards and Geoanalytical Research* 36.2, pp. 161–175.

Wall, M. and G. Nehrke (2012). “Reconstructing skeletal fiber arrangement and growth mode in the coral Porites lutea (Cnidaria, Scleractinia): a confocal Raman microscopy study”. In: *Biogeosciences* 9.11, pp. 4885–4895.

Wall, M., J. Fietzke, G. M. Schmidt, A. Fink, L. C. Hofmann, D. de Beer, and K. E. Fabricius (2016). “Internal pH regulation facilitates in situ long-term acclimation of massive corals to end-of-century carbon dioxide conditions”. In: *Sci Rep* 6, p. 30688.

Wall, M., J. Fietzke, E. D. Crook, and A. Paytan (2019). “Using B isotopes and B/Ca in corals from low saturation springs to constrain calcification mechanisms”. In: *Nat Commun* 10.1, p. 3580.

Watling, L., S. C. France, E. Pante, and A. Simpson (2011). “Biology of Deep-Water Octocorals”. In: *Advances in Marine Biology*. Vol. 60, pp. 41–122.

Wise, S. and R. Watters (2012). “Certificate of Analysis, Standard Reference Material 610”. In: *National Institute of Standards and Technology (NIST)*.

Yoshinari, A. and J. Takano (2017). "Insights into the Mechanisms Underlying Boron Homeostasis in Plants". In: *Front Plant Sci* 8, p. 1951.

Zeebe, R. E. (2005). "Stable boron isotope fractionation between dissolved B(OH)3 and B(OH)4-". In: *Geochimica et Cosmochimica Acta* 69.11, pp. 2753–2766.

Zeebe, R. E., A. Sanyal, J. D. Ortiz, and D. A. Wolf-Gladrow (2001). "A theoretical study of the kinetics of the boric acid–borate equilibrium in seawater". In: *Marine Chemistry* 73.2, pp. 113–124.

Zhang, S., M. J. Henehan, P. M. Hull, R. P. Reid, D. S. Hardisty, A. V. S. Hood, and N. J. Planavsky (2017). "Investigating controls on boron isotope ratios in shallow marine carbonates". In: *Earth and Planetary Science Letters* 458, pp. 380–393.

Zweng, M. M., J. R. Reagan, J. I. Antonov, R. Locarnini, A. V. Mishonov, T. P. Boyer, H. E. Garcia, O. K. Baranova, D. R. Johnson, D. Seidov, and M. M. Biddle (2013). "World Ocean Atlas 2013, Volume 2: Salinity". In: *NOAA Atlas NESDIS*. Ed. by S. Levitus and A. Mishonov. Vol. 74, p. 39.

5 Conclusion and outlook

5.1 Conclusion

The overarching goal of this thesis was to evaluate the potential of bamboo corals to record environmental conditions at high resolution in their high-magnesium calcite skeleton. The relative importance of environmental and physiological impacts on the skeleton composition was studied on the micrometre scale. Specimens from the Atlantic and Pacific Ocean were mapped using different techniques such as LA-MC-ICPMS, confocal Raman microscopy and EMPA. For B isotope measurements, these techniques were supported by a solution-based approach involving conventional drill sampling.

In the first manuscript (chapter two) of this thesis, skeletal Mg and Ba distributions were investigated aiming to resolve in how far these elements record environmental temperature and nutrient conditions. Both elements show concentric and in case of Mg also zigzag patterns in skeletal sample sections of an Atlantic coral. We concluded that long-term skeletal Mg/Ca and Ba/Ca variations can be used as in situ temperature and $[Ba]_{SW}$ proxies. Nevertheless, high-resolution compositions of the bamboo coral internodes vary significantly stronger than expected based on instrumental time series and are therefore likely driven by coral physiology. In particular, the attachment of coral tissue to the skeleton by desmocytes has been identified to impact the small-scale skeletal chemical composition.

Aiming at the suitability of Na and S as environmental or biomineralisation proxies, the third chapter addressed the spatial Na and S compositions of two Atlantic bamboo coral internodes at the micrometre scale. Similarly to Mg and Ba, concentric bands and zigzag structures were found. The observed anti-correlation of Na and S in bamboo corals has been explained with a biomineralisation model

that involves proton and bicarbonate pumping, assuming conservative behaviour of both elements in the CF. Based on the ability of the model to explain skeletal Na variations, Na as a potential salinity proxy has been ruled out because Na/Ca variations seem to be driven by the Ca concentration of the CF. Organic matter may have limited impact on the Na and S composition of the skeleton. The nonconcentric fine-scale structures found for the elemental composition of the internodes rule out high resolution environmental reconstructions. However, long-term variations may still be useful as environmental proxies.

Chapter four discussed the B elemental and isotopic composition of bamboo coral HMC, investigating whether seawater or CF carbonate parameters can be reconstructed from the skeleton. We observed a positive correlation between skeletal B/C and δ^{11}B values. This correlation can be used for preliminary estimates of spatial variation of δ^{11}B values on bamboo coral samples. The comparison of the laser ablation and solution-based methods on an Atlantic and a Pacific sample showed that the range resulting from the laser ablation mapping exceeds the one of the solution-based method. The disagreement in range was explained by smoothing induced by the spatial resolution of the applied methods and through compositional differences of the bulk and the bleached skeletal phase. The latter was assumed to be the main driver of the disagreement. Therefore, we concluded that laser ablation that is targeting bulk carbonate as opposed to the pure carbonate fraction, is less suitable to reconstruct pH of seawater or the CF, while bleached samples analysed using solution-based techniques may show the pH of the CF. In agreement with other studies, this study confirmed that bamboo corals show a lower pH upregulation, if at all, in their CF. Nevertheless, our results suggest that, besides a potential influence of boron isotopic fractionation with organic matter and kinetic isotope effects borate transport to the CF can influence the skeletal boron isotopic composition. The latter would cause the borate concentrations in the CF not to be representative of seawater. If this suggestion should turn out to be correct, then the offset of the CF boron isotopic composition in the CF from seawater needs to be

taken into account for calculations of the pH of CF from skeletal B isotopic compositions.

Taken together, the various proxy records in the investigated bamboo corals show a variety of microstructural patterns in their chemical compositions which were shown to arise from environmental but also from physiological factors, e.g. temperature or precipitation rate. Despite their complexity, bamboo corals still represent potential archives for paleoenvironmental reconstructions of for example temperature or $[Ba]_{SW}$ as long as the impact of physiological factors is understood and considered. This is likely the case for reconstructions based on empirical proxy calibrations on the decadal scale. In contrast, variations on the spatial scale of annual growth (i.e. at the micrometre level) should be insightful to gain a better understanding of the calcification process in calcifying octocorals.

5.2 Outlook

This thesis provides insights on the potential cause of skeletal B, $\delta^{11}B$, Ba, Mg, Na and, S variations in bamboo corals but many questions remain unanswered. Future projects would have to look into the cellular mechanisms which influence calcification and therefore the build-up of the bamboo coral proxy archive. These mechanisms include for example the transport pathways of ions from seawater to the CF. Cellular pumps and channels capable of transporting ions need to be identified and their relative importance to each other should be quantified. Further, the possible roles of organic matter in the CF as template of crystal formation, complexing agent or nucleation seed have to be investigated. Besides the classical crystallisation theory, various other pathways of biogenic carbonate formation including the involvement of ACC were suggested. The discovery of the real crystallisation pathway is essential to explain observed elemental and isotopic properties of the skeleton. Furthermore, little is known on the CF, even though information such as better constraints regarding its volume is crucial for model calculations. Finally, the composition and the role of skeletal organic matter for growth and thriving, or the

causes of the ring and zigzag patterns seen in many samples remain poorly understood. These questions open up a range of possible research areas aiming at evaluating and validating different geochemical parameters used on bamboo corals to reconstruct environmental conditions. Future research needs to address the diverse open questions on the field of bamboo coral calcification to establish these calcifiers as a proxy archive that can reliably substitute instrumental time series.